SSI-DT46205030

Doctoral Thesis

Estimation of Hosting Capacity of Photovoltaic Generations in Distribution Networks using Hybrid Particle Swarm and Gradient Descent Optimization

粒子群最適化と勾配降下法のハイブリッド最適化による配電系統における太陽光発電接続可能 量の推定

Esau Zulu

December 2023

Division of Systems Science and Informatics

Graduate School of Information Science and Technology

Hokkaido University

Doctoral Thesis

Submitted to Graduate School of Information Science and Technology

Hokkaido University

In partial fulfilment of the requirements for the degree of

Doctor of Information Science

Esau Zulu

Dissertation Committee:

Associate Professor Ryoichi Hara

Professor Hiroyuki Kita

Professor Hajime Igarashi

Publications and conferences

Journal Papers:

1. Esau Zulu, Ryoichi Hara, Hiroyuki Kita, "A flexible stochastic PV hosting capacity framework considering network over-voltage tolerance", *Energy Reports*, Vol. 9, Supplement 1, pp.529-538 (March,2023). https://doi.org/10.1016/j.egyr.2022.11.101
2. Esau Zulu, Ryoichi Hara, Hiroyuki Kita, "An efficient hybrid particle swarm and gradient descent method for the estimation of the hosting capacity of photovoltaics by distribution networks", *Energies* **2023**, 16, 5207. https://doi.org/10.3390/en16135207

Conference presentations:

1. Esau Zulu, Ryoichi Hara, Hiroyuki Kita, "Utilization of Electric Vehicles and Battery Energy Storage Systems for Enhancement of PV Hosting Capacity in A Distribution Network" *International Council on Electrical Engineering (ICEE 2023)*, 2-6 July 2023, Hong Kong, China.
2. Esau Zulu, Ryoichi Hara, Hiroyuki Kita, "A flexible stochastic PV hosting capacity framework considering network over-voltage tolerance", *9th International Conference on Power and Energy Systems Engineering (CPESE 2022)* Online September 9-11, 2022, Nagoya, Japan.
3. Esau Zulu, Ryoichi Hara, Hiroyuki Kita, "Distribution network PV hosting capacity improvement by inverter volt/var optimization using hybrid PSO/GD algorithm", *IEEJ annual general conference*, 6-161, pp.264-265, online (March 2022).
4. Esau Zulu, Ryoichi Hara, Hiroyuki Kita, "Distribution Network PV Hosting Capacity Evaluation using Hybrid Particle Swarm Optimization and Gradient Descent Algorithm", *IEEJ Conference – Hokkaido Chapter*, online (August 2021).

Estimation of Hosting Capacity of Photovoltaic Generations in Distribution Networks using Particle Swarm and Gradient Descent Optimization

Esau Zulu

Abstract

The excessive dependence on fossil fuels such as coal, oil and gas for energy production has led to massive emission of CO_2. This huge emission of CO_2 in the atmosphere has led to deterioration of the ozone layer. The subsequent impact of this has been rapid global temperature rise and, ultimately, climate change. To avoid further deterioration of the ozone layer and avoid deepening the climate change crisis, the world has, over the last few decades, resorted to the use of clean green-energy resources such as wind, photovoltaic (PV) etc., for the world's energy needs. In the same vein, electrical vehicles (EV) with battery energy storage systems (BESS) have increased in the share of the transportation industry to replace fossil fuel dependent transportation.

PV power sources have been increasingly adopted in large quantities and accounts for nearly ninety percent of green-energy power sources in the electrical power distribution networks (DN). This is because PV is relatively easy to install, has higher scalability and is cheaper than other renewable energy options. However, the adoption of PV in huge quantities can lead to various challenges in the operation of the distribution networks. The greatest challenge posed by PV is the risk of over-voltages during times of high solar irradiation (with subsequent high-power output) at times of low power demand. Other risks include, thermal capitulation of network lines and cables, reverse power flows, and high harmonics. Therefore, there is a need to determine the amount of PV power which a particular DN can accommodate without abrogating the network's operational limits. This amount is referred to as the PV hosting capacity (PVHC).

This study proposes an efficient method for estimating the PVHC of a DN. This method uses swarm intelligence in combination with gradient descent. The method harnesses the excellent exploration capabilities of particle swarm optimization (PSO) and the powerful exploitation of the optimum solution espoused by the gradient descent algorithm. In hybridizing the PSO and the GD algorithms, the proposed method also gets rid of the ills of each method.

The proposed method's efficacy in depth and speed of calculation was tested on several DN test systems including the IEEE 33 bus test DN, the IEEE 69 test DN and the existing 136 bus in Sao Paulo, Brazil to estimate the PVHC of these networks. The proposed method was also

used in the study of the effects of BESS and EV on the PVHC of a DN. The results of the calculations were compared with several other methods. The numerical results of the simulations proved that the proposed method was more efficient compared with other methods found in literature.

The study also proposes the use of the deterministic approach in combination with the stochastic methods to produce a fast optimization algorithm for estimating the PV hosting capacity distribution networks operating under the uncertainties which inherent in the network variables. In this part of the research, the PSO-GD was combined with the PEM-based probabilistic load flow analysis to synthesize a powerful tool for estimating the acceptable limit of PV which can be safely installed into the distribution network without violating the network performance limits. This tool can be used for network planning purposes at the conception stage of the DN or for system expansion planning purposes.

Keywords: Deterministic load flow, Distribution network, Gradient Descent, Hosting capacity, Over-voltage, Photovoltaic, Particle swarm optimization, Probabilistic load flow, Stochastic analysis

Table of Contents

1. Introduction 2
1.1 Background and Significance of the research 2
1.2 Challenges of PV integration in power distribution networks 3
1.2.1 Risk of Overvoltage Occurrence 3
1.2.2 Reverse Power Flow 4
1.2.3 High Harmonics due to high PV penetration 4
1.2.4 Risk of Overheating of Line Conductors and Cables 5
1.3 State-of-the-art in PV Hosting Capacity Estimation 5
1.3.1 Deterministic Approach 5
1.3.2 Stochastic/Probabilistic Approach 7
1.3.3 Time-series Approach 9
1.4 Distribution Network PVHC improvement Strategies 10
1.4.1 Line Capacity enhancement 11
1.4.2 Volt-var control using Smart Inverter 11
1.4.3 Battery Energy Storage Systems and Electric vehicles 12
1.4.4 Network Reconfiguration 12
1.4.5 Optimal Sizing and Placement of PV generation units 12
1.5 Motivation 13
1.6 Relevance of the Research 14
1.6.1 Importance of Research 14
1.6.2 Aim of Research 14
1.6.3 Objectives of the Research 14
1.7 Thesis Structure 15
1.8 Chapter Summary 16
2. Particle Swarm and Gradient Descent Algorithm 18
2.1 Overview 18
2.2 Conceptual Framework of PSO-GD Algorithm 18
2.2.1 Gradient Descent Algorithm 18
2.2.2 Original Particle Swarm Optimization 20
2.2.3 Challenges of standard particle swarm optimization 23
2.2.4 The Proposed PSO-GD Algorithm 23

2.3 Chapter Summary 26
3. PV Hosting Capacity of a Distribution Network 29
3.1 PV Hosting Capacity Problem Definition 29
3.1.1 PVHC estimation formulation 29
3.1.2 Solution Approach: Estimation of PVHC by PSO-GD 32
3.2 Case studies 33
3.2.1 Case I: Estimation of PVHC of IEEE 33 test bus DN 33
3.2.2 Performance of PSO-GD against other methods 37
3.2.3 Case II: Estimation of PVHC of IEEE 69 bus test DN 39
3.2.4 Case III: Existing Brazilian 136 bus DN 42
3.2.5 Case IV Comparison of Proposed PSO-GD and Original PSO 44
3.3 Stability Analysis of PSO-GD 45
3.4 Chapter Summary 46
4. PVHC Enhancement using PV Inverter Volt-Var Control 49
4.1 Proposed Reactive Power Compensation technique. 49
4.2 Implementation of VVC during PVHC estimation 50
4.3 Chapter Summary 55
5. Estimation of PVHC with Uncertainty Consideration 57
5.1 Chapter Overview 57
5.2 Stochastic PVHC estimation using PSO-GD 58
5.2.1 Hong's PEM Schemes 58
5.2.2 Implementation of Stochastic PSO-GD for PVHC estimation 61
5.2.3 Probabilistic Modelling of PV Output 61
5.2.4 Probabilistic Modelling of Load Demand 62
5.3 Case Studies 63
5.3.1 Case IA: Conservative Stochastic PVHC 63
5.3.2 Case IB: Flexible Stochastic PVHC 64
5.4 Efficacy and Speed of Proposed Method 69
5.4.1 Computation Accuracy 69
5.4.2 Computation Speed 72
5.5 Chapter Summary 72
6. Impacts of BESS and EV on PVHC in DN 75

6.1 BESS Charging load demand Model 75
6.2 EV charging load demand model 76
6.3 Quantification of the Effects of BESS and EV deployment in DNs on PVHC 78
6.4 Case Studies 79
6.4.1 Case A: EV Charging Station and BESS Located at PV Installation Sites 79
6.4.2 Case B: EV Charging Station Randomly Located within DN 82
6.5 Chapter Summary 83
7. Conclusions 86
References 89
Acknowledgements 99
Appendix I-A: Line power flows of IEEE 33 without PV 100
Appendix I-B: Line Flows for IEEE 33 with PV 101
Appendix II: PSO-GD Program Code 102
Appendix II-A Main Program Code 102
Appendix II-B: PSO-GD Sub-routine 102
Appendix II-C: PVHC Cost-function Sub-routine 106
Appendix II-D: Lagrange Gradient Sub-routine 107
Appendix II-E: LoadFlowAnalysis Sub-routine 108
Appendix II-F: Volt-Var Control Sub-routine 111
Appendix II-G: PEM Moments Generator 112
Appendix II-H: Main program for comparison of PSO-GD/PEM and MCS 115
Appendix II-I: PEM-based PVHC Estimation sub-routine 116
Appendix II-J: MCS-based PVHC Estimation sub-routine 118

LIST OF FIGURES

Figure 1.1: Percentage of power generation technologies 2015-2021 2
Figure 1.2: Typical node voltage variations with/without PV installations 3
Figure 1.3: Typical flow chart for deterministic PVHC estimation 6
Figure 1.4: Flowchart of the PVHC estimation using stochastic analysis. 8
Figure 1.5: Typical time-series based PVHC estimation process flow chart. 10
Figure 1.6: Structure of the thesis. 15
Figure 2.1: Solution search for the method steepest gradient descent in the solution space. 20
Figure 2.2:Movement of particles of standard PSO in the solution search space 21
Figure 2.3:Movement of a particles of original PSO from one position to the next 22
Figure 2.4:Movement of particles in PSO-GD optimization from one position to the next 24
Figure 2.5:Update process of a single particle in PSO-GD optimization 24
Figure 2.6: Flow chart of the PSO-GD algorithm 25
Figure 3.1:PVHC defined under different operational limits. 29
Figure 3.2: IEEE 33 bus test network with optimal locations and PV sizes. 33
Figure 3.3: Optimal PV locations and sizes for IEEE 33 bus test DN 34
Figure 3.4: Voltage profiles obtained with/without PV installations in IEEE 33 bus test DN. 35
Figure 3.5: Line current, actine power, reactive power w/without PV installation 36
Figure 3.6: PVHC convergence plots obtained for IEEE 33 bus for different methods. 38
Figure 3.7: voltage profiles obtained using different PVHC estimation methods. 38
Figure 3.8: Configuration of the IEEE 69 bus test DN with optimal PV locations 39
Figure 3.9: Line current, actine power, reactive power w/without PV installation 40
Figure 3.10: Comparison of PVHC estimates obtained for IEEE 69 bus test DN 41
Figure 3.11: Configuration of existing 136 DN in Sao Paulo, Brazil. 41
Figure 3.12: 136-bus voltage profile and line flows with/without PV installations 43
Figure 3.13: Comparison of convergence plots of original PSO against proposed PSO-GD 44
Figure 3.14: PVHC values of IEEE-33 bus, and IEEE-69 bus test DNs for stability analysis. 45
Figure 4.1: Inverter VVC characteristics for node voltage. 50
Figure 4.2: Flowchart of PVHC estimation with inverter VVC. 51
Figure 4.3: Voltage profiles of the IEEE bus network for three different scenarios 52

Figure 4.4: (b) Reactive power generated at the nodes in the IEEE 33 bus for each scenario..... 53
Figure 5.1: Flow chart for Hong's 2m+1 PEM scheme 60
Figure 5.2: Flowchart for the PVHC estimation process in DN using stochastic PSO-GD..... 62
Figure 5.3: PDFs of maximum node voltages at each installed PV size..... 64
Figure 5.4: PVHC (a) with hard voltage constraint (b) with flexible voltage constraint 65
Figure 5.5: Probability density functions of maximum node voltages for different PV sizes. 66
Figure 5.6: PDF of maximum node voltages for Installed PV capacities 3.2 - 5 MW 67
Figure 5.7: Probability of voltage violations as a function of Installed PV capacity..... 67
Figure 5.8: PVHC as a function of flexible voltage limit constraints. 68
Figure 5.9: Probability of over-voltages as a function of installed PV size..... 70
Figure 5.10: PVHC and error as a function of voltage violation probability..... 71
Figure 6.1: Flow chart of multi-stage estimation of PVHC of DNs with EV and BESS. 78
Figure 6.2: PDFs of the maximum node voltages in each EV and BESS penetration scenarios. . 79
Figure 6.3: Variations of mean and standard deviation of maximum node voltages..... 80
Figure 6.4: Variations of PVHC estimates with BESS/EV load for each scenario..... 81
Figure 6.5: Net demand on the DN nodes for each scenario 81
Figure 6.6: Variations of PVHC estimates in simulation runs against number of EVs. 82
Figure 6.7: PVHC estimate as a function of EV charging load. 83

NOMENCLATURE

λ:	Lagrange multipliers on equality constraints of the optimization problem
μ:	Lagrange multipliers on inequality constraints of the optimization problem
ε_r:	Relative error in the estimation
ε_{rmse}:	Root mean square error in the estimation
μ_{r_l} :	Mean value of a random variable r_l
σ_{r_l} :	Standard deviation of a random variable r_l
$\xi_{l,k}$:	Standard location of the input random variables
$\omega_{l,k}$:	Weights of standard locations of the input random variables
α_i:	Slope of the PV inverter volt-var control characteristic
δ_n:	Phase angle of the voltage at the n −th node
ζ_h^{BESS}:	Binary variable for the status of the battery energy storage charging
η_{ch}^{BESS}:	Charging efficiency of battery energy storage system
η_{dis}^{BESS}:	Discharging efficiency of battery energy storage system
ζ_h^{EV}:	Binary variable for the status of the electric vehicle (charging/discharging)
η_{ch}^{EV}:	Charging efficiency of electric vehicles
η_{dis}^{EV}:	Discharging efficiency of electric vehicles
$\mathcal{L}(\cdot)$: $\mathbb{R}^n \to \mathbb{R}$:	Lagrange function resulting from the optimization problem
$\boldsymbol{\nabla f}$:	Gradient of the objective function of the optimization problem
$\boldsymbol{\nabla \mathcal{L}}$:	Gradient of the lagrange function of the optimization problem
B_{nm}:	Susceptance of the line joining node n to node m
c_1:	Individual acceleration coefficient for the particles
c_2:	Cultural (population) acceleration coefficient for the particles
$C_{v,j}$:	Penalty factor applied for violating the j −th inequality constraint
G_{nm}:	Conductance of the line joining node n to node m
$f(\cdot)$: $\mathbb{R}^n \to \mathbb{R}$:	Objective function an optimization problem with real valued terms
$g_p(\cdot)$: $\mathbb{R}^n \to \mathbb{R}^c$:	Equality constraints on active power flows of the optimization problem
$g_q(\cdot)$: $\mathbb{R}^n \to \mathbb{R}^c$:	Equality constraints on reactive power flows of the optimization problem
$h(\cdot)$: $\mathbb{R}^n \to \mathbb{R}^c$:	Inequality constraints of the optimization problem
$\boldsymbol{gbest^k}$:	Global best position for all particles after k − iterations

$\boldsymbol{pbest_i^k}$:	Best position taken by the i −th particle after k − iterations
P_{ch}^{BESS}:	Charging power requirement of battery energy storage system
P_{ch}^{EV}:	Charging power requirement of electric vehicles
P_j^{pv}:	Installed PV size at the j −th node in the distribution network
P_n:	Net active power at the $n-th$ node in the distribution network
P_n^G:	Generated active power by conventional generators at the $n-th$ node
P_n^L:	Active power load demand at the $n-th$ node
$Pr(a \geq b)$:	Probability of a variable a being greater than b
Q_j^{pv}:	Reactive power from installed PV inverter at the j −th node
Q_n:	Net reactive power at the $n-th$ node in the distribution network
Q_n^G:	Generated reactive power by conventional generators at the $n-th$ node
Q_n^L:	Reactive power load demand at the $n-th$ node
r_1:	Randomizer for individual acceleration of particles ($r_1 \in \{0,1\}$)
r_2:	Randomizer for cultural acceleration of particles ($r_1 \in \{0,1\}$)
S_{nm}:	Apparent power flow from node n to node m
V_n:	Voltage magnitude at node n
$\boldsymbol{v_i^k}$:	Velocity vector of the i −th particle at the k −th iteration of the PSO
$\boldsymbol{v_i^{k+1}}$:	Updated velocity vector of the i −th particle after the $k+1$ −th iteration
w:	Inertia weight on the velocity of the particles
$\boldsymbol{x_i^k}$:	Incumbent position of i −th particle of PSO at the k −th iteration
$\boldsymbol{x_i^{k+1}}$:	Updated position of i −th particle of PSO after the k −th iteration

LIST OF ABBREVIATIONS

BESS:	Battery Energy Storage System
CTLBO:	Comprehensive Teaching Learning-Based Optimization
CDF:	Cumulative Distribution Function
DG:	Distributed Generation
DN:	Distribution Network
DPF:	Deterministic Power Flow
DSO:	Distribution System Operator
EV:	Electric Vehicle
GA:	Genetic Algorithm
I-DBEA:	Improved Decomposition -Based Evolutionary Algorithm
IMOEHA:	Improved Multi-Optimization Elephant Herding Algorithm
MCS:	Monte Carlo Simulation
MINLP:	Mixed Integer Non-Linear Programming
PCC:	Point of Common Coupling
PDF:	Probability Density Function
PEM:	Point Estimate Method
PPF:	Probabilistic Power Flow
PSO:	Particle Swarm Optimization
PSO-GD:	Particle Swarm and Gradient Descent Optimization
PV:	Photo-Voltaic
PVHC:	Photo-Voltaic generation Hosting Capacity
QOTLBO:	Quasi-Oppositional Teaching Learning-Based Optimization
RDN:	Radial Distribution Network
RE:	Relative Error
RMSE:	Root Mean Square Error
SoC:	State-of-Charge
VVC:	Volt-Var Control

CHAPTER ONE
INTRODUCTION

1. Introduction

1.1 Background and Significance of the research

Photovoltaics (PV) integration in electric power generation and electrical power systems has been increasing rapidly for the past few decades. In fact, the global total installed PV in 2021 was 168.8 GW from 139.2 GW in 2020 [1]. The projections for future installations are even higher with PV set to enjoy 56% of total distributed renewable energy installation. This increased use of PV generation has been necessitated by the need to curb the use of fossil fuel-based power generation which is leading the way for climate change and global warming.

PV power generation is highly sustainable, offers capacity credit by reducing the demand that must be met by conventional generators during periods of high demand and provides flexible scalability [2]. With the upsides to solar integration coupled with ever decreasing cost associated with PV technologies [3], rooftop PV penetration is projected to reach between 44 GW and 76.5 GW globally.

Figure 1.1 shows the progression of the solar installation from 2015 to 2021 relative to other electrical power generation sources. Solar installation has increased its global generation footprint from 1.1% to 3.7%. Thus, PV installations have increased their share by 2.6 percentage points compared to 2.3 percentage points for other renewables. This is significantly a higher increase than all the other renewable energy alternatives combined.

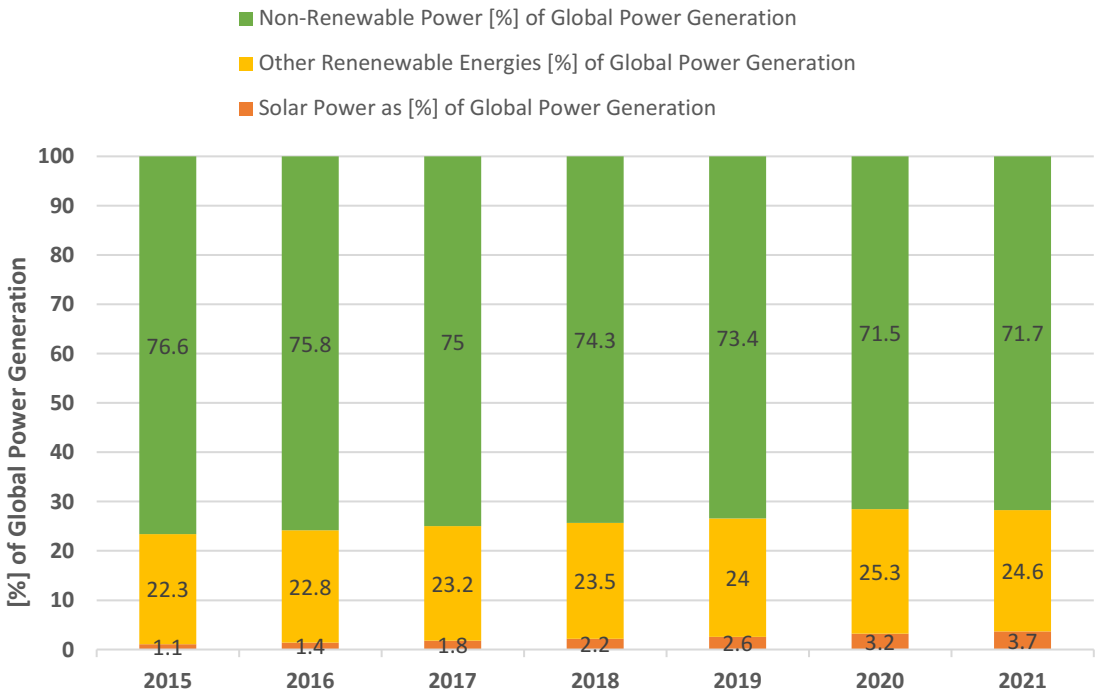

Figure 1.1: Percentage of power generation technologies 2015-2021

1.2 Challenges of PV integration in power distribution networks

The advantages of PV power generation range from technical benefits such as peak power shaving, network reliability enhancement, line power loss reduction [4] to environmental impact reduction, such as de-escalation of climate change brought by continued and excessive use of fossil fuels [5].

However, unlike power from conventional generators such as coal-powered thermal plants or nuclear power plants, PV power output is variable during short timescales due the dependence on solar irradiation which may be affected by cloud cover its diurnal nature. This variability produces several pertinent challenges in its interactions with the power distribution network [6]. These challenges include, but are not limited to, reverse power flow-which affects the network protection operation, increased harmonics, and line congestion-which may lead to thermal capitulation of network cables and conductors, over-voltages and voltage unbalance [7]-which might affect the insulation of associated equipment and devices. They also present a problem of unintentional islanding [8].

1.2.1 Risk of Overvoltage Occurrence

Any kind of distributed generation (DG) raises the local voltage at the point of common coupling (PCC). In some instances, this voltage rise might be beyond the acceptable range. This situation may be worsened by PV inverters if these inverters inject pure active power only.

Figure 1.2 shows the whole-year variation of voltage at a node in a typical DN with and without PV injection. It has been observed that PV injection improves the undervoltage issues which may occur in networks without PV installation at high load conditions but, it also brings about the challenge of over-voltages at moments of high irradiation and low network loading.

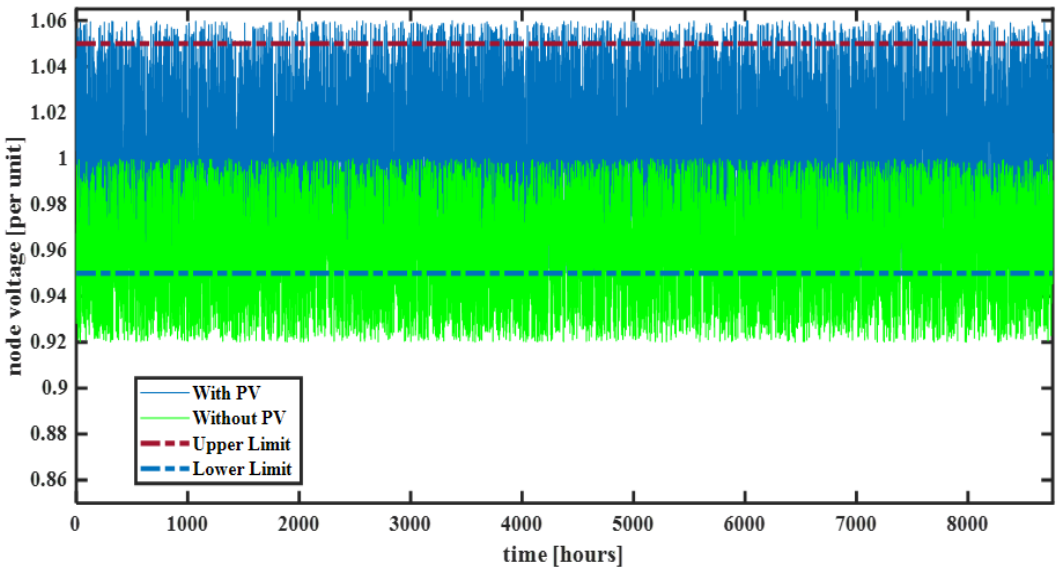

Figure 1.2: Typical node voltage variations with/without PV installations

The over-voltage problem brought about by the excessive proliferation of PV generation in power distribution networks is perhaps the biggest challenge faced in DNs. This is one of the main reasons for limiting the amount of PV connected in the network [9]. Limiting the amount of installed PV helps prevent the system from operating at undesirable conditions of over-voltages. This technique is referred to as 'active power curtailment'. It restricts the PV output to prevent over-voltage occurrences. This technique reduces the PV generator's financial potential. The authors in [10] and [11]argue that the loss of green energy and an economic loss to curtail generation with near zero marginal costs may, at times, be an unacceptable solution.

To reduce the risks of over-voltages without restricting the PV generator's output, advanced inverters are used. These PV inverters have the capability of voltage control using reactive power compensation. During conditions of high PV injections, these PV inverters absorb reactive power at the PCC to regulate the voltage downwards. At other times, they inject reactive power to support the voltage at the PCC.

1.2.2 Reverse Power Flow

In the traditional historical sense, the distribution network was designed to deliver power from the generating centers to the consumers in one direction. However, with the increased adoption of demand side power generation mainly by widespread PV deployment in distribution networks, power can now flow in both directions [12], [13]. At times of high demand compared to local generation, power is delivered in the conventional direction from the distribution substation to the loads. At times of high local generation, power flows from the load side into the substations.

Ideally, there is no fundamental issue with power flowing in either direction as the network cables or line conductors can carry as much power in one direction as they would in the other direction. The problem with reverse power flows, however, is that they affect the operation of control and protection devices [6]. Reverse power flows can cause improperly configured controllers and relays to maloperation. These may have catastrophic ramifications on the entire network such as wrongful isolation of healthy parts of the power network at the expense of the unhealthy sections.

1.2.3 High Harmonics due to high PV penetration

PV generates direct current (DC) power. Many distribution networks and devices operate with alternating current (AC) power. Therefore, inverters are used to convert the DC power from PV sources to AC power required by the distribution network. This conversion process usually produces harmonic distortions of the current and voltages [8].

Increased penetration of PV power sources increases the amount of harmonic content in the currents and voltages the network. Consequently, this heightened level of harmonics culminated into poor power quality at the customer PCC [14], [15]. There is a set limit to the amount of harmonic content that can be imposed by the power supplier at the PCC.

Therefore, the amount of PV that can be interconnected to a network can by restricted by the amount of harmonic content in the PV output.

1.2.4 Risk of Overheating of Line Conductors and Cables

The authors [16] contend that, much like the node voltage levels, the feeder current carrying capacity (ampacity) is a serious limiter to the maximum amount of PV generated power that a particular distribution network can accommodate. In essence, high PV penetration in the network potentially results in increased power flows between nodes in a feeder. This prospect of an increase in line power flows increases the prospect of thermal line congestion. Thus, the PV penetration in the network must be restricted to amounts which would not lead to thermal capitulation of conductors or network cables.

1.3 State-of-the-art in PV Hosting Capacity Estimation

Considering the challenges of PV integration into the power distribution networks highlighted in section 1.2, it is necessary to determine the maximum amount of PV that a particular network can hold without violating the network's performance limits on voltage, harmonics, line ampacity et cetera. The authors [17], [18], [19], [20] define the maximum amount of PV which can be injected into a distribution network without violating the operational limits of voltages, line thermal capacities, acceptable harmonic content etc., as the network's 'PV hosting capacity' (PVHC).

PVHC is a very important metric in modern power distribution networks with high penetration of distributed PV generation. It is used by network planners during the network design stage to simulate the network's capability to accommodate new photovoltaic installations [21]. PVHC is also used by network planners and operators to determine areas which need structural reinforcements and areas simply needing network reconfigurations [22]. PV hosting capacity estimation is aimed at maximizing the return on investment in the installed PV in distribution network by the distribution network operators (DSO).

There are several methods which have been developed for the estimation of PV hosting capacity in power distribution networks. The main methods used for PVHC estimation include:

1. deterministic methods,
2. stochastic/probabilistic approach and,
3. time-series based estimation.

1.3.1 Deterministic Approach

The deterministic approach applies known and fixed input data to a process model [23]. The process model then generates a set of fixed output data such as node voltage levels, line power flows, network harmonic content and direction of power flow [24], [25] and [26]. These outputs are then analyzed to determine the PVHC.

In the deterministic approach, the process model uses deterministic load flow (DLF) analysis to give information on output variables [27]. The information on the output variables is used as a guide to estimate the network operating state. If any of the indices are violated by a particular PV installation size, the system has reached its PV absorption potential and thus, its PV hosting capacity is estimated using this potential.

Figure 1.4 provides a crude flowchart of the deterministic approach to PVHC estimation. The implementation of the approach starts with inputting the DN data and initialization of the installed PV sizes at each site. The system state is then calculated using DLF analysis. The obtained output variables are then tested against preset limits. If any of the limits are violated, the process is shut down and the PVHC is estimated to be the sum of all initial PVs installed otherwise, The PV size is incremented in a predefined step at each site and the procedure repeated until there is a violation of any performance variable.

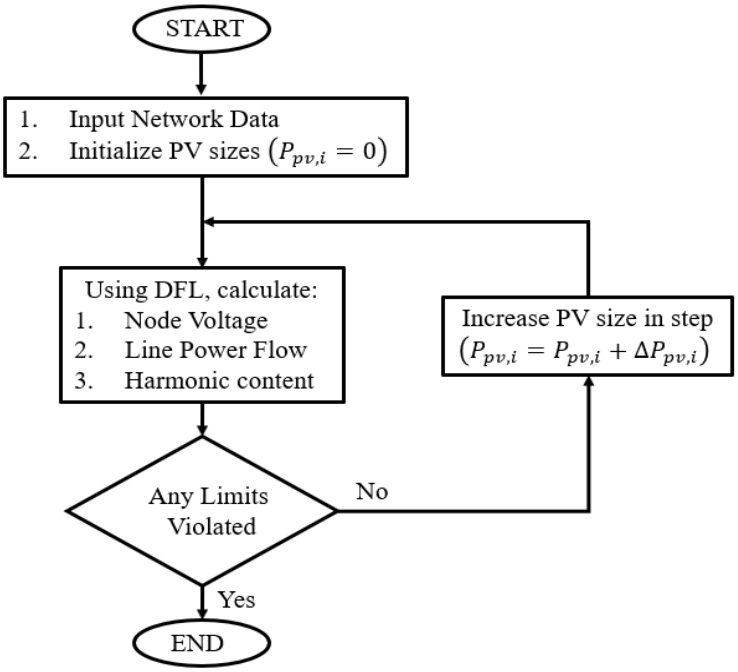

Figure 1.3: Typical flow chart for deterministic PVHC estimation

The procedure described above is a typical analytical method. Another class of the deterministic approach employs meta-heuristic optimization strategy to estimate the optimal PV sizes and locations. In this approach, PV hosting capacity is set up as a maximization problem and the performance indices are set as constraints to the optimization problem whose limits are not to be abrogated.

In [28], a nature inspired improved elephant herding optimization was used to estimate the optimal PV sizes in predetermined locations of distribution networks. [29] and [30] used the comprehensive teaching-learning-based optimization algorithm (CTLBO) and the improved decomposition-based evolutionary algorithm (I-DBEA) respectively to obtain optimal locations and sizes of PV systems on the IEEE 33-bus, 69-bus, and 118-bus test distribution networks. Furthermore, a framework based on hybrid genetic algorithm and

particle swarm optimization (GA/PSO) was used to estimate the PV hosting capacity of a distribution network with enhanced voltage regulation and voltage stability [31].

Table 1.1 lists some of the available literature on deterministic PV hosting capacity.

Table 1. 1: Representative deterministic methods for estimating PVHC found in literature.

Method	Network Type	Reference
Analytical	Existing rural grid - Japan	[32]
Analytical	Existing grid - USA	[33]
Analytical	IEEE 30 Bus Test DN	[34]
Analytical	EPRI J1 - USA	[35]
Analytical	EPRI Ckt7	[36]
Analytical	Urban area - Australia	[37]
Meta-heuristic	IEEE 33 bus Test DN	[30]
Meta-heuristic	IEEE 33 and 69 bus DN	[38]
Meta-heuristic	IEEE 33 and 123 bus DN	[29]
Meta-heuristic	IEEE 33,69 and 123	[39]
Meta-heuristic	IEEE Test DN	[31]

Both the analytical and meta-heuristic deterministic approaches provide a quick and computationally sound method of estimating the PV hosting capacity of the distribution network. However, because they employ DLF in their analysis, they are unable to handle uncertainties in the input variables [19] such as the random nature of PV power generation and the variations in the system loading. As a result, the models and results obtained using this method are not realistic.

1.3.2 Stochastic/Probabilistic Approach

Solar PV power output depends on solar irradiation and temperature to an exceedingly large extent [40]. Therefore, the PV output power is characterized by random behavior. Further, the load demand imposed on the network is highly variable and is also a random phenomenon [41]. Thus, the loading on the network is an uncertain variable. Consequently, the PVHC estimated using the stochastic approach is modeled as a stochastic phenomenon characterized by randomly generated uncertain parameters and input variables with random output variables. Authors [42] and [43] present network parameters, such as plausible locations for PV installations, and random variables, such as PV output and installed size, and variations in load conditions using their probability density functions (PDF). In fact, the output of the PV at installation sites is modeled as a beta distribution [44] while the load is modeled as a normal probability distribution. Figure 1.4 shows the flow chart of the PVHC estimation using stochastic analysis.

The PVHC estimation using stochastic methods begins with generating random distributions of input variables. Unlike the deterministic approaches which use the DLF, the stochastic approach uses these uncertain random variables in conjunction with the

probabilistic load flow (PLF) to obtain the probabilistic distributions of output variables of interest [19]

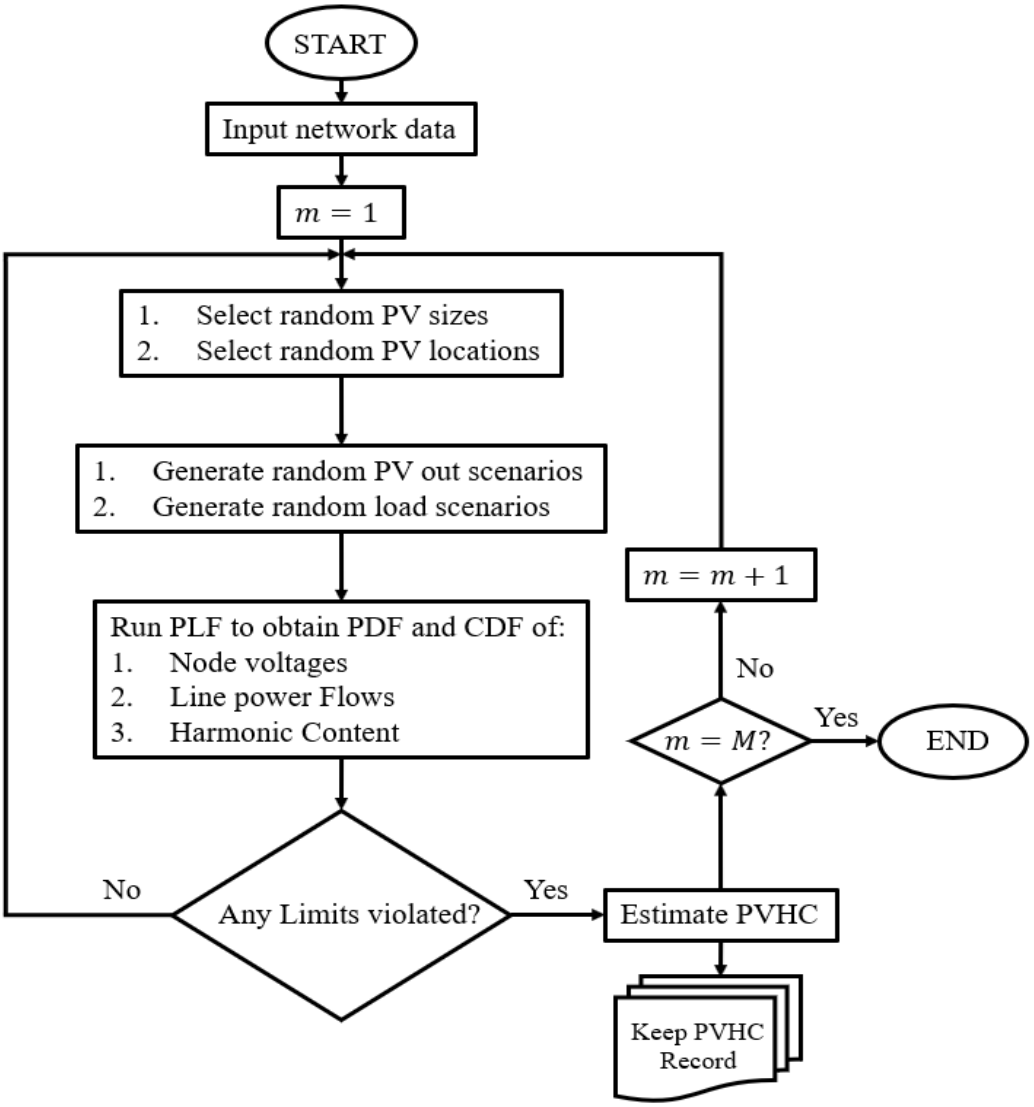

Figure 1.4: Flowchart of the PVHC estimation using stochastic analysis.

The PVHC estimation using stochastic methods begins with generating random distributions of input variables. Unlike the deterministic approaches which use the DLF, the stochastic approach uses these uncertain random variables in conjunction with the probabilistic load flow (PLF) to obtain the probabilistic distributions of output variables of interest [19].

The most widely used PLF analysis employs the Monte-Carlo simulation (MCS) strategy [43], [20]. The MCS is the most straight forward method. It entails running repeated simulations with values derived from random variables' PDFs [45]. However, despite the MCS high accuracy, it is computationally heavy because it requires to run DLF analysis at every iteration. The alternative to the MCS is the approximate methods. Among the approximate methods are the point estimate methods (PEM) which are computationally efficient and fast [46]. In [47], Hong's 3m PEM was used to approximate the PVHC of a

network with electric vehicle (EV) charging load. Here, it was shown that the PEM method is very fast compared to the MCS while giving a very accurate result. A similar conclusion was reached by [48] where the $2m + 1$ PEM was applied in estimating the maximum amount of photovoltaic which could be hosted by a DN.

The weaknesses of the stochastic approach are two fords. As alluded to earlier, they are computationally heavy and thus are very slow. Added to this, if the input variables are left free to assume any values within the solution space, they may produce an infinite number of scenarios which may not give a solution in a plausible time or, give a solution at all.

Table 1.2 summarizes the reviewed literature detailing the stochastic methods with the typical performance characteristics studied.

Table 1.2: Summary of some Stochastic methods for PVHC estiamtions in literature

Stochastic technique	Impact studied	Reference
PLF using Latin Hypercube Sampling with Cholesky Decomposition	Network demand, voltage magnitude, fast voltage variation	[49]
PLF using Heuristic Algorithm	Node voltage magnitude	[50]
Probabilistic direct voltage unbalance calculation	Voltage unbalance	[51]
Probabilistic power flow using first-order second-moment method	Voltage magnitude	[52]
Probabilistic power flow using enhanced cumulants	Voltage magnitude	[53]
probabilistic load flow using Unscented Transformation-UT	Voltage magnitude and Power losses	[54]
Probabilistic power flow utilizing simplified Monte Carlo Simulations	Voltage magnitude, voltage unbalance and loading	[55]
Probabilistic power flow formulated with a mixed-integer nonlinear optimization and genetic algorithm	voltage magnitude and unbalance	[56]

1.3.3 Time-series Approach

Time series methods utilize actual system measurements and historical data of power consumption and solar PV production as input variables in their PVHC estimation process. The process model in this approach uses a time-series power flow-based analysis to calculate the output variables of interest at a specific time resolution. These methods are a very realistic method of finding correlations between input variables and output variables.

In [57], quasi-static time series (QSTS) approach was used to estimate the maximum PV which could be hosted by a DN in specific times at a 1 second resolution. Similarly, [58] used fast QSTS with vector quantization determine the time dependent impacts of PV installations in the DN. Figure 1.6 shows the basic flow chart for the time series based PVHC estimation process.

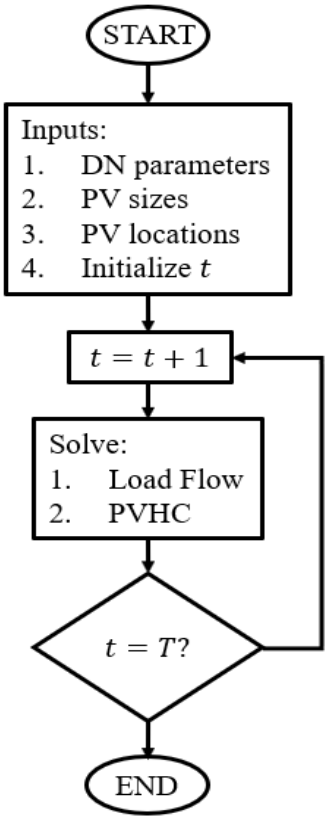

Figure 1.5: Typical time-series based PVHC estimation process flow chart.

The QSTS simulations are not widely used in industry because of the computational burden associated with running yearlong simulations at 1 second granularity resolution, which is required to capture PV variability. Furthermore, because time-series calculations offer point-by-point PVHC estimations in time domain, they may be suitable for DN operational PV injection scheduling but fall short on PV installation planning.

1.4 Distribution Network PVHC improvement Strategies

Given the need to limit the power generation from fossil fuel-propelled sources to limit the carbon emissions, there is a greater need to increase the proportion of power generation from renewable sources [59]. However, as alluded to in section 1.1, there is a restriction on the maximum amount of renewable energy which can be safely injected into the DN without risking violation of the limits on operational performance indicators such as voltage, line thermal capacity, and harmonic content [60]. Therefore, ways of improving the PVHC of the DN have been devised.

The strategies by which the PVHC of a DN are enhanced can be classified in two (2) broad categories vis a vie:

1. Network reinforcement-based enhancement strategies and,
2. Non-reinforcement-based strategies.

The first strategy involves system structural equipment improvements while the second involves the use of technical solutions. The techniques' applicability for a particular DN depend on investment costs, technology readiness, impact on congestion, compliance with applied grid codes etc. [61].

The network reinforcement-based strategies include, but are not limited to:

1. Line capacity enhancement
2. Smart inverter utilization (volt-var control VVC strategy)
3. Battery Energy Storage System (BESS) installation
4. Electric Vehicle (EV) Charging

The no-reinforcement strategies include:

1. Network re-configuration
2. Strategic optimal sizing and placement of the generating sources

1.4.1 Line Capacity enhancement

Line capacity enhancement is a necessity where the thermal rating of the network must be increased [62]. It involves either using a larger conductor size with higher current carrying capacity or erecting a new set of conductors in parallel with the existing lines. This is an expensive undertaking and must only be applied when it is necessary.

1.4.2 Volt-var control using Smart Inverter

The most prominent challenge to excess PV installation in DNs is the high risk of over-voltages [63], [64] and [65]. Therefore, active control of voltage can potentially lead to increased space in the network for higher PV size installation vis-a-vie increased PVHC. Several techniques are employed to achieve this including, but not restricted to, transformer online tap changing (OLTC), static compensation (STATCOM), smarter inverter volt-var control (VVC). In [66] proposed a method of node voltage approximation and control using OLTC. Reactive power compensation for voltage control using active devices to enhance the PVHC was explored by authors [67]. Smarter inverters with VVC functionality are the most recent advance in PVHC enhancement. The inverter performs dual functionality of power processing and voltage control [68] to increase the PVHC [69].

1.4.3 Battery Energy Storage Systems and Electric vehicles

The DN is undergoing many structural and technical changes due to introduction of Battery Energy Storage Systems (BESS) and Electric Vehicles (EV) [70]. The aggregate charging load imposed by different EV fleets at different times is highly stochastic but could lead to higher PV self-consumption and increase PVHC. have recently been engaged to improve PV self-consumption. [71] and [72] contend that optimal coordination of EV aggregators increases PV hosting capacity of DN. Furthermore, deployment of EVs in residential settings with rooftop PV is thought to mitigate the voltage drop problems for end-use residential customers [73].

Similarly, it has been argued by authors [74] that by using BESS to increase PV self-consumption and network resilience, BESS installation can improve the PVHC of the DN. BESS and EV impose similar loading demand on the DN with the only difference being that, while the BESS is more or less permanently connected to the network, the EVs have to plug-in and plug-out of the DN by the very nature of their operation.

1.4.4 Network Reconfiguration

The role of network reconfigurations was explored by [75]. The authors argued that DG hosting capacity can be increased by both static and dynamic grid reconfiguration. The static reconfiguration of the grid is applied during the planning stages of the DN hosting capacity while dynamic reconfiguration is realized through remote switching using active network management (ANM) schemes. For large networks, the switching possibilities for reconfiguration may be enormous. For this reason, [76] proposed a method of maximizing hosting capacity of DN by network reconfiguration by dividing the problem into several subproblems. The subproblems were then compressed into zero-suppressed binary decision diagram (ZDD) to avoid a huge combinatorial explosion. These ZDDs were thus easier to solve than the original problem.

The practical disadvantage of network reconfiguration is the cost of equipment deterioration due to switching. This disadvantage is exacerbated by the need to recalculate the reconfiguration problem in several timeframes.

1.4.5 Optimal Sizing and Placement of PV generation units

Strategic placement and optimal sizing of the PV generators is cardinal to ensuring that the maximum amount of PV in installed without the risks of over-voltages, thermal limit violations, voltage quality problems due to high harmonic content, reverse power flows etc. As alluded to in section 1.2.1, correct location of PV generation resources can result in enhanced PVHC. Authors [77], [78], [79] all conclude that there is a strong correlation between the placement of PV and its size in the DN. This is because the location of PV influences the subsequent thermal impacts and power flow directions. Furthermore, installed PV sizes at respective locations have an impact on the maximum node voltage

which could arise in the DN [80], [81]. Therefore, optimal location and sizing of PV installation is essential to maximizing the capacity of the DN.

1.5 Motivation

This research proposes a combination of deterministic/stochastic approaches to estimating the PV hosting capacity (PVHC) of a distribution network. At the center of the deterministic approach, a hybrid particle swarm with gradient descent mechanism is proposed. The gradient mechanism is aimed at regulating and the inertia constant of the standard particle swarm optimization through the steepest descent gradient and re-directing the velocity component of standard PSO orthogonal to the gradient of the objective function of the PVHC problem. This makes the solution approach acquiescent to the structure and nature of the problem because it requires the problem's derivative relationships.

The stochastic analysis involves the use of approximate probabilistic load flow analysis using point estimate method (PEM). These have excellent mechanisms for capturing uncertainties in the variables while retaining a reasonable calculation speed.

Deterministic methods have excellent calculation ability and speed but do not incorporate uncertainties in input variables. This makes the results of these methods unrealistic and, often, unapplicable in real systems. Stochastic/probabilistic approaches, on the other hand, have excellent capabilities of handling uncertainties in input variables. However, just like time-series based methods, they usually take an enormous amount of calculation time and effort to produce realistic models.

Because of the above-mentioned upsides and downsides to each method, there a need to develop a tool which combines the excellent speed and power of calculation offered by the deterministic approaches with the good uncertainty handling capability of the stochastic/probabilistic approaches.

The research presented in this thesis has been devoted to developing an approach that seeks to augment the excellent capabilities of both the deterministic and stochastic approaches while trying to address the downsides present in each individual approach. To that end, this research has managed to:

1. develop a method for estimating the PVHC of DN using hybrid particle swarm and gradient descent (GD) optimization (PSO).
2. develop a hybrid method of approximating the PVHC of DN under uncertainty of PV output power and load demand using PSO-GD and probabilistic analysis,
3. highlight the impact of use of smart PV inverters, which use the volt-var control mechanism to control the node voltages at the PCC, on DN's PVHC and,
4. investigate and underpin the impacts of EVs and BESS on the distribution network's PVHC by developing models for incorporating EV & BESS charging demand into the PVHC formulation.

1.6 Relevance of the Research

1.6.1 Importance of Research

The research carried out in this study is of utmost importance in modern power distribution network design and expansion planning [6].

The estimation of the PV hosting capacity of the distribution network enables the distribution system operator to:

1. pre-emptively determine or predict the response of the distribution network to various scenarios of PV deployments (involving both the PV sizes and the installation locations). This is a very important part of the network design to ensure proper operation of the network once commissioned but also to ensure appropriate PV sizes in different locations are accepted for integration in the network.
2. identify operational limits which can be relaxed and in which areas this can be considered for allowing higher levels of PV to be installed. This is particularly important when planning the expansion of PV generation expansion in the distribution network.
3. properly install battery storage facilities to improve system resilience performance by optimally locate, size, and control these facilities. Battery energy storage facilities help to ensure continuity of power supply in the network when there is disruption to normal generation facilities. To ensure the batteries are nearly always charged, they must be located near the PV installation sites so that at least they can be charged by PV power.

1.6.2 Aim of Research

The main objective of this research is to develop a method for estimating the PV hosting capacity of a power distribution network using a combination of the deterministic approach and the stochastic approach. This could help alleviate the problems present in each approach while augmenting the advantages of each approach.

1.6.3 Objectives of the Research

To achieve the aim stated above, and address the importance attached to this research the following objectives were set:

1. develop an accurate and effective PV hosting capacity estimation method.
2. investigate the effects of relaxing operational limits on certain performance indices in relation to PV hosting capacity estimation.
3. study the impacts of battery energy storage systems (BESS) and electric vehicles (EV) deployments in distribution networks on PV hosting capacity of the distribution network.

1.7 Thesis Structure

The thesis is structured as shown in figure 1.6. It has seven interrelated chapters starting from the introduction all the way to the conclusion.

Chapter 1 introduces the thesis by giving the background of the study, motivation, importance and aims of the research. It also provides a literature review on the state of the research on PV hosting capacity.

In Chapter 2, the proposed particle swarm and gradient descent (PSO-GD) algorithm is explained in detail. It begins by giving an overview of both the original particle swarm optimization (PSO) and the gradient descent (GD) approaches and ends by explaining how the two approaches are combined to realize the proposed PSO-GD method.

Chapter 3 analyzes the results obtained by applying the proposed PSO-GD method to various test systems including the IEEE-33 bus test DN, the IEEE-69 bus test DN and the existing 136 bus test DN in Sao Paulo

Chapter 4 highlights the importance of inverter volt-var control. Chapter 5 describes the estimation of PVHC under uncertainty conditions while Chapter 6 gives the results of the study of the impacts of BESS and EV on PVHC in DN. Chapter 7 gives the conclusions of the research.

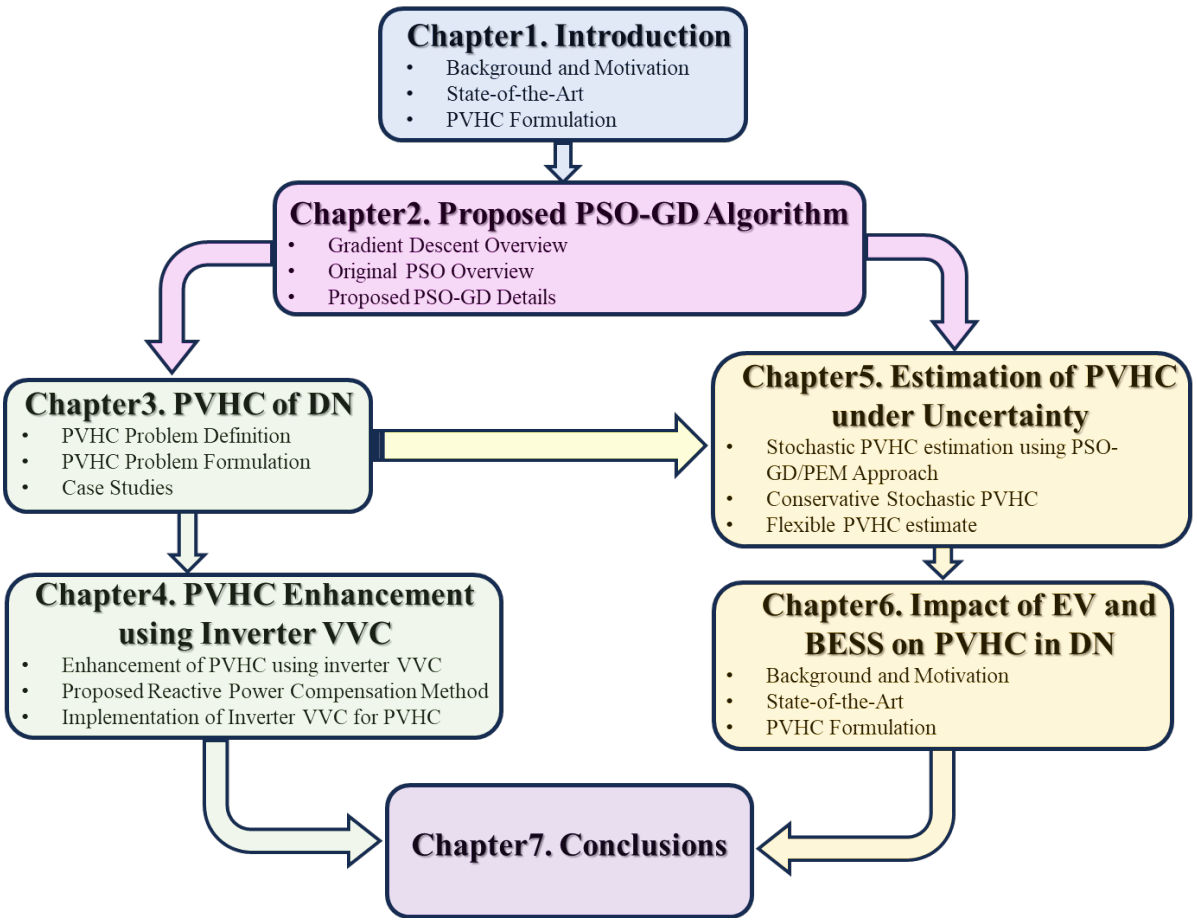

Figure 1.6: Structure of the thesis.

1.8 Chapter Summary

This chapter has presented the significance of estimating the PVHC of a particular DN. It has highlighted the main methods used, and the PVHC enhancement techniques which maybe be employed.

The table below is a list of advantages and disadvantages of each of the methods as highlighted in the literature considered in this study.

Table 1.3: Advantages and disadvantages of different PVHC estimation methods

Method	Advantages	Disadvantages
Deterministic	◆ Input parameters are easy to access. ◆ It is easy to implement. ◆ It is fast	◆ Does not incorporate uncertainty in input variables. ◆ PVHC obtained is a 1-snapshot scenario thus is not a true representation of network potential.
Stochastic	◆ Incorporates uncertainties in input variables. ◆ Generates realistic models and accommodates many PDFs	◆ Huge computational time and storage requirement ◆ Becomes increasing more complex with increases in number of variables. ◆ Fails to accommodate time dependent nature of variables
Time-series	◆ Considers correlations in grid power and PV production. ◆ Presents a realistic overview of the PVHC at different time scales	◆ Requires a lot of measurement data. ◆ Needs a lot of simulations at very high time resolutions. ◆ Very huge computational and storage demand

CHAPTER TWO PARTICLE SWARM AND GRADIENT DESCENT

2. Particle Swarm and Gradient Descent Algorithm

2.1 Overview

In the introductory chapter, it was discussed that meta-heuristic optimization methods are used as deterministic methods to estimate the PVHC of DNs. In this chapter, a gradient descent (GD)-based particle swarm optimization (PSO) proposed in this research is described in detail. The chapter begins the chapter by describing the steepest gradient descent algorithm based on steepest movement from point to point of in the solution search space orthogonal to the gradient of the objective function. It then describes classical PSO which mimics natural search behavior before uniting the GD and PSO algorithm into the proposed hybrid PSO-GD. The chapter concludes by providing numerical simulation results obtained by applying PSO-GD on several test DNs.

2.2 Conceptual Framework of PSO-GD Algorithm

2.2.1 Gradient Descent Algorithm

The generic Newton's GD has been applied to optimal power flow problems since the 1960s. Authors [82] proposed a method of solving the optimal power flow problem to minimize power systems power losses by obtaining optimal values for control variables such as real and reactive power and transformer tap ratios.

The classical optimization problem involves minimizing a function $f(x,u)$ with a set of variables x and u subject to equality and inequality constraints $g(x,u)$ and $h(x,u)$ respectively vis-a-vie:

$$min\ f(x,u) \tag{2.1}$$

$$s.t: g_i(x,u) = 0 \tag{2.2}$$

$$h_j(x,u) \leq 0 \tag{2.3}$$

The problem of (2.1) - (2.3) could be solved using the solution of Lagrange multipliers by introducing auxiliary variables on equality constraints and applying penalties on inequality constraints. The Lagrange function is then given by:

$$\mathcal{L}(x,u) = f(x,u) + [\lambda_i]^T.[g_i(x,u)] + \left[\mu_j\right]^T.\left[h_j(x,u)\right] \tag{2.4}$$

Where λ_i are the auxiliary variables introduced into the optimization problem for equality constraints, μ_j are penalty parameters for violation of inequality constraints. i are the indices for the equality constraints, j are the indices for inequality constraints.

At the optimum point (u', x') the partial derivatives of the Lagrange function are equal to zero, i.e.,

$$\left[\frac{\partial \mathcal{L}(x',u')}{\partial x}\right] = \left[\frac{\partial f(x',u')}{\partial x}\right] - [\lambda^T]\left[\frac{\partial g(x',u')}{\partial x}\right] - [\mu^T]\left[\frac{\partial h(x',u')}{\partial x}\right] = 0 \tag{2.5}$$

and,

$$\left[\frac{\partial \mathcal{L}(x',u')}{\partial u}\right] = \left[\frac{\partial f(x',u')}{\partial u}\right] - [\lambda^T]\left[\frac{\partial g(x',u')}{\partial u}\right] - [\mu^T]\left[\frac{\partial h(x',u')}{\partial u}\right] = 0 \quad (2.6)$$

Where the inequality constraints $h(x,u)$ only become active when the constraints are violated otherwise, they are inactive. Therefore,

$$\mu_j = k_{p,j}\begin{cases} 1\ for\ h_j(x,u) \geq 0 \\ 0\ for\ \ h_j(x,u) < 0 \end{cases} \quad (2.7)$$

Where $k_{p,j}$ are the penalty constants imposed on the Lagrange function for inequality constraint violation.

Therefore, when no inequality constraint violations are observed, the solutions are obtained by using partial derivatives and the Karush-Kuhn-Tucker (KKT) necessary conditions [83]. It follows then that, for an optimum solution, the conditions are:

$$\left[\frac{\partial \mathcal{L}}{\partial x}\right] = \left[\frac{\partial f}{\partial x}\right] + \left[\frac{\partial g}{\partial x}\right]^T . [\lambda] = 0 \quad (2.8)$$

$$\left[\frac{\partial \mathcal{L}}{\partial u}\right] = \left[\frac{\partial f}{\partial u}\right] + \left[\frac{\partial g}{\partial u}\right]^T . [\lambda] = 0 \quad (2.9)$$

$$\left[\frac{\partial \mathcal{L}}{\partial \lambda}\right] = g(x,u) = 0 \quad (2.10)$$

The values of the variables which give an optimal solution are obtained by:

evaluating the auxiliary variables using (2.11):

$$[\lambda] = -\left[\frac{\partial g}{\partial x}\right]^{-T} . \left[\frac{\partial f}{\partial x}\right] \quad (2.11)$$

analyzing the Lagrange gradient using (2.12):

$$[\nabla \mathcal{L}] = \left[\frac{\partial \mathcal{L}}{\partial u}\right] = \left[\frac{\partial f}{\partial u}\right] + \left[\frac{\partial g}{\partial u}\right]^T . [\lambda] \quad (2.12)$$

If the Lagrange gradient is sufficiently small, the minimum has been reached, otherwise, a new set of variables is calculated. The common approach is to use the steepest descent in the orthogonal direction of the gradient by updating the variables as given by (2.13) and depicted in figure 2.1. The update process is repeated using (2.11) to (2.13) until a sufficiently small value of the Lagrange gradient is obtained.

$$[u^{new}] = [u^{old}] - c.[\nabla \mathcal{L}] \quad (2.13)$$

c is the step-size which must be selected carefully. Too small a value assures convergence but requires too many adjustment cycles. Too big a value causes oscillations around the optimum.

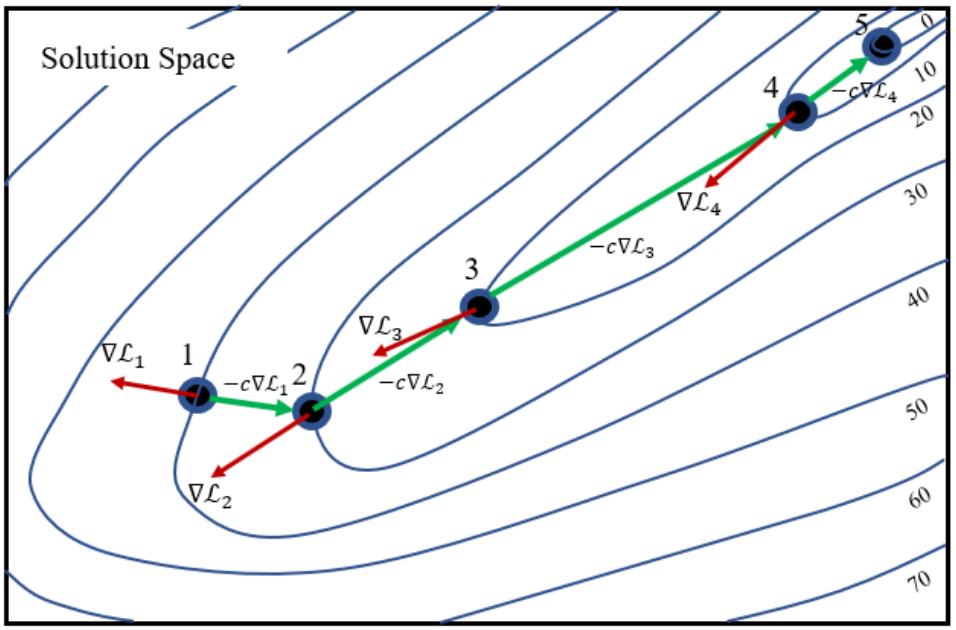

Figure 2.1: Solution search for the method steepest gradient descent in the solution space.

So far, the problem has been assumed not to violate the inequality constraints. This is not a practical assumption and most of the optimization problems are constrained by inequalities which may be abrogated from time to time. In [84], the authors proposed a method of solving non-linear problems by combining the treatment of equality and inequality constraints with the objective function.

However, Newton's gradient descent approach has difficulties handling inequality constraints in mixed integer non-linear, non-convex linear programming (MINLP) problems [85]. Thus, new methods involving meta-heuristics have been employed.

2.2.2 Original Particle Swarm Optimization

The original PSO was developed by Kennedy and Eberhart [86]. In its concept, it simulates flocking of birds (particles) in a two-dimensional space. The flocking of these particles optimizes a certain objective function. The value objective function of each particle is a function of its position and velocity in the space under consideration. The particles share information about their best experiences (personal best). Thus, the best experience is determined for the entire flock (global best) is obtained from the particle with the best objective value among the flock (population).

Each particle in the population is characterized by its current position x_i^k in the solution search space. k is the iteration number representing current condition, i is the particle number in the population. The objective value of the particle is calculated at the current position by $f(x_i^k)$. The particles in the population move from the current position to the next position using equation (2.14).

$$\boldsymbol{x_i^{k+1} = x_i^k + v_i^{k+1}} \tag{2.14}$$

Where v_i^{k+1} is the updated velocity component from the current position of the particle to the next. This updated velocity is derived relative to the personal best $pbest_i^k$ position of the particle experiences, the global best experience of all the particles in the population $gbest^k$ and the initial velocity of the individual particle. Therefore, the velocity is updated via equation (2.15).

$$\boldsymbol{v_i^{k+1}} = w\boldsymbol{v_i^k} + c_1 r_1\left(\boldsymbol{pbest_i^k} - \boldsymbol{x_i^k}\right) + c_2 r_2\left(\boldsymbol{gbest^k} - \boldsymbol{x_i^k}\right) \tag{2.15}$$

Where w is an inertia constant to the movement of the particles, c_1, c_2 are acceleration constants for relative movements towards the best position and the global best respectively, r_1, r_2 are randomly generated values $r_1, r_2 \in \{0,1\}$.

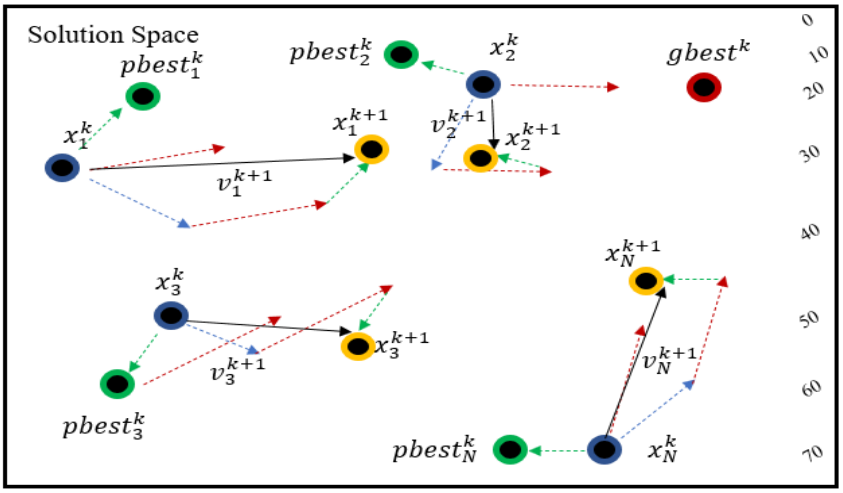

Figure 2.2:Movement of particles of standard PSO in the solution search space

Figure 2.2 shows the conceptual movement of particles in an N population original PSO. Green arrows are the particle movement vectors towards the best particle positions per individual experience, red arrows are the particle movement vectors towards the global best experience for the entire population and blue for the initial velocity components for the individual particles. Blue dots are the particle positions at the $k-th$ iteration while yellow dots are the particle positions at the $(k+1)-th$ iteration.

Figure 2.3 shows a detailed illustration of how one particle transits from the current position to the new position. The final position (yellow dot) is a vector sum (movement) of three components, vis-a-vie, the velocity component (blue arrow), the acceleration towards the personal best (green arrow) and the acceleration towards the global best position (red arrow).

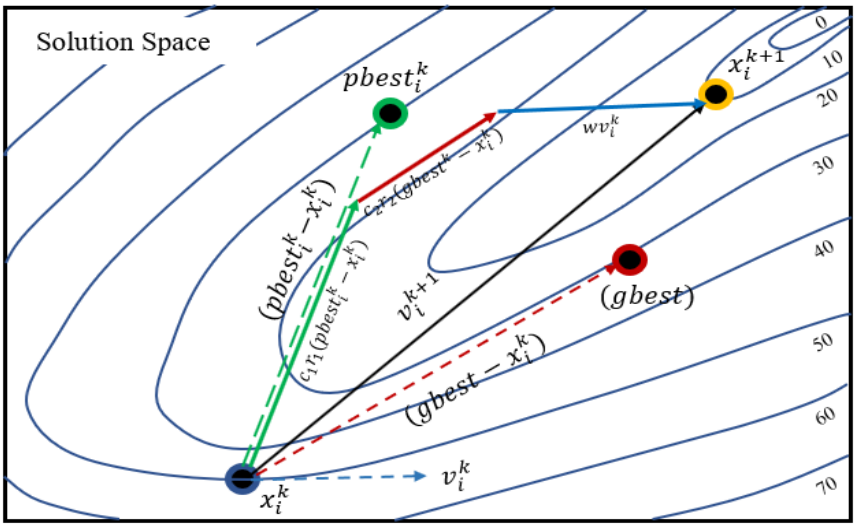

Figure 2.3:Movement of a particles of original PSO from one position to the next

The algorithm for original PSO is as follows:

1. Initialize control parameters, set fitness function $f_i(\cdot)$, population size N, Set maximum number of iterations $iter_{max}$
2. *For* each particle $i = 1$ to N
   A) Initialize particle positions $x_i^{(1)} = \left[x_1^{(1)}, x_2^{(1)}, \ldots\ldots x_N^{(1)}\right]$ randomly.
   B) Initialize particle velocities $v_i^{(1)} = \left[v_1^{(1)}, v_2^{(1)}, \ldots\ldots v_N^{(1)}\right]$ randomly.
   C) Evaluate each particle's fitness value at the particles' initial position $pbest_i^{(1)}$, $f_i(x_i^{(1)}) = \left[f_1\left(x_1^{(1)}\right), f_2\left(x_2^{(1)}\right), \ldots\ldots f_N\left(x_N^{(1)}\right)\right]$.
   D) Compare the particles fitness to select the particle with best position. Set this as global best position $gbest^1$.
3. *End For*,
4. *For* $iter = 1: iter_{max}$
5. *For* each particle $i = 1$ to N
   A. Update velocity component according to (2.2).
   B. Update particle position according to (2.1)
   C. Evaluate particle fitness.
   D. Compare particle with best fitness to global best fitness in previous iteration.
   E. *If* $f\left(pbest_i^{(iter+1)}\right)$ is better than $f((gbest)^{iter})$
   $gbest^{(iter+1)} = pbest_i^{(iter+1)}$
   Else
   End If
6. *End For*
7. *End For*
8. Return the global optimal $gbest^{(iter_{max})}$

The parameters given to the original PSO do not depend on the structure and nature of the problem being solved. This makes PSO have a good global search exploration and not converge prematurely. However, it has a major disadvantage in exploiting the local optima

as the particles are likely to have many oscillations around the optima given the random nature of the velocity component update [39]. Therefore, this research proposes a modification to the original PSO to improve its local solution exploitation while retaining its global exploitation capabilities.

2.2.3 Challenges of standard particle swarm optimization

In many versatile domains, PSO has been effectively applied to obtain solutions to a varied number of optimization problems [87]. It has been applied in fields in a wide spectrum of optimization problems ranging from medical applications, industrial, smart cities to engineering problems.

- It offers the following advantages:
- It is simple to implement.
- It has very few parameters and most of these parameters do not require tuning.
- It is capable of multi-objective and parallel computation.
- It is highly robust.
- It has higher efficiency and probability to find the global optimum solution.
- Requires less computational time.
- Can be applied to solve complex problems through its ability to build accurate mathematical models [88].

However, there are many challenges which need to be addressed. Some of the critical problems and issues with PSO include:

- The PSO algorithm does not carry out a sensitivity analysis on the problem being addressed. This makes PSO not amiable to the nature and structure of the problem [89].
- There is greater difficulty to initialize control parameters.
- It sometimes suffers from Premature convergence and trapping into the local optima especially when solving high-dimensional problems.

2.2.4 The Proposed PSO-GD Algorithm

In this research, a hybrid method combining PSO and GD is proposed to get rid of the problems associated with each individual method and to enhance the excellent qualities of each.

The method involves the use of the gradient vector of the particle towards the global best solution to not only redirect the velocity component, but also to regulate its magnitude. In this regard, (2.15) is modified to include the GD component as in (2.16).

$$\boldsymbol{v_i^{k+1}} = |\nabla f^k|\boldsymbol{v_i^k} + c_1 r_1\left(\boldsymbol{pbest_i^k} - \boldsymbol{x_i^k}\right) + c_2 r_2\left(\boldsymbol{gbest^k} - \boldsymbol{x_i^k}\right) \tag{2.16}$$

Figure 2.4 depicts how the particles are affected by the GD in the transitions between iterations.

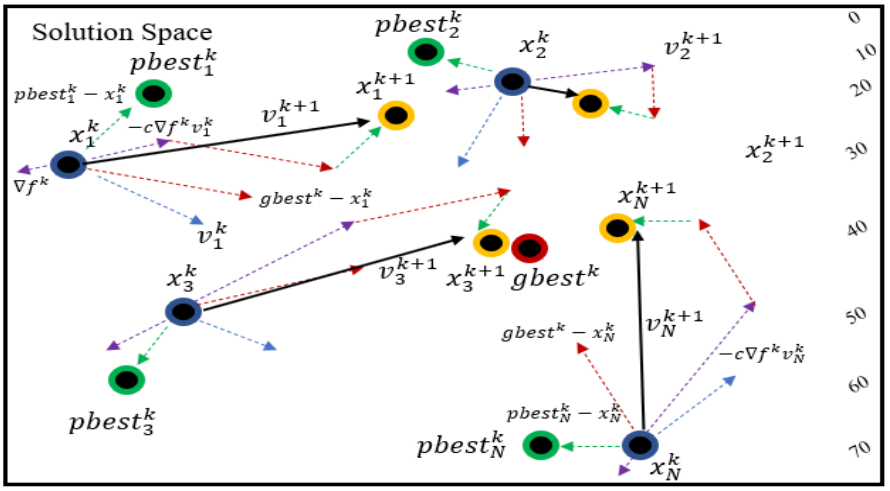

Figure 2.4:Movement of particles in PSO-GD optimization from one position to the next

As depicted in fig. 2.3, the velocity component is redirected to point in the anti-gradient component of the particle. The gradient of the particle movement is orthogonal to the tangent of the particle. Since the particle velocity is redirected and regulated by the gradient component, the particles respond to the structure of the problem. This is particularly advantageous in ensuring that particles exploit the local optimum search while retaining the global exploration capabilities as the acceleration towards the particle best position and the global best position are not altered.

Figure 2.5 shows the in-depth outlook of the movement of a single particle from one position to another in one iteration.

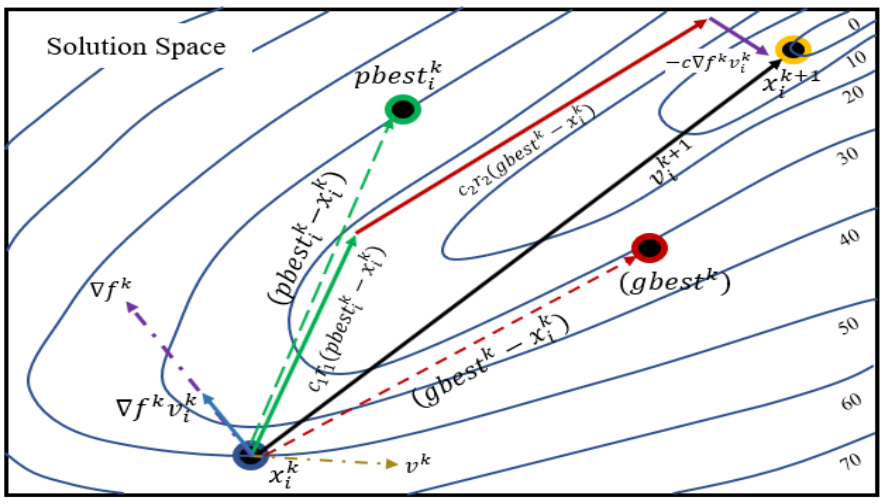

Figure 2.5:Update process of a single particle in PSO-GD optimization

It can be noted that, in the proposed method. The magnitude and direction of the velocity component is regulated and influenced by the orthogonal movement of the gradient vector

of the langrage function extracted using equations (2.4) – (2.12). This helps the proposed method to aggressively exploit the optimum points within the search perimeter.

Figure 2.6 shows the flow chart of the PSO-GD algorithm.

The PSO-GD algorithm starts with generation of random particle positions and random particle velocities. At the same time the global best solution and the iteration count are initialized.

Next, each particle's fitness is evaluated and then the particle's new velocity and position is updated using (2.16) and (2.14) respectively. The update process in (2.16) ensures the use of the gradient component of the particle to redirect and regulate the magnitude of the velocity of the particle.

Once all the particles in the population are evaluated, they are compared among themselves to select the best positioned particle according to the superiority of feasibility rules [90] and [91] as set forth in table 2.1.

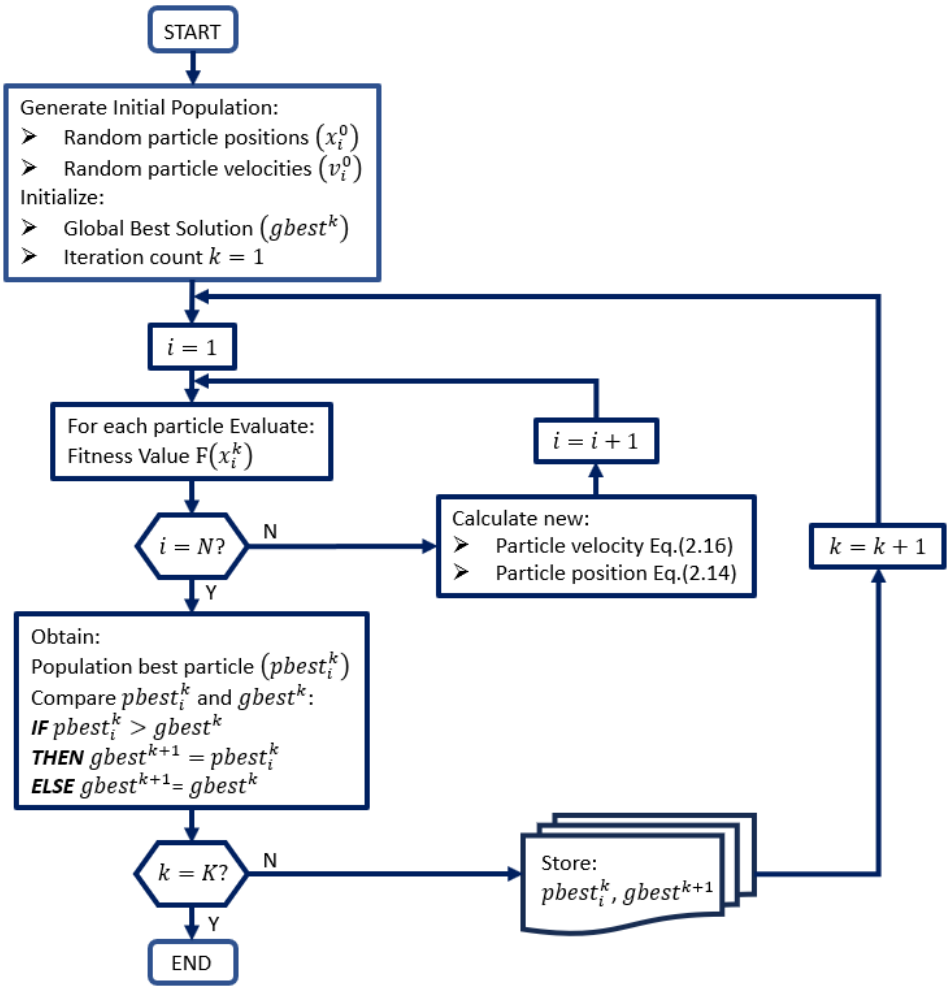

Figure 2.6: Flow chart of the PSO-GD algorithm

The second application of the gradient component of each particle is in the selection of the best particle position. Here, it is set as part of the conditions for the superiority of feasibility of the particle.

Table 2.1: Superiority of feasibility procedure for selecting personal best solution.

Algorithm 2: Selection of Personal Best Particle in population at iteration *k*
A particle is superior to another if: 1. It is feasible while the one being compared with is not. 2. Both particles are feasible, but the particle has better fitness evaluation than the one being compared to. 3. Both particles have the same feasibility and fitness value, but the particle has a lower absolute objective function gradient than the one being compared with. 4. Both particles have the same feasibility, fitness value and absolute objective function gradient, but the particle has less constraint violations than the other particle.

After the selection of the best particle in the population, a secondary comparison of the best particle and the global best particle position is made. The rules guiding the selection of the global best solution are set out in table 2.2.

Table 2.2:Superiority of feasibility procedure for selecting global best solution.

Algorithm 3: Selection of Global Best Particle at iteration *k*
A personal best particle is superior to global best particle if: 1. It is feasible and the global best is not. 2. Both particles are feasible, but the personal best particle has better fitness evaluation than the global best. 3. Both particles have the same feasibility and fitness value, but the personal best particle has a lower absolute objective function gradient. 4. Both particles have the same feasibility, fitness value and absolute objective function gradient, but the personal best particle has less constraint violations than the other. 5. The personal best solution becomes the global best solution if it satisfies 1-4. Otherwise, the global best solution is retained.

Finally, the iteration count is incremented, and the procedure repeated until a predetermined number of iterations is exhausted.

2.3 Chapter Summary

This chapter presents the conceptual framework of the proposed hybrid particle swarm and gradient descent algorithm. It gives the concepts of PSO and GD and the hybridization of the two algorithms to attain the hybrid PSO-GD algorithm.

The proposed method has the advantage of making the solution approach amiable to the structure of the problem by employing the first derivative of the optimization problem to modify the velocity vector in the standard PSO. This redirects particles to point in the direction orthogonal to that of the gradient of the objective function. This helps improve

the solution search exploitation capabilities while retaining the exploration prowess of the algorithm.

Methods for selection of personal best and global best solutions based on the superiority of feasibility of the evaluations of each particle have also been presented in this chapter.

CHAPTER THREE
PV HOSTING CAPACITY OF A DISTRIBUTION NETWORK

3. PV Hosting Capacity of a Distribution Network

3.1 PV Hosting Capacity Problem Definition

The maximum amount of PV that a Distribution Network can accommodate safely without the network operating outside of its limits on node voltages, line power flows, harmonics etc., is defined as the network's hosting capacity. This capacity depends on various factors [92]. The factors include, but are not limited to, the network layout and topology, types of loads in the network, irradiance levels, network operational limits, connection type vis-a-vie single phase or three phase etc. The PV hosting capacity may also be defined as the minimum amount of PV which causes violation of at least one technical limit [93]. Figure 3.1 depicts the PV hosting capacity defined under three different operational constraints.

As can be seen from figure 3.1, the PVHC can be defined at different values depending on

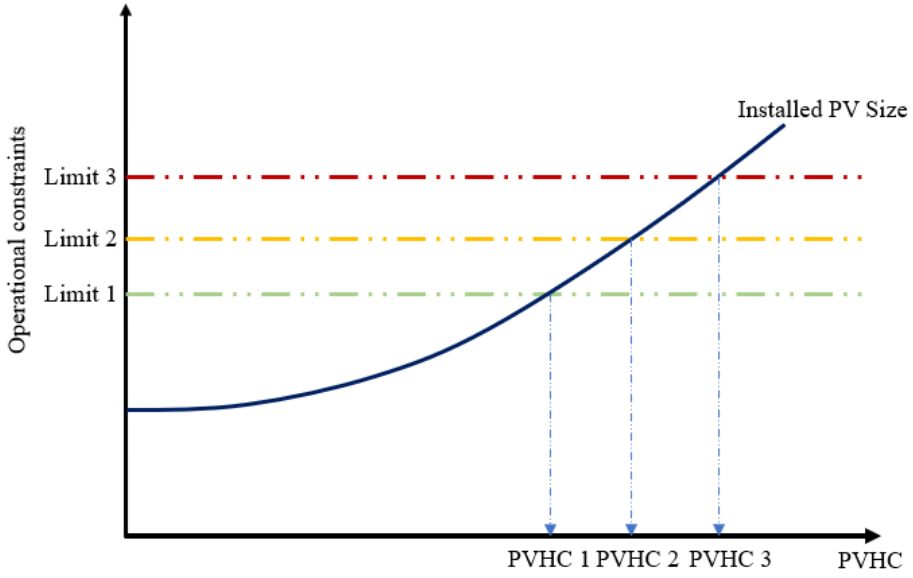

Figure 3.1:PVHC defined under different operational limits.

the level of restriction applied to the estimation process. Under constraint limit 1, the PVHC is the lowest and under constraint limit 3, the PVHC is highest. If all the constraints are considered for the estimation, therefore, the PVHC is to be taken as PVHC1. However, if relaxations are allowed on limit 1 and 2, the PVHC could be as high as PVHC3.

In most considerations, the operational constraint of great importance is the upper operating voltage limit [94], [17]. Therefore, in most deliberations in this study, the voltage limits are taken as the limiting factor for PV proliferation of the distribution network. Other factors such as line power flows play a role as well.

3.1.1 PVHC estimation formulation

The PVHC problem is formulated in many different forms with different objectives. In [28] and [29] it was formulated as an optimization problem with multiple objectives. These objectives were power loss and voltage deviation minimization. [80] formulated the

problem as a stochastic optimization problem with the objective of maintaining the voltage within a specified range for all PV penetrations.

However, the underlying principle of PVHC estimation is a PV installation maximization with two important variables of interest: PV size and location, while maintaining the operational constraints within acceptable ranges [79], [62].

In this research, the PVHC is formulated as a PV installation size maximization and PV location optimization as illustrated by equation (3.1).

$$PVHC = max\{\sum_{j=1}^{N} P_j^{pv}\} \tag{3.1}$$

Where, P_j^{pv} is the installed PV size at the j −th location in the DN and N is the total number of possible PV locations in the DN. $j \in \{1,2,3,\ldots\ldots,N\}$

Equation (3.1) is constrained by the power balance conditions laid out in (3.2) and (3.3).

$$P_n = P_n^G - P_n^L + P_n^{pv} = \sum_{m=1}^{N} V_n V_m \{G_{nm} cos(\delta_n - \delta_m) + B_{nm} sin(\delta_n - \delta_m)\} \tag{3.2}$$

$$Q_n = Q_n^G - Q_n^L + Q_n^{pv} = \sum_{m=1}^{N} V_n V_m \{G_{nm} cos(\delta_n - \delta_m) - B_{nm} sin(\delta_n - \delta_m)\} \tag{3.3}$$

Where, P_n^G , Q_n^G are conventional active and reactive power generation at bus n respectively; P_n^L , Q_n^L are conventional active and reactive load demand at bus n respectively; P_n^{pv} , Q_n^{pv} are PV output active and reactive power injection at bus n respectively; V_n, V_m are respective voltages at nodes n and m; G_{nm}, B_{nm} are the respective conductance and susceptance of line $n - m$; $\delta_n$and δ_m are the voltage angles at nodes n and m respectively.

Furthermore, the problem is constrained by generator limitations and caters for thermal limitations as outlined in equations (3.4) and (3.5).

$$P_{min}^G \leq P_n^G \leq P_{max}^G \tag{3.4}$$

$$Q_{min}^G \leq Q_n^G \leq Q_{max}^G \tag{3.5}$$

$$0 \leq P_j^{pv} \leq P_{max}^{pv} \tag{3.6}$$

$$Q_{min}^{pv,inv} \leq Q_n^{pv,inv} \leq Q_{max}^{pv,inv} \tag{3.7}$$

Where, P_{min}^G , P_{max}^G are the minimum and maximum active power generations of conventional generators respectively; Q_{min}^G, Q_{max}^G are the minimum and maximum reactive power generations of conventional generators respectively; Q_{min}^{pv}, Q_{max}^{pv} are the minimum and maximum reactive power capacity of the PV inverters.

Finally, the problem is bound by constraints on equipment and line conductor operational limits on voltages and line power flows as shown in equations (3.8) - (3.10).

$$V_n^{min} \leq V_n \leq V_n^{max} \tag{3.8}$$

$$I_{nm}^{min} \leq I_{nm} \leq I_{nm}^{max} \tag{3.9}$$

$$S_{nm}^{min} \leq S_{nm} \leq S_{nm}^{max} \tag{3.10}$$

From equations (2.17) to (2.26), it can be appreciated that the problem is a mixed integer, non-linear, non-convex programming (MINLP) problem with principal objectives of evaluating optimal PV locations and installation sizes.

The gradient of the objective function can be calculated using the derivation outlined in the following sequence of formulae.

The PVHC problem as defined in equations 3.1 can be rewritten as:

$$PVHC = \max f = \left\{\sum_{j=1}^{N} P_j^{pv}\right\} \tag{3.11}$$

Assuming the inequality constraints are not violated, the Lagrangian of the optimization problem is given by equation (3.12)

$$\mathcal{L}(\delta, V, P_{pv}, \lambda) = f(P_{pv}) - \lambda_p[P_n] - \lambda_q[Q_n] \tag{3.12}$$

The gradient of the Lagrangian function is given by equation (3.13) as follows [95] :

$$\boldsymbol{\nabla \mathcal{L}} = \left[\boldsymbol{\nabla \mathcal{L}_{\delta,V}}\ \boldsymbol{\nabla \mathcal{L}_{P_{pv}}}\ \boldsymbol{\nabla \mathcal{L}_{\lambda_p}} \boldsymbol{\nabla \mathcal{L}_{\lambda_q}}\right] \tag{3.13}$$

Where,

$$\boldsymbol{\nabla \mathcal{L}_{\delta,V}} = \left[\frac{\partial f}{\partial \delta}\ \frac{\partial f}{\partial V}\right]^T - \left[\frac{\partial P_n}{\partial \delta}\ \frac{\partial P_n}{\partial V}\right]^T [\lambda_p] - \left[\frac{\partial Q_n}{\partial \delta}\ \frac{\partial Q_n}{\partial V}\right]^T [\lambda_q] \tag{3.14}$$

$$\boldsymbol{\nabla \mathcal{L}_{P_{pv}}} = \left[\frac{\partial f}{\partial P_{pv}}\right] - \left[\frac{\partial P_n}{\partial P_{pv}}\right]^T [\lambda_p] - \left[\frac{\partial Q_n}{\partial P_{pv}}\right]^T [\lambda_q] \tag{3.15}$$

$$\boldsymbol{\nabla \mathcal{L}_{\lambda_p}} = P_n = 0 \tag{3.16}$$

$$\boldsymbol{\nabla \mathcal{L}_{\lambda_q}} = Q_n = 0 \tag{3.17}$$

Considering the KKT necessary conditions equations 3.14 and 3.15 can be rewritten as:

$$\boldsymbol{\nabla \mathcal{L}_{\delta,V}} = \begin{bmatrix} \frac{\partial f}{\partial \delta} \\ \frac{\partial f}{\partial V} \end{bmatrix} - \begin{bmatrix} \frac{\partial P_n}{\partial \delta} & \frac{\partial Q_n}{\partial \delta} \\ \frac{\partial P_n}{\partial V} & \frac{\partial Q_n}{\partial V} \end{bmatrix} \begin{bmatrix} \lambda_p \\ \lambda_q \end{bmatrix} = 0 \tag{3.18}$$

But $\begin{bmatrix} \frac{\partial P_n}{\partial \delta} & \frac{\partial Q_n}{\partial \delta} \\ \frac{\partial P_n}{\partial V} & \frac{\partial Q_n}{\partial V} \end{bmatrix} = J^T$ is the transpose of the Jacobian of the power flow equations. Therefore, equation (3.18) can be written as equation (3.19) to calculate the auxiliary variables:

$$\begin{bmatrix} \lambda_p \\ \lambda_q \end{bmatrix} = J^{-T} \begin{bmatrix} \frac{\partial f}{\partial \delta} \\ \frac{\partial f}{\partial V} \end{bmatrix} \tag{3.19}$$

Substituting equation (3.19) into equation (3.15) and applying the KKT necessary conditions yields:

$$\nabla \mathcal{L}_{P_{pv}} = \left[\frac{\partial f}{\partial P_{pv}}\right] - \begin{bmatrix} \frac{\partial P_n}{\partial P_{pv}} \\ \frac{\partial Q_n}{\partial P_{pv}} \end{bmatrix}^T \begin{bmatrix} \lambda_p \\ \lambda_q \end{bmatrix} = 0 \tag{3.20}$$

The gradient of the objective function is thus obtained using equation (3.20) as:

$$[\nabla f] = \begin{bmatrix} \frac{\partial P_n}{\partial P_{pv}} \\ \frac{\partial Q_n}{\partial P_{pv}} \end{bmatrix}^T \begin{bmatrix} \lambda_p \\ \lambda_q \end{bmatrix} \tag{3.21}$$

3.1.2 Solution Approach: Estimation of PVHC by PSO-GD

In this research, the proposed approach is to solve the PVHC problem described by equations (3.1) – (3.10) using the proposed PSO-GD algorithm presented in section 2.2.3.

The summary of the procedure for estimating the PVHC of the DN is described as follows:

1. All parameters are initialized. The objective function is set to equation (3.1) and the global best solution for fitness is set to zero (the worst possible sum of PV sizes).
2. Random PV sizes at all the nodes in the DN are generated as:

$$\begin{bmatrix} PV_1^{(0)} \\ PV_2^{(0)} \\ \vdots \\ PV_m^{(0)} \end{bmatrix} = \begin{bmatrix} P_{1,1}^{pv(0)} & P_{2,1}^{pv(0)} & \cdots & P_{j,1}^{pv(0)} \\ P_{1,2}^{pv(0)} & P_{2,2}^{pv(0)} & \cdots & P_{j,2}^{pv(0)} \\ \vdots & \vdots & \cdots & \vdots \\ P_{1,m}^{pv(0)} & P_{2,m}^{pv(0)} & \cdots & P_{j,m}^{pv(0)} \end{bmatrix} \tag{3.22}$$

   Where m is the total number of PV particles for the PSO-GD population.
3. A DLF analysis is run for each PV size to determine whether the variables used for ascertaining the equality and inequality constraints are in violation status. The objective value of each PV size is evaluated using equations (3.1) and (3.23).

$$\begin{bmatrix} f(PV_1^{(0)}) \\ f(PV_2^{(0)}) \\ \vdots \\ f(PV_m^{(0)}) \end{bmatrix} = \begin{bmatrix} P_{1,1}^{pv(0)} + P_{2,1}^{pv(0)} + \cdots + P_{j,1}^{pv(0)} \\ P_{1,2}^{pv(0)} + P_{2,2}^{pv(0)} + \cdots + P_{j,2}^{pv(0)} \\ \vdots \\ P_{1,m}^{pv(0)} + P_{2,m}^{pv(0)} + \cdots + P_{j,m}^{pv(0)} \end{bmatrix} \tag{3.23}$$

   Fitness of each PV distribution is then then evaluated by subtracting a penalty for constraint violation from the objective value. i.e.,

$$Fitness_m = \begin{bmatrix} f(PV_1^{(0)}) \\ f(PV_2^{(0)}) \\ \vdots \\ f(PV_m^{(0)}) \end{bmatrix} - \sum_{j=1}^{N_c} \mu_j \times C_{v,j} \times \begin{bmatrix} h_j(PV_1^{(0)}) \\ h_j(PV_2^{(0)}) \\ \vdots \\ h_j(PV_m^{(0)}) \end{bmatrix} \quad (3.24)$$

Where N_c is the total number of constraints under consideration; $C_{v,j}$ is the penalty factor for violation of j −th constraint.

4. The gradient of each PV penetration scenario is evaluated using equations in (3.12) to (3.21).
5. Using the rules in tables 2.1 and 2.2, the population best solution and the global best solutions are obtained and recorded.
6. The iteration count is incremented and the PV sizes at each node are updated using equations (2.14) and (2.16)
7. Procedure 3-6 is repeated until a preset iteration count is exhausted.

3.2 Case studies

The efficacy, validity and robustness of the PSO-GD algorithm was tested on the IEEE 33-bus test DN, IEEE 69-bus test DN and the existing 136 bus radial distribution network (RDN) to determine the optimal PV locations and sizes which can be installed into these networks, and to validate the stability of the algorithm.

The proposed algorithm was implemented in the MATLAB environment and simulations were conducted on a PC with a 64-bit dual core™ i9-9900K CPU @ 3.6 GHz processor and 64.00 GB RAM. For comparison, IMOEHO, QOTLBO, PSO-GA, and CTLBO were also modeled on the same platform. The results are as presented in the graphs and tables in the proceeding sections.

3.2.1 Case I: Estimation of PVHC of IEEE 33 test bus DN

The technical specifications (including the topology and line parameters) of the IEEE 33-bus RDN are given in [96]. This network has a 5000 kVA, 12.66 kV substation with a total active load of 3715 kW and a lagging reactive power demand of 1800 kVAr. It has 33 nodes

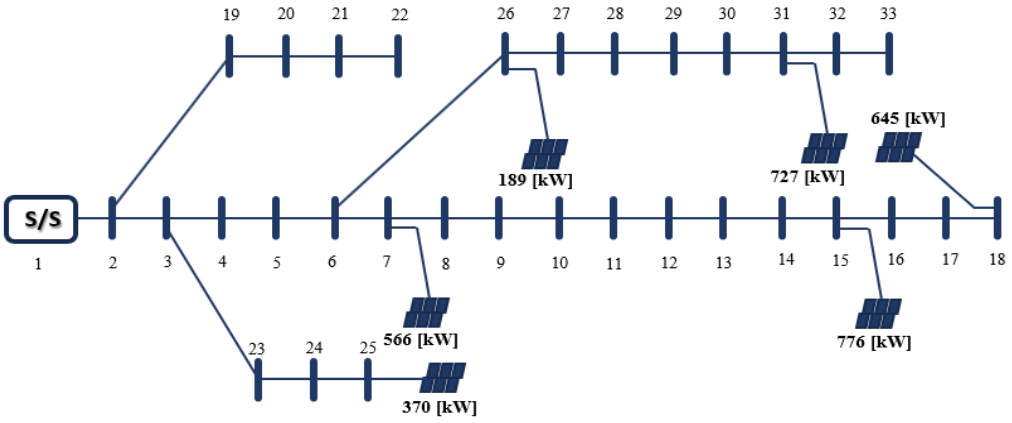

Figure 3.2: IEEE 33 bus test network with optimal locations and PV sizes.

with 32 branches. Figure 3.2 shows the configuration of the IEEE 33 bus test distribution network. It also shows the optimal locations (nodes) and sizes of installed PV evaluated using PSO-GD algorithm.

The network PVHC was simulated using the proposed PSO-GD method with all the point loads fixed at their average values (without consideration of uncertainty in PV output nor load variations). The largest size of PV is along the lateral line 1-18 at node (location) 15. The estimated size at this node is 776 kW. The second largest estimate is 727 kW at node 31. Subsequent sizes and respective nodes are 645 kW at node 18, 566 kW at node 7, 370 kW at node 25 and 189 kW at node 26.

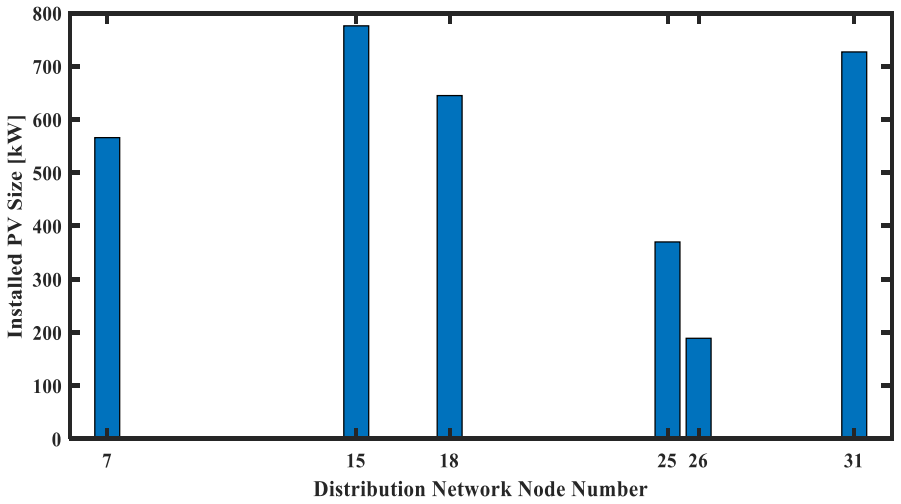

Figure 3.3: Optimal PV locations and sizes for IEEE 33 bus test DN

Figure 3.3 shows a bar graph of the optimal PV sizes estimated using the PSO-GD algorithm at respective optimal locations. The sizes range from as low as 189 kW at node 26 to as high as 776 kW at node 15. Figure 3.4 shows that the voltage profiles obtained when PV installed has node voltages ranging between 0.96 [pu] at node 33 and 1.05 [pu] at nodes 18 and 23 while the profile obtained without PV installation has an upper value of 1.00 [pu] and a lower value around 0.92 [pu]. This means that the voltages generally increase across the network when there is PV integration. It is observed that nodes with PV installed experience high voltage gains compared with those without PV installations.

However, the voltages are maintained within the acceptable range ($0.95pu \leq V \leq 1.05pu$). Therefore, no voltage violations are observed in this case, but some node voltages lie on the boundary of operating limit.

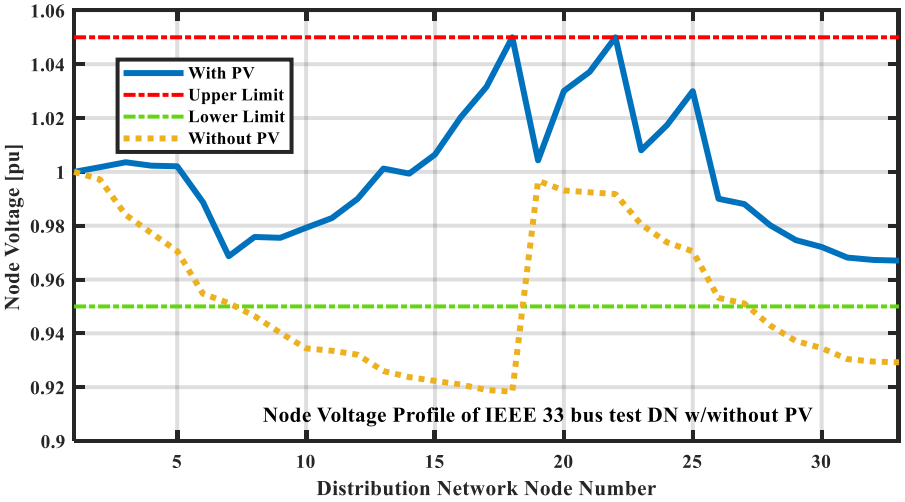

Figure 3.4: Voltage profiles obtained with/without PV installations in IEEE 33 bus test DN.

Figure 3.5 shows the line current flows, line active power flows and the line reactive power flows with and without installing PV at the determined locations respectively. The numerical results are also given in appendix I-A and appendix I-B respectively.

It can be observed that without PV installation all current, active power and reactive power flows in a positive direction (in this case from the distribution substation to the network nodes). This is strongly because there is only one source of power, and the network is configured in a radial topology. The highest power flow occurs from the substation to the adjacent node. In subsequent interconnecting branches downstream, the power flow magnitude reduces until end node 18 in the first radial line. This trend is also observed in radial lines starting 2-22, 3-25 and 6-33. No 'reverse power' flows are observed.

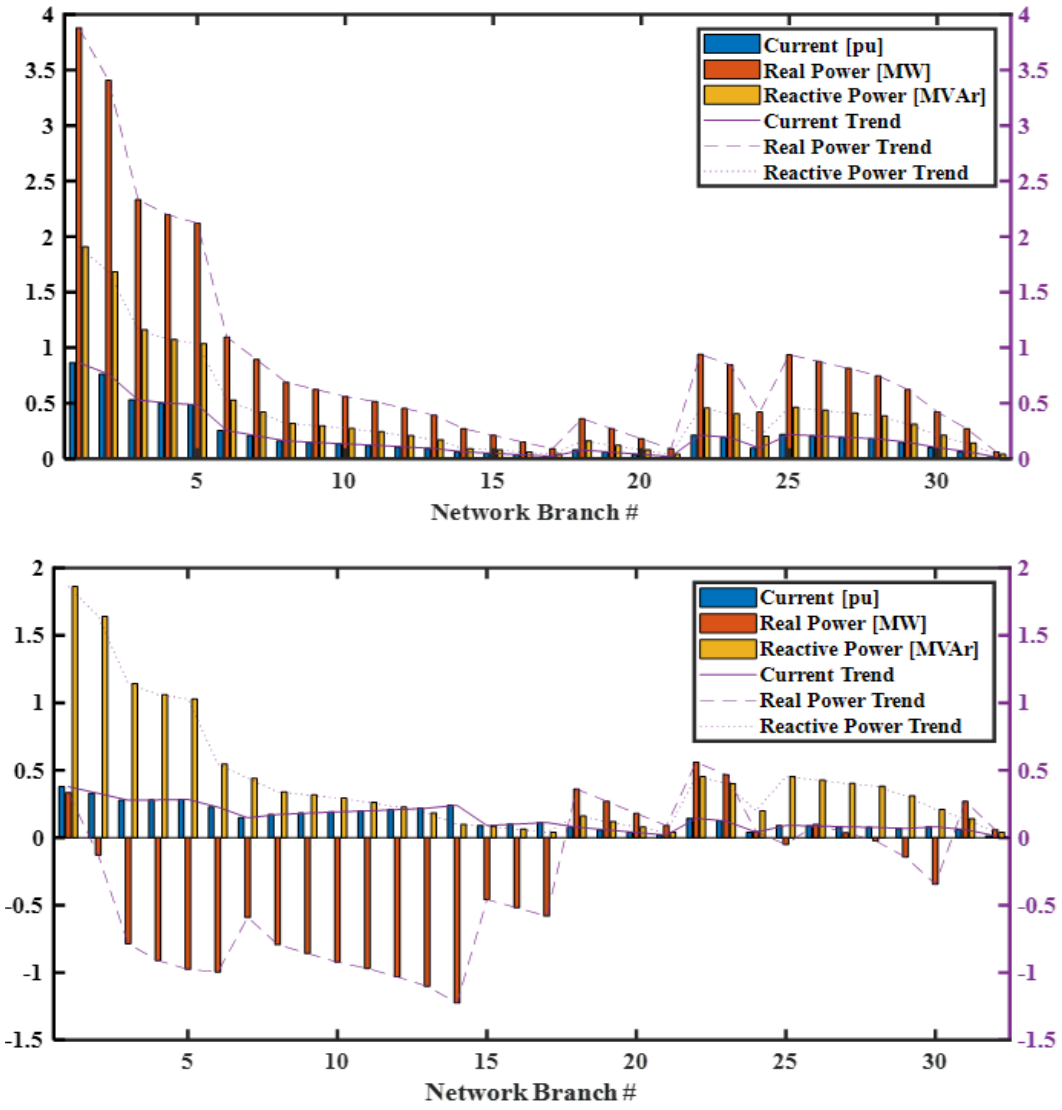

Figure 3.5: Line current, actine power, reactive power w/without PV installation

In the case with PV installed, however, the power flow from the substation reduces substantially from 3. 879 MW to 0.335 MW. This reduction is echoed through the other

branches with only a few exceptions. In both cases the active power is maintained within the required bounds ($-1pu \leq P_{ij} \leq 1pu$).

In terms of reactive power, the line flows remain substantially unaffected by this change in all branches and are also maintained in the required bounds. This is testament to the fact that the PV inverters are only injecting pure active power. There is no burden of voltage control placed upon the inverter for this section. Therefore, the PV inverters do not attempt to inject or absorb reactive power into or from the PCC respectively. Line current flows only change slightly at the substation (node 1) where the current drops from around 0.85 pu in the case without PV installed to about 0.4 pu in the case with PV installed. This is mainly attributed to the local generation being able to supply the local loads at nodes where PV is installed.

Furthermore, we observe reverse power flows in certain branches. These reverse power flows are occurring in regions located near PV installation sites. Because the power being generated is greater than the local demand in almost all cases, the excess power is being transferred to other areas from the PV hosting nodes resulting in reverse power flows. As alluded to earlier in chapter one, this may be problematic if the protection system were not properly set up.

Overall, the estimated values of PV installed by PSO-GD do not result in constraint violations when applied to the IEEE 33 bus distribution network. Only reverse line power flows are observed. However, even the line reverse power flows are within acceptable limits thus no line congestion is experienced.

3.2.2 Performance of PSO-GD against other methods

The PSO-GD algorithm's performance was compared with the performance of other deterministic methods which have been employed to estimate the PVHC of radial distribution networks. These methods include variations of PSO with GA (PSO-GA), IMOEHO, CTLBO and QOTLBO.

Table 3.1 shows the results obtained for estimated PVHC using the proposed PSO-GD compared with other meta-heuristic based methods.

Table 3. 1:Optimal locations for PV installation and estimated PVHC for different methods

Method	PV locations	Hosting Capacity [kW]
CTLBO	13, 25, 30	2951.1
PSO-GA	11, 16, 32	2991.0
QOTLBO	12, 24, 29	3014.2
IMOEHO	7,14, 25,31	3176.0
PSO-GD	7,18, 22, 25, 26, 31	3461.9

From table 3.1, PSO-GD finds more PV installation locations (six optimal PV installation sites) because of its superior optima exploitation and diversely intense global search exploration.

Subsequently, the PVHC of the IEEE 33 bus test DN estimated by PSO-GD is much higher at 3461.9 kW than that obtained using other approaches. Compared with IMOEHO whose estimate is 3176.0 kW in 4 locations, the PSO-GD approach provides an estimate that is 8.26% greater. Similarly, the QOTLBO estimates PVHC at 3014.2 kW which stands at 12.93% lower than PSO-GD. Worse still, PSO-GA and CTLBO provide even smaller PVHC estimates at 2991.0 kW and 2951.1 kW respectively representing around 13.60% and 14.75% adrift of the PSO-GD PVHC estimate.

Clearly, PSO-GD algorithm has a superior calculation depth compared to the other meta-heuristic approaches. The convergence plots for each of the approaches are shown in figure 3.6.

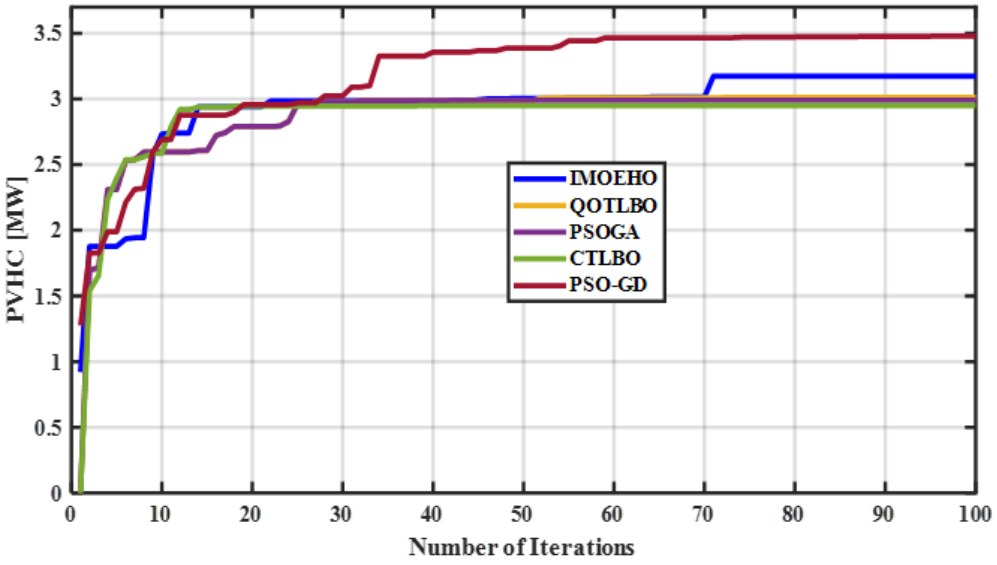

Figure 3.6: PVHC convergence plots obtained for IEEE 33 bus for different methods.

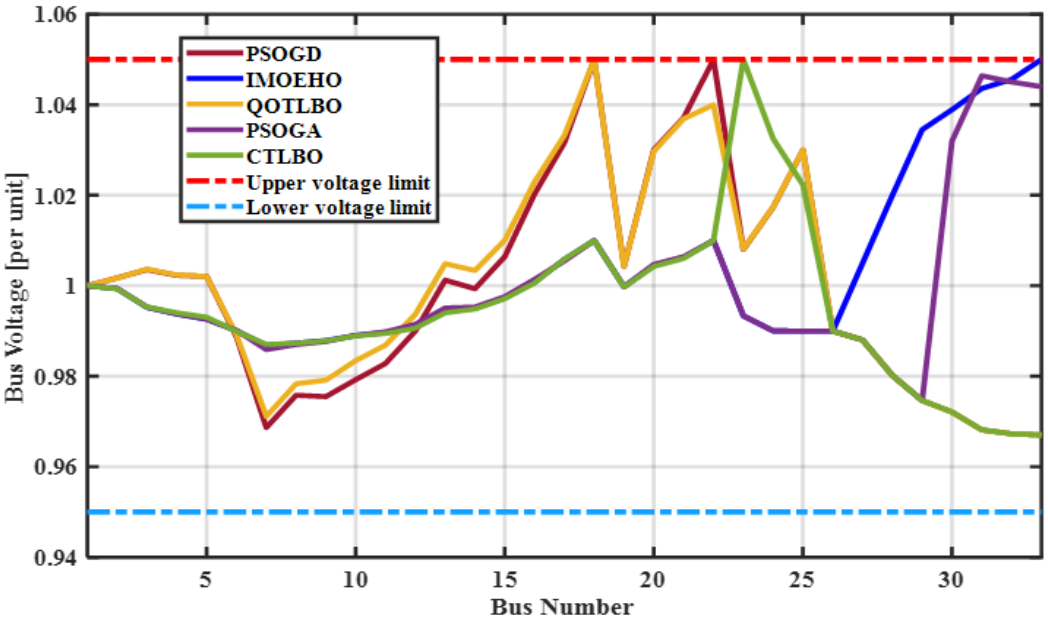

Figure 3.7: voltage profiles obtained using different PVHC estimation methods.

It can be observed that compared with PSO-GD, the other methods, except for IMOEHO, converge very quickly and, perhaps, prematurely. This is the reason why their objective evaluations at the final iteration are much lower than the PSO-GD evaluation. Consequently, their estimations of PVHC fall very short of the PSO-GD estimation as alluded to earlier.

Figure 3.7 shows the network voltage profiles obtained by using respective approaches mentioned above. It is observed that the voltages for all methods lie within the acceptable lower and upper voltage boundaries. As the network is maximized for PV injection, the node voltages observed all reach the periphery of the upper voltage boundary but are way above the lower voltage limit. Thus, it should be appreciated that in all the approaches applied, a maximum amount of PV is injected above which voltage constraint violations would become apparent.

3.2.3 Case II: Estimation of PVHC of IEEE 69 bus test DN

A similar study to the one conducted on the IEEE 33 bus test DN was carried out on the IEEE 69 bus test DN. Technical details of the IEEE 69 bus network are found in [30], [97].

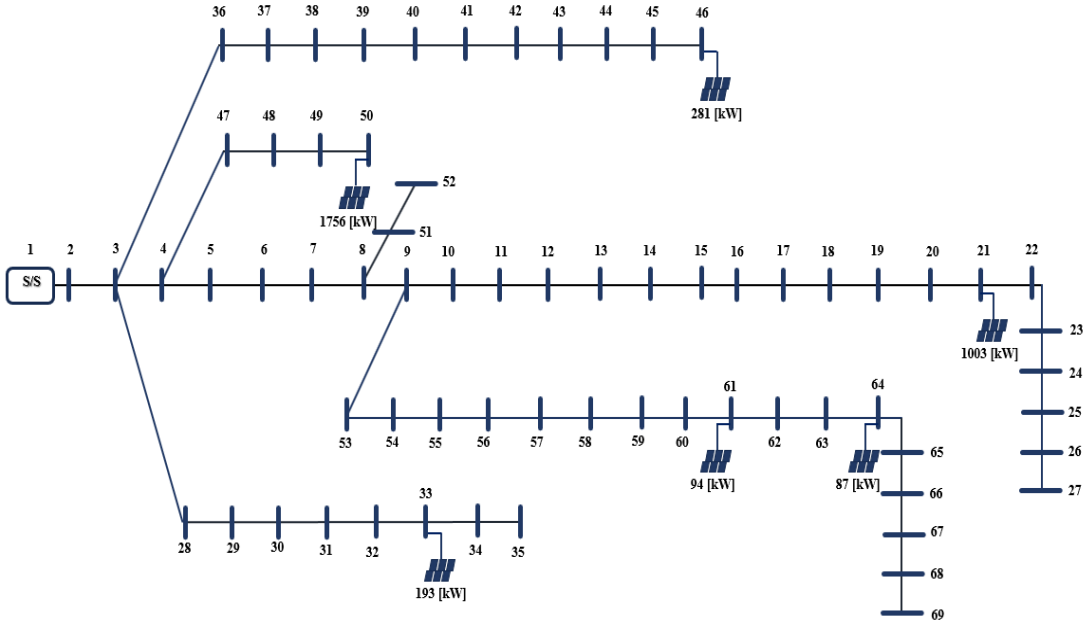

Figure 3.8: Configuration of the IEEE 69 bus test DN with optimal PV locations

Figure 3.8 shows the topology of the network with the optimal locations and sizes of PV. There are six optimal locations (nodes) determined for this case. Node 50 has the largest PV installation size of 1756kW followed by node 21 with 1003 kW. The other nodes contribute significantly lower sizes with node 46 having 281 kW, 33 with 193kW and 61 and 64 contributing a miserly 94kW and 87kW respectively.

Figure 3.9 shows a comparison of the current, active, and reactive power flows with the PV installed and without PV installations.

In the IEEE 69 bus test DN, it is observed, as in the case of the IEEE 33 bus network, that with no PV installation all the power flows in the direction from the source to the load vis-a-vie, no reverse power flows. Similarly, the voltages, line active and reactive power flows also line within acceptable margins as defined for the network. However, with PV installation, there are reverse power flows in some branches albeit within acceptable margins.

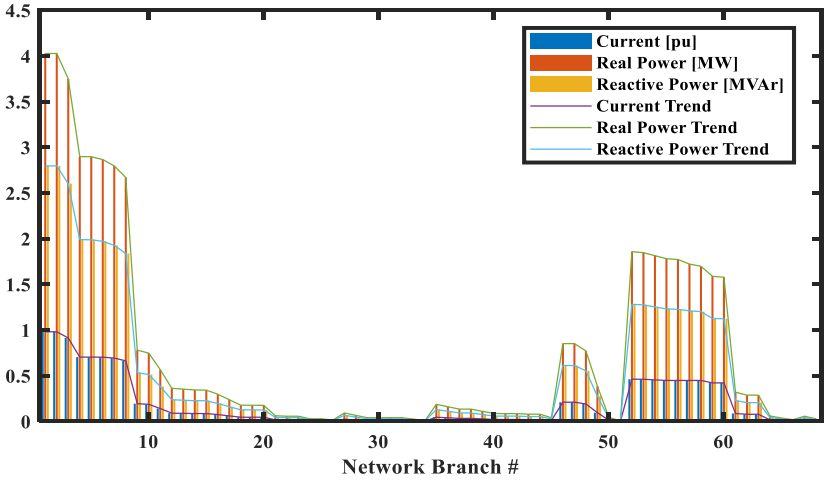

(a) Line current, active power and reactive power for IEEE 69 bus without PV

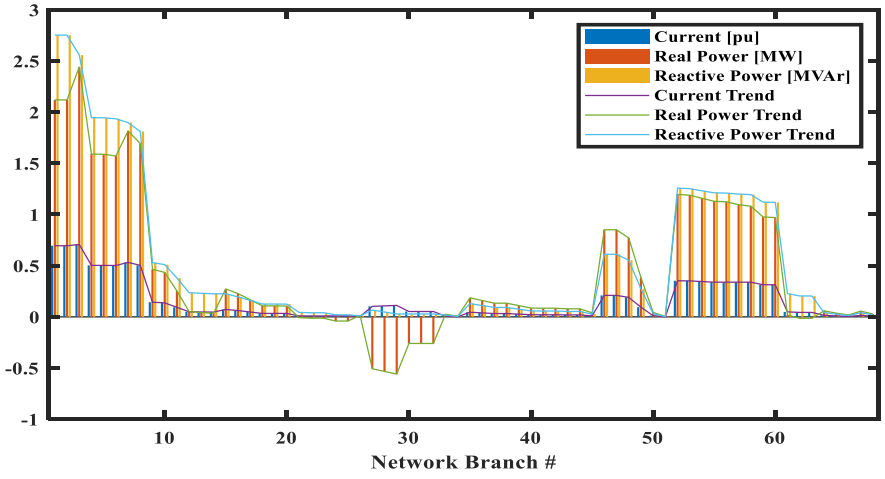

(b) Line current, active power and reactive power for IEEE 69 bus with installed PV

Figure 3.9: Line current, actine power, reactive power w/without PV installation

The line current and active/reactive power flows between bus 20 and bus 45 is very minimal in the case without installed PV. Huge currents and power flows from the substation of the DN. In the case with PV installed, a significant reverse active power flow is observed. This power emanates from the excess PV generation in the installed PV plants at node 21.

Figure 3.10 shows a comparison of the results obtained when PSO-GD is used against the results obtained when other methods are employed. As can be seen, PSO-GD produces a superior result compared to the other methods.

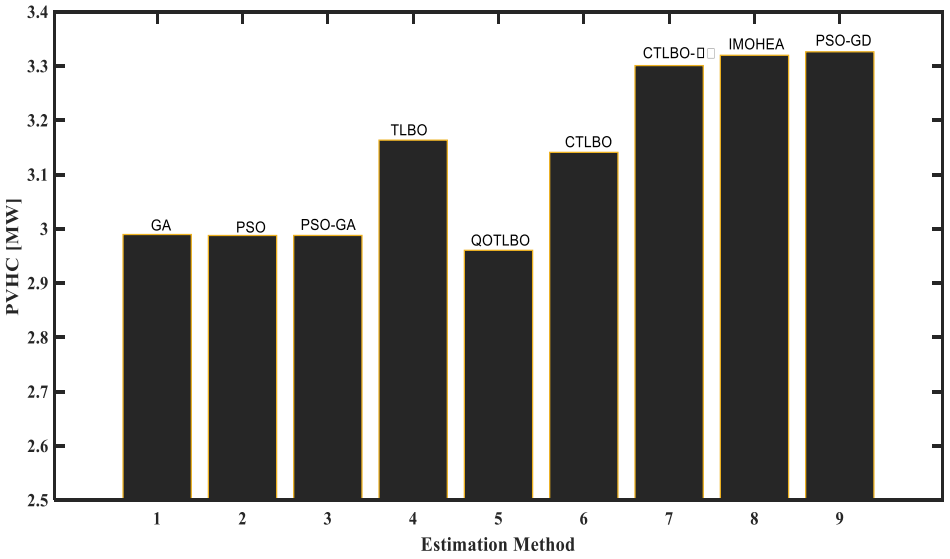

Figure 3.10: Comparison of PVHC estimates obtained for IEEE 69 bus test DN

It can be appreciated that PSO-GD outperforms most of the methods outlined in figure 3.10. IMOEHA has nearly the same performance in terms of the final solutions but needs a lot of parameters tuning which is very difficult to achieve. The other variant of PSO, the PSO-GA, is way too inferior to the proposed algorithm as it generates a solution which is about 11% lower than that estimated by the proposed PSO-GD algorithm.

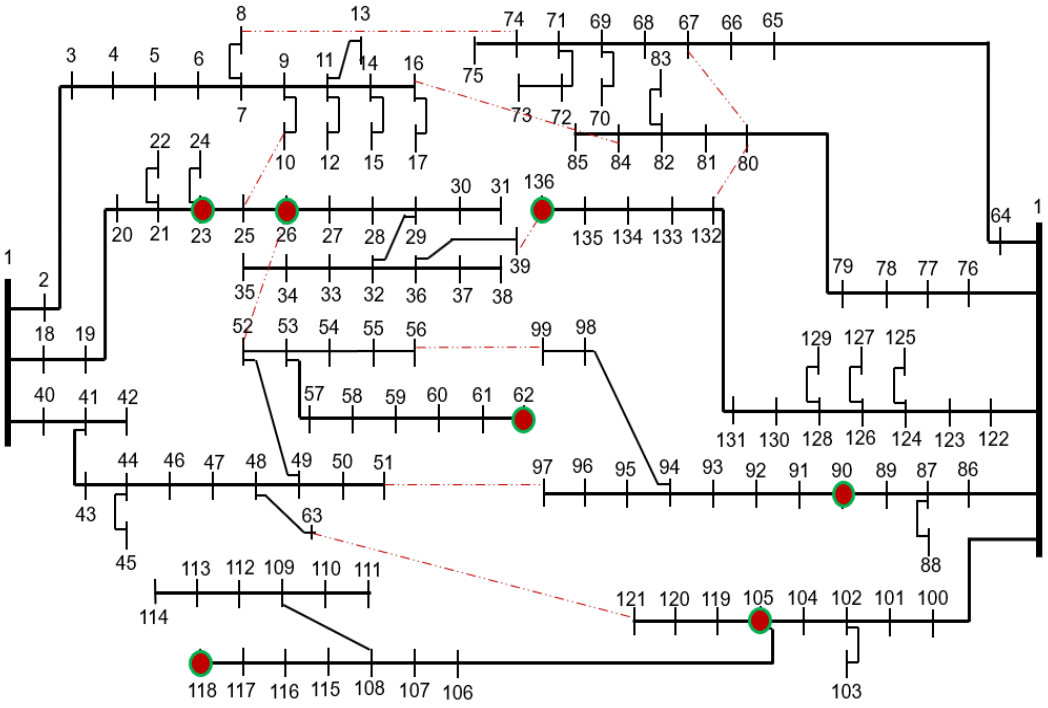

Figure 3.11: Configuration of existing 136 DN in Sao Paulo, Brazil.

3.2.4 Case III: Existing Brazilian 136 bus DN

The technical details of the 136 bus DN are published in [98] and [99]. The network configuration together with its optimal locations of PV plants as determined using PSO-GD are shown in figure 3.11.

There are seven locations identified as the optimal locations of the PV plants. These include nodes 23, with PV size 923.5 kW, 26 with 145.5 KW, 90 with 3500 KW, 105 with 138kW, and 118 with 3409.5 kW. The total installed PV size is thus 8116 kW representing about 48% of the total power demand of the network.

The situation with the Brazilian 136 bus network is slightly different. Reverse line power flows are in both the case with PV and the case without PV installation. This is because the network is configured in a 'ring', rather than radial as is the case with the IEEE-33 and IEEE-69 bus test systems using section interconnectors. Thus, power can flow in either direction.

It is worth noting that while the active power demand for the IEEE-33 and IEEE-69 from the substation drops significantly by about 91.37% and when PV is installed, it completely vanishes in the existing 136 bus DN. Figure 3.12 shows the voltage profiles, line current, branch active and reactive power flows for both networks.

However, the important inference here is that, in all the examined cases the power contribution from the source significantly reduces. The reduction occurring during periods of high solar (irradiation) could help the distribution network operator to minimize the net demand from the main power grid, save costs or move the network towards self-sufficiency.

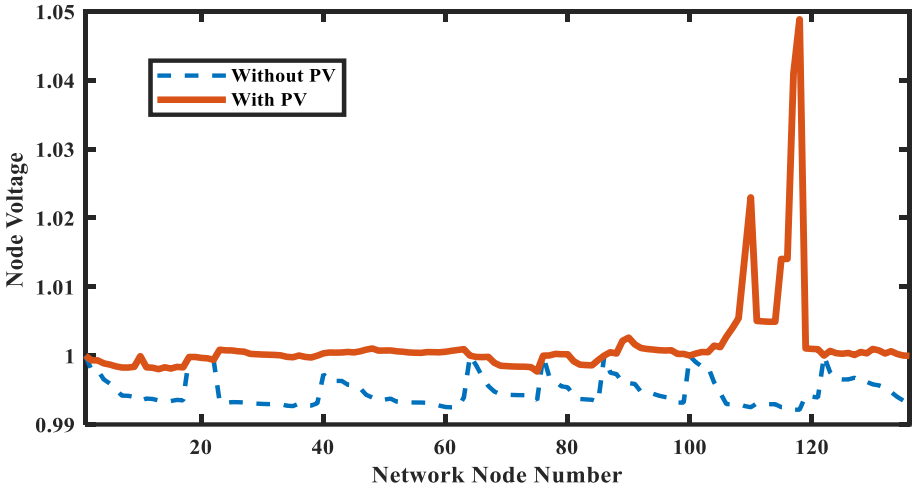

(a) Voltage profile of the 136-bus w/without PV installation

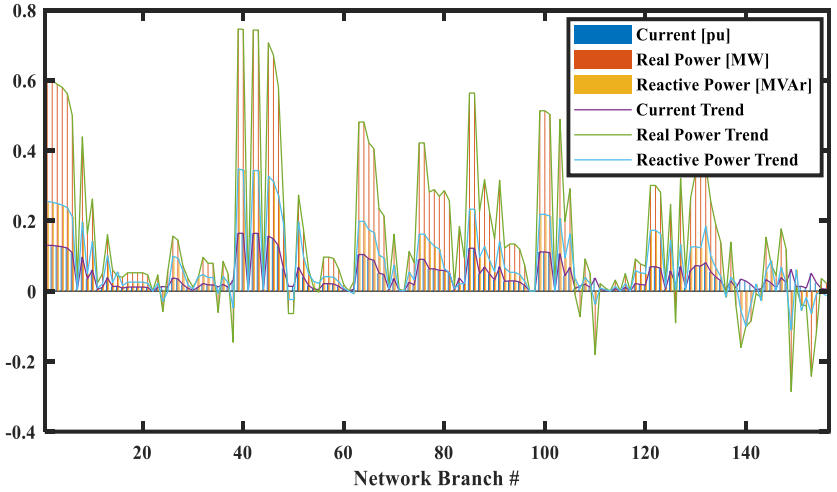

(b) Line flows for the 136-bus without PV installation

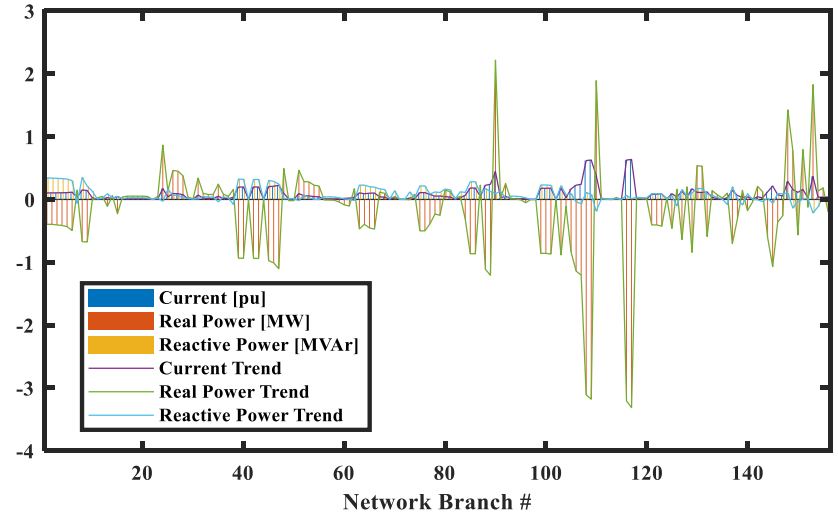

(c) Line flows for the 136-bus with PV installation

Figure 3.12: 136-bus voltage profile and line flows with/without PV installations

3.2.5 Case IV Comparison of Proposed PSO-GD and Original PSO

To compare the efficacy of the proposed method against the original PSO approach, the proposed PSO-GD algorithm results of the PVHC estimation for IEEE-33 bus test DN and the IEEE-69 bus test DN were compared.

Figure 3.13 shows the variation of the objective values obtained in respective cases. For the IEEE- 33 bus test DN the iterations for the simulation were 100 while the iterations for IEEE-69 bus were 150. The difference was because in the IEEE-33 bus convergence was reached earlier than in the IEEE-69 bus network.

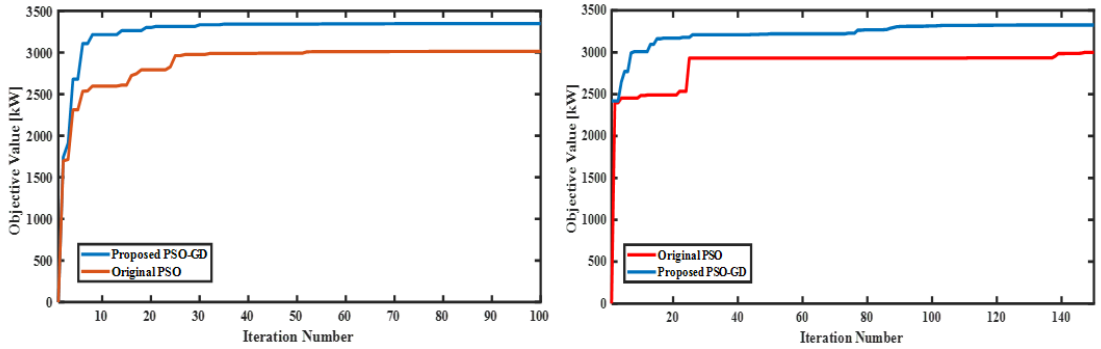

(a) IEEE-33 bus test DN (b) IEEE-69 bus test DN

Figure 3.13: Comparison of convergence plots of original PSO against proposed PSO-GD

In both cases, the objective evaluations obtained using the proposed method are comparatively higher than those obtained using the original PSO approach. By running the two algorithms several times on the same test DNs, the results obtained are tabulated in table 3.2.

Table 3. 2: Comparison of results obtained using original PSO and PSO-GD

Method	Test System	IEEE - 33	IEEE - 69
Original PSO	Lowest PVHC [kW]	3014	2971
	Highest PVHC [kW]	3162	3004
Proposed PSO-GD	Low PVHC [kW]	3429	3317
	Highest PVHC [kW]	3461	3326

In both the IEEE – 33 and IEEE – 69 test DNs, the proposed method gives greater PVHC values. For the lowest values, the proposed method gives a 13.77% better result compared with original PSO on the IEEE – 33 bus test DN. Similar results are obtained for others.

The differences in estimates for the proposed PSO-GD between the lowest and highest values for the 2 test systems are 32 kW and 9 kW. These are comparatively much lower than for original PSO which are 148 kW and 33 kW respectively. Therefore, the proposed method manifests a better retainability of the estimated solution than the original PSO.

3.3 Stability Analysis of PSO-GD

One of the most important aspects of an optimizer is its computation stability. Stability refers to the optimizer's ability to generate the same solution for the same problem, starting from different initial values [100]. There are several stability analyses and definitions for different meta-heuristics.

Authors of [101] contend that to ensure convergence, it is not enough to simply apply the order-1 stability defined by equation (3.25) to obtain the stability operating region but, there is a need to also calculate the order-2 stability.

$$\lim_{t\to\infty} \boldsymbol{E}[\boldsymbol{x}(\boldsymbol{t})] = \boldsymbol{y} \tag{3.25}$$

Where $\boldsymbol{E}[\boldsymbol{x}]$ is the expectation of a random variable $\boldsymbol{x}$ which results in order-1 stability. Order-2 stability condition aims to reduce the standard deviation or the variance. It is given in equation (3.26).

$$\lim_{t\to\infty} \boldsymbol{E}[\boldsymbol{x}(\boldsymbol{t}) - \boldsymbol{y}]^2 = 0 \tag{3.26}$$

To validate the stability of the proposed PSO-GD algorithm for both order-1 and order-2 stability, it was tested for stability by applying PSO-GD on the IEEE 33 and 69 test RDN. Several simulations were run on the networks to ascertain the algorithm's robustness in retaining the same output starting from different initial values.

A 100-iteration simulation was run and repeated 25 times, starting from random positions for each simulation, to ascertain the stability and robustness of the algorithm. Figure 3.14 shows the values of PVHC obtained for respective networks.

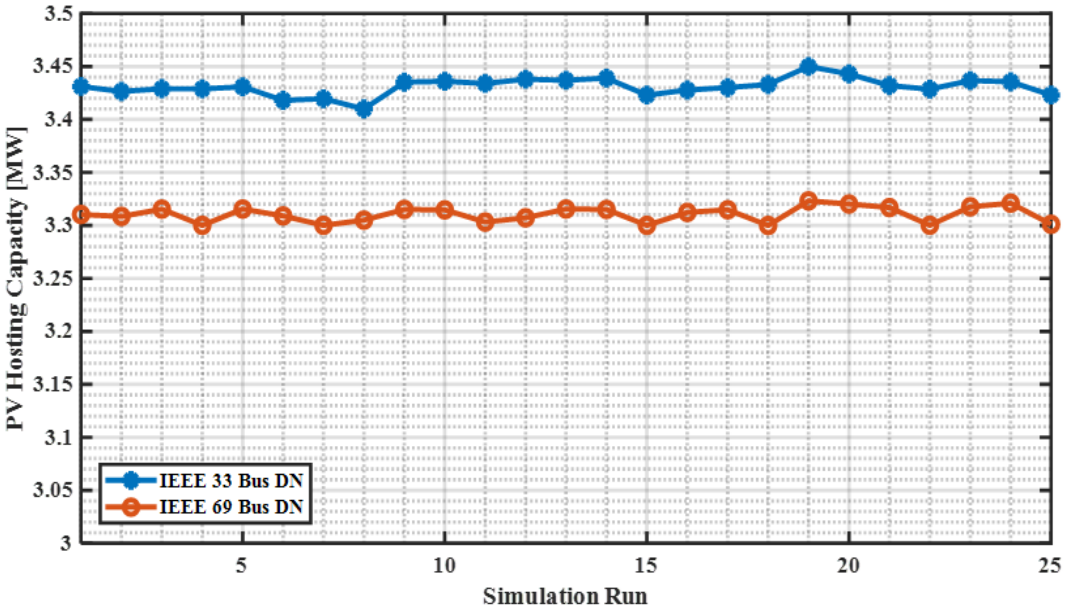

Figure 3.14: PVHC values of IEEE-33 bus, and IEEE-69 bus test DNs for stability analysis.

Similarly, 25 runs of 100-iteration PSO-GD for estimating the PVHC of the IEEE 33-bus test network was simulated. It was observed that the fitness plots converged to nearly the same point at the 100th iteration in both cases. Figure 3.13 shows the final values obtained at the end of each run for both the IEEE 33-bus and IEEE 69-bus test DNs. For the IEEE 33-bus test DN, the mean value of PVHC estimated from the 25 runs was around 3.431 MW with a standard deviation of 0.0084 MW. Similarly, the respective values from the simulations on IEEE 69-bus test DN were 3.3105 MW and 0.0075 MW.

The mean μ_{PVHC} and standard deviation σ_{PVHC} of the observed final PVHC for each of the 25 iterations performed on IEEE 33 and 69 DNs are summarized in table 3.3.

Table 3. 3: Mean and Standard deviation in PV HC estimated by PSO-GD over 25 simulations.

Test case	μ_{PVHC} [MW]	σ_{PVHC} [MW]
IEEE-33 bus	3.4310	0.0084
IEEE-69 bus	3.3105	0.0075

With the standard deviations being 0.245% and 0.226% of the mean PVHC estimates for IEEE-33 and IEEE-69 bus test DN respectively, the estimated values for each simulation only vary insignificantly. This means that the calculated values lie in high-end precision level and, consequently, the PSO-GD algorithm is order-1 and order-2 stable.

3.4 Chapter Summary

In this chapter, the PV hosting capacity of the distribution network has been defined. The problem structure has been given and a formulation for a deterministic approach has been carefully and comprehensively described. The PVHC problem was presented as a mixed integer nonlinear programming (MINLP) problem whose objective is to maximize the amount of PV size which can be installed in the DN without violating the network set limits on the node voltages, line current and power flows, acceptable reverse power flow levels etc.

The chapter showcased the use of the proposed PSO-GD in estimating the PVHC of distribution network networks through its applications on standard IEEE test systems such as the IEEE 33 bus test DN and the IEEE 69 test DN. The application of PSO-GD for PVHC estimation was also extended to the existing 136 bus network in Sao Paulo, Brazil.

The stability of the proposed network was also presented in this chapter by considering the order-1 and order-2 stability criteria for meta-heuristics.

The performance of the proposed PSO-GD method in estimating the PVHC of electrical power distribution systems was compared to other methods found in literature. The results showed that the PSO-GD is superior to other methods found in literature because not only was the result for PVHC better, but the proposed method also produced more locations for PV installation sites compared to the counterpart methods.

Finally, the results also indicated that the proposed PSO-GD method is order-1 and order-2 stable when calculating the PVHC of a distribution system.

CHAPTER FOUR
PVHC ENHANCEMENT USING INVERTER VOLT-VAR CONTROL

4. PVHC Enhancement using PV Inverter Volt-Var Control

The past few decades have seen a high proliferation of PVs in power distribution networks [102]. Part of this drive has mainly been because of the need to reduce the dependence on fossil fuels for electrical power generation and, in turn, reduce carbon emissions. However, as alluded to earlier, the amount of PV installed in the network is heavily constrained by the risk of over-voltages.

To negate this voltage security challenge, transformer tap changers and reactive power compensation techniques are employed. Transformer tap changers, in a limited capacity, can help regulate the voltage within a certain feasible range. Reactive power compensation seeks to inject reactive into or absorb from the system nodes when the voltage is low or high respectively. This helps regulate the voltage through a wide range.

In this chapter, inverter voltage control using reactive power compensation is highlighted as one of the means for achieving greater PVHC sizes in distribution networks. The chapter proposes a method of utilizing three distinct inverter characteristics for over-voltage control, under-voltage control, and dead-band action phases.

4.1 Proposed Reactive Power Compensation technique.

The most significant issue emanating from the injection of PV power for distribution networks is over and under voltage problems. This is because there is a high probability of over-voltages at light loads and high PV injection, and a likelihood of under-voltages at heavy loads and low PV injection at the point of common coupling (PCC). Therefore, implementation of the inverter voltage support function to the PV system has the potential of hosting capacity improvement [103].

Authors [38] contend that the volt/var function of the PV inverter is designed so that the voltage deviation can be compensated by means of reactive power compensation technique. Considering the negative sensitivity nature between voltage and reactive power, reactive power injection by inverter is typically defined as equation (4.1) and the guidelines of IEEE 1547 Standard for interconnection and interoperability of Distributed Energy Resources with Associated Electric Power Systems Interfaces [104].

$$Q_i = \begin{cases} Q_{max,i}, & V_i < V_{min} \\ -\alpha_i(V_i - V_{d1}), & V_{min} \le V_i \le V_{d1} \\ 0, & V_{d1} \le V_i \le V_{d2} \\ -\alpha_i(V_i - V_{d2}), & V_{d2} \le V_i \le V_{max} \\ Q_{min,i}, & V_i > V_{max} \end{cases} \tag{4.1}$$

Where, V_{d1}, V_{d2}: the dead-band voltage range; α_i: slope of the i-th inverter volt/var characteristic; V_i: voltage at i-th node; $Q_{max,i}$, $Q_{min,i}$: maximum and minimum values of

reactive power for i-th inverter; V_{max}, V_{min}: maximum and minimum allowable voltages at i-th node.

The slope of inverter volt/var control dictates the rate at which the reactive power is injected into or absorbed from the network node. It is determined by the set dead band as given in equation (4.2).

$$\alpha_i = \frac{Q_{max}}{(V_{min} - V_{d1})} \tag{4.2}$$

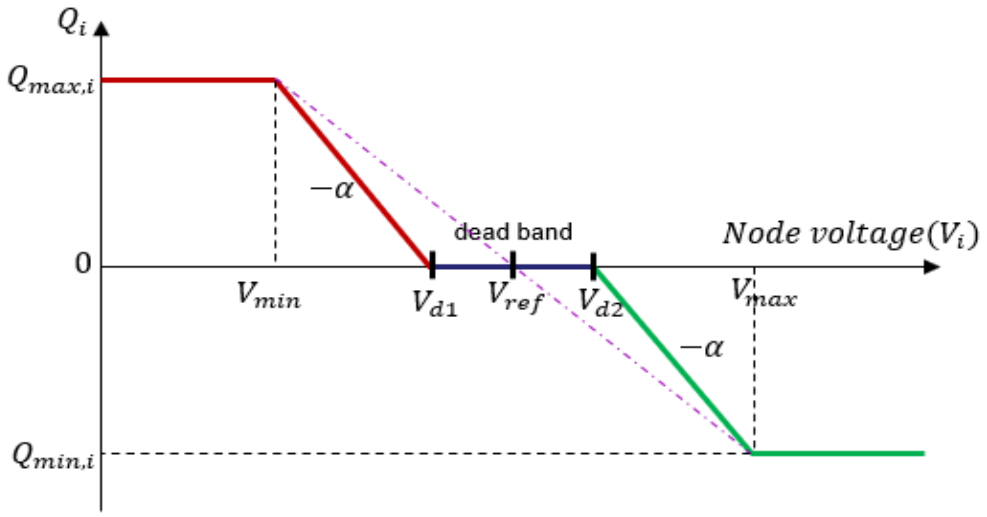

Figure 4.1: Inverter VVC characteristics for node voltage.

The inverter volt/var control horizon is given by figure 4.1. The upper part (red) being for reactive power injection to support the voltage. The lower part (green) for absorption of reactive power when there is a high injection of active power by PV resources resulting in a rise of voltage on the node.

The upper half of the characteristic curve is used for controlling voltages when they fall below the minimum allowable values. That is, when the voltage is below a certain prescribed minimum, the inverter injects reactive power to increase the voltage until it goes above the minimum. The converse happens when the voltage goes above the maximum prescribed limit. In this case, the inverter absorbs reactive power from the node until the voltage drops to acceptable levels. In the dead band region, the voltages are deemed to be in the acceptable range and so, no volt/var action is required from the inverter. The dead band is adjusted to meet the requirements of each node.

4.2 Implementation of VVC during PVHC estimation

Estimation of PVHC in the wake of inverter volt/var control with uncertainty consideration is carried out as outlined in chapters 2 and 3 with the only difference being that the inverter is allowed at inject/absorb a certain amount of reactive power. This, in turn, makes the node

voltages relatively lower than for the same amount of PV installed at the nodes. Subsequently, this opens the nodes for greater PV installation.

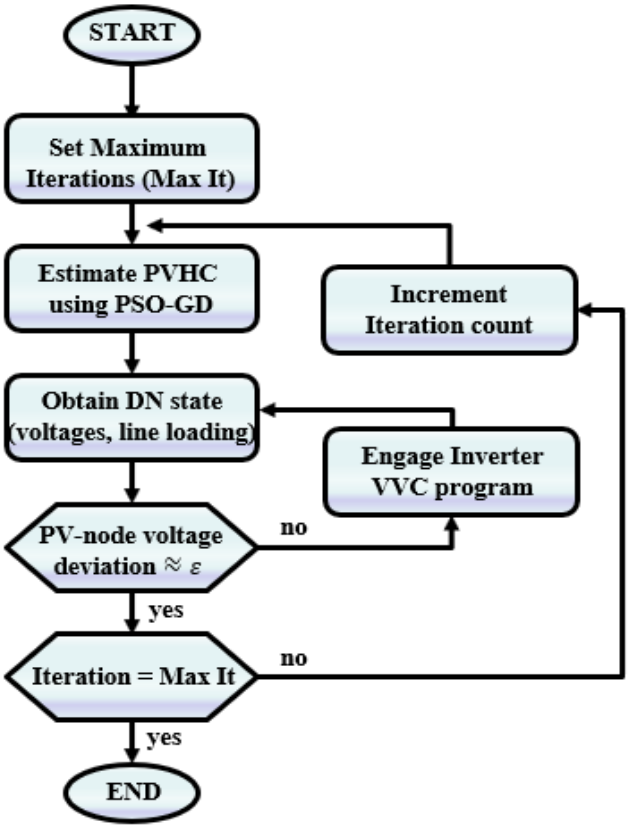

Figure 4.2: Flowchart of PVHC estimation with inverter VVC.

Figure 4.2 shows the proposed computation flow chart for the optimization process incorporating inverter VVC. The PV injection locations together with the PV sizes are determined using PSO-GD optimization algorithm as described in chapter 2. Then the inverter volt/var settings are calculated to optimize the voltage profile of the distribution network using equations (4.1) and (4.2). This process continues until there is no capacity left for more PV injections in the network according to either the voltage limits, line power flow limits or the maximum system loading possible.

The algorithm was tested on the IEEE 33 bus test DN used in chapter 2 and a comparison with a case where VVC was not employed was done. Table 2 shows a comparison of the results of PVHC estimation obtained when inverter VVC is not activated and when its activated.

The PVHC was evaluated using the method proposed in chapters 2 and 3 with reactive power compensation using the PV inverter with VVC capability. The line and bus parameters of the test network are indicated earlier in chapter 3. Three distinct scenarios were considered: A no installed PV scenario, a scenario with PV but no VVC for the PV inverter and a scenario with PV installed and the PV inverter VVC actualized. Table 4.1 shows the results.

Table4. 1: Estimates of PV sizes at optimal nodes of IEEE 33 bus DN with/without inverter VVC.

Location (Node number)	Installed PV size [kW]	
	Without VVC	With VVC
7	566.31	606.56
15	776.16	832.62
18	645.23	672.14
25	370.11	374.52
26	189.38	209.72
31	726.78	764.63
TOTAL	3273.97	3460.19

The PVHC without inverter volt-var control is estimated at about 3273.97 kW, while that with inverter volt-var control is about 3460.19 kW. This represents a significant 186.22 kW (or 5.688%) increase in PVHC. The increase is because, with volt-var control, the inverter actively engages in ensuring that the node voltages are kept within the acceptable limits by injecting or absorbing reactive power when the voltages fall below or rise above the set limits, respectively. This, in turn, creates extra space for more PV installations without abrogating the voltage limit requirements.

Figure 4.3 shows the voltage profiles obtained for three principal scenarios: case (a) is the base case scenario of the IEEE 33-bus test DN with no PV installation; case (b) represents a scenario with PV installations but no VVC; and case (c) gives a scenario with PV and VVC engaged. As can be observed, in the base-case scenario, some node voltages are below the set voltage minimum boundary. In the two cases with PV installation, there is an

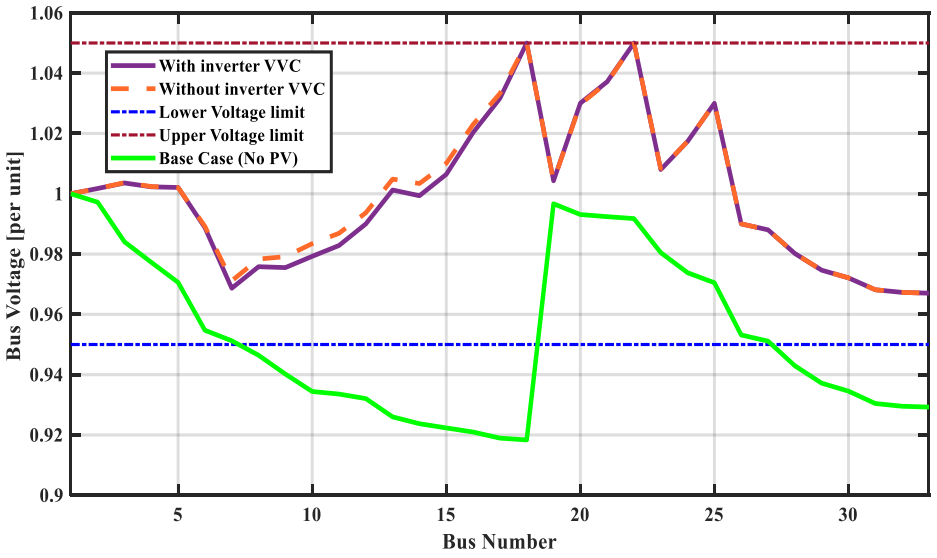

Figure 4.3: Voltage profiles of the IEEE bus network for three different scenarios

improvement in the voltage profile such that in both cases, all the node voltages lie within the set boundaries, but some nodes operate at the periphery of the upper voltage boundary.

Despite the network voltage profiles for the scenario with PV without VVC and the scenario with PV and with VVC being substantially, the installed PV size in the former scenario is much greater than in the later scenario. The bar charts of figures 5.4 and 5.5 show the estimated sizes of installed PV and the required reactive power to support the voltages respectively.

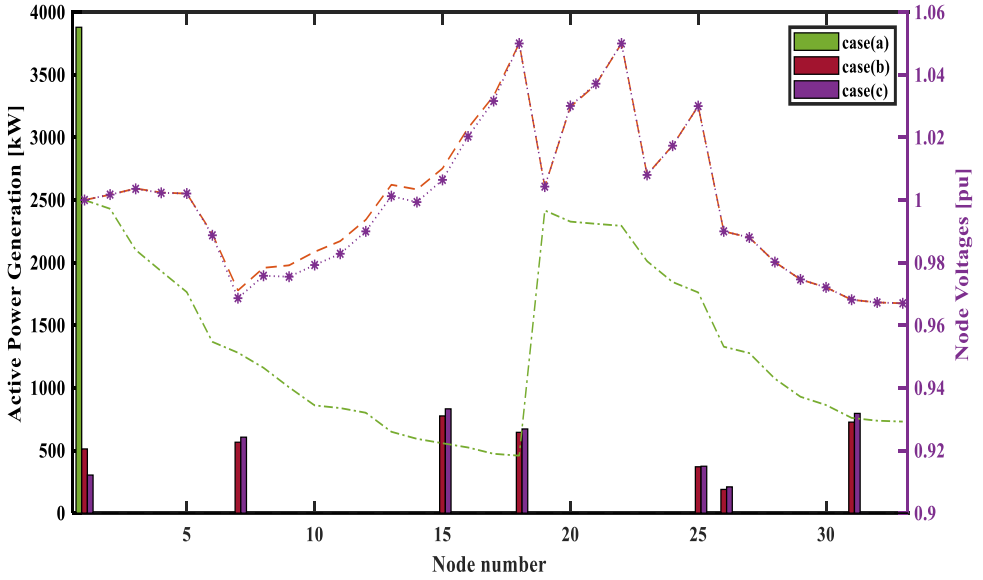

Figure 4.4: (a) Active power generated at the nodes in the IEEE 33 bus for each scenario.

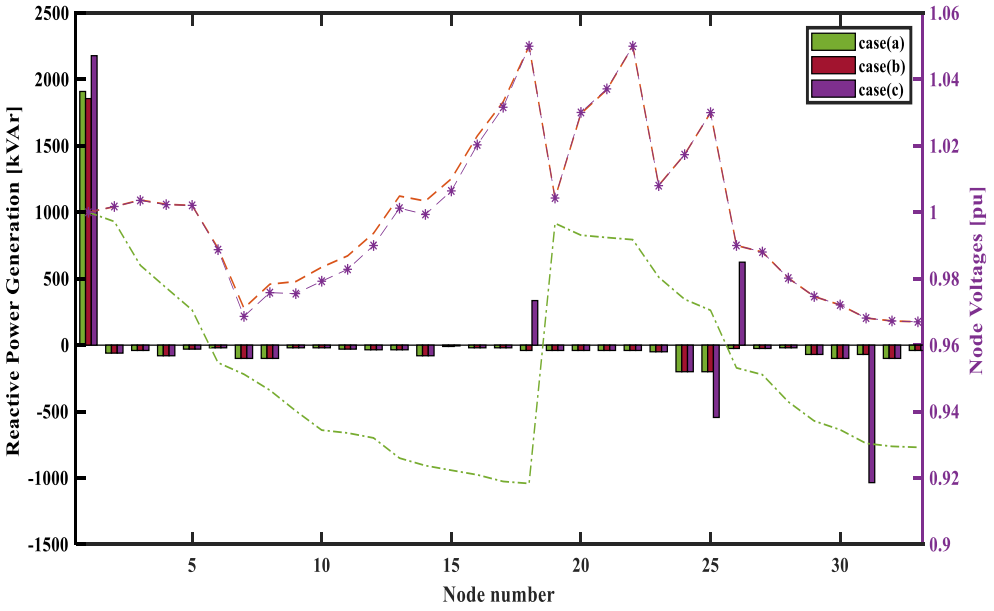

Figure 4.4: (b) Reactive power generated at the nodes in the IEEE 33 bus for each scenario.

It is evident that the use of the PV inverter with volt-var control functionality offers an improvement in the PVHC of the network.

Figure 4.4 shows the trend of the power generation from the reference situation vis-a-vie case (a) with no PV installation and inverter VVC functionality to case (b) with PV installation but no VVC functionality and case (c) with PV installation and inverter VVC functionality. The active power supply in case (a) is unilaterally from the distribution substation to a tune of 3879.50 kW. In case (b) where there are PV installations on some nodes, the power is supplied from all nodes with PV installations and a significantly lower amount of about 500 kW comes from the distribution substation. The total power supplied from all generating units in this case is 3795.97 [kW]. In the final case where there is PV installation and inverter VVC, an even smaller amount of power is obtained from the distribution substation (about 280 kW) with the total power from all sources amounting to 3786.53 kW.

Considering the DN total of 3715.00 kW, case (a) results in the highest power loss of 164.5 kW compared to 80.97 kW in case (b) and 70.53 kW in case (c). Therefore, it can be inferred that the optimal location and sizing of PV installation reduces the power losses significantly. Further to this, it can be appreciated that the use of VVC not only increases the size of the PV installation but also reduces the power losses.

From figure 4.4, case (b) vis a vie the base case with no PV nor inverter VVC, all the nodes absorb reactive power supplied by the substation. In this case, the substation supplies nearly 2000 kVAr. In case (b), a similar trend as in case (a) is observed with all the nodes absorbing the same amount of reactive power except for the substation (virtual slack node) which supplies the reactive power.

In case (c) however, there are differences in reactive power trends on 4 nodes with installed PV. On nodes 18 and 25, reactive power is injected into the nodes to support the voltages at these nodes. On nodes 26 and 31 reactive power is absorbed to prevent over-voltages as these nodes experience large PV power injections.

The absorption/injection of reactive power on the 4 nodes mentioned in the paragraph above enables the control of the node voltages. The control of the node voltages invariably leads to higher PV size installations being permitted.

Therefore, there is an inevitable increase in PVHC in the distribution network when the PV inverter employs the volt/var control functionality. In the case under consideration, the PVHC increased from 3273.97 kW to 3460.19 kW, a rise of about 5.69 %. This is a considerable increase particularly in large systems demanding hundreds or thousands of megawatts.

4.3 Chapter Summary

The chapter presented a proposed use of the PV inverters with voltage control capability using reactive power compensation to improve the PVHC of distribution networks. The characteristics provided were driven by the conclusions of the IEEE 1547 standard on renewable energy resources interconnection and interoperability with their associated devices.

The numerical results showed that the use of the PV inverter with volt-var control capability greatly enhances the PVHC of the distribution network. The results also showed that even the voltage profiles could be operating around the maximum boundary, the control mechanism ensures that the highest possible PV sizes could be installed.

Furthermore, the active power contributions from the distribution network substation are significantly reduced from 3879.5 kW, in the scenario without PV, to 500 kW, in the case with PV but without VVC and a merger 279 kW in the case with PV and VVC present. This means the substation has freed up capacity to supply a greater load demand for future expansions.

CHAPTER FIVE ESTIMATION OF PVHC UNDER UNCERTAINTY CONSIDERATION

5. Estimation of PVHC with Uncertainty Consideration

5.1 Chapter Overview

In chapter 2, a deterministic approach to PVHC estimation in DNs using PSO-GD was proposed. This approach combines the use of steepest gradient descent in the update process of the PSO velocity component to influence the rate of particle movement. The method proved to be efficient and stable when it was applied to estimate the PVHC of the IEEE 33-bus test DN, 69-bus test DN and the 136-bus existing RDN.

However, the intermittent characteristics of PV generation [49] and the variability in the load demand cannot be included in deterministic methods [105]. Thus, the foregoing approach did not produce realistic PVHC models [106].

To include uncertainty brought by PV intermittency and load demand variability, stochastic/ probabilistic methods are employed. The traditional probabilistic methods employing the Monte Carlo simulations (MCS) or conventional convolution, solve several thousands of scenarios of PV outputs and load demands to produce a probabilistic result [107], [108]. The generated models are very realistic because they incorporate the uncertainties in network variables and parameters. However, these methods impose a huge computation burden when the uncertain variables and parameters are many. There is also a loss of generality as the number of uncertain variables increases. More modern probabilistic methods such as the point estimate method (PEM) and Latin Hypercube Sampling with Cholesky Decomposition provide faster solutions. However, these too are affected by the complexity of the problem and require some linearization. Consequently, their result is an approximate solution.

In this research, a combination of the deterministic and stochastic approach to the PVHC problem is proposed. The deterministic approach (PSO-GD) is used for estimating the optimal sizes and locations of PV while the stochastic approach (PEM) is used to assimilate the uncertainties in the input variables. The PEM-based probabilistic analysis is an approximate method but if carefully modeled, gives a very accurate result.

The numerical results obtained using hybrid PSO-GD/PEM are benchmarked against the hybrid PSO-GD/MCS method in [20]. While it is established that there is very little variation in the PVHC results obtained using both hybrid methods, the PSO-GD/PEM method is extremely faster compared with PSO-GD/MCS approach. This is especially advantageous when dealing with a very big network in which there are many uncertain variables and parameters.

5.2 Stochastic PVHC estimation using PSO-GD

Several point estimate method (PEM) schemes have been developed and applied in many fields over the years. Table 3.1 shows the most popular schemes, their efficiency and what type of variables they are associated with [109].

Table 5. 1 Description of PEM schemes

Scheme	Number of simulations	Efficiency	Ability to handle:	
			Correlated variables	Asymmetric variables
Rosenblueth	2^m	Very low	Yes	Yes
Li	$O(m^3)$	low	Yes	Yes
Harr	$2m$	high	Yes	No
Hong	Km / $Km+1$	high	No	Yes

The choice of scheme to use for a particular application depends on the nature of the input variables. For example, Harr's scheme [110] and Li's scheme [111] are applicable to asymmetric and correlated input variables which are asymmetric.

Rosenblueth's scheme performs well with random input variables which are both correlated and asymmetric [112]. Unlike Harr's and Hong's schemes, whose evaluations increase linearly with increase in the number of input variables, Rosenblueth's scheme can impose a very huge calculation burden for large systems (even more than MCS) because the evaluations increase exponentially as the number of variables increase.

For the PVHC problem, the random input variables are narrowed down to PV output power and load demand (active and reactive power). These variables have been shown to be uncorrelated and asymmetric and therefore, we will limit our discussion to Hong's $2m+1$ PEM because the scheme renders itself suitable for the variables of interest [113], [114].

5.2.1 Hong's PEM Schemes

In Hong's $2m+1$ PEM scheme, the statistical information obtained from the central moments of input random variables on 2 points are condensed to produce concentrations $(r_{l,k}, \omega_{l,k})$ where $r_{l,k}$ and $\omega_{l,k}$are the location and relative weight (importance) of the l th input random variable at the k th concentration respectively, $l = 1,2, \dots \dots, m$, $k = 1,2$.

A function F linking the input random variables to the output is then evaluated at these concentrations for each input random variable $r_{l,k}$ by replacing the l th variable at the k th concentration while holding the other input random variables to their mean values, $(\mu_{r_1}, \mu_{r_2}, \dots \dots, \mu_{r_{l,k}}, \dots \dots \mu_{r_{m-1}}, \mu_{r_m})$. An extra evaluation of F at the expected values of all the input random variables is carried out to complete the evaluation.

On every evaluation of F, the raw moments of the output variables are updated until the final input random variable is used. One advantage of this method is that the function F

linking the inputs to the outputs can be a linear or non-linear function. Thus, for probabilistic load flow (PLF) analysis, each evaluation can accommodate a full AC deterministic power flow evaluation and output variables such as node voltages, line power flows, network power losses can be obtained from these evaluations.

The locations of the input random variables are calculated using (5.1):

$$r_{l,k} = \mu_{r_l} + \xi_{l,k}\sigma_{r_l} \tag{5.1}$$

Where $\xi_{l,k}$ is the standard location for the input random variable and is determined using (5.2), and μ_{r_l}, σ_{r_l} are the mean and standard deviation of the random variable r_l respectively.

$$\xi_{l,k} = \frac{\lambda_{l,3}}{2} + (-1)^{3-k}\sqrt{\left(\lambda_{l,4} - \frac{3}{4}\lambda_{l,3}^2\right)} \tag{5.2}$$

Where, $\lambda_{l,3}$ and $\lambda_{l,4}$ are the skewness and kurtosis of the input random variable respectively. The associated weights for the locations are computed using (5.3) and (5.4), with (5.4) being associated with the evaluation of F at the mean values of the input random variables.

$$\omega_{l,k} = \frac{(-1)^{3-k}}{\xi_{l,k}\left(\xi_{l,1} - \xi_{l,2}\right)} \tag{5.3}$$

$$\omega_0 = 1 - \sum_{l=1}^{m} \frac{1}{\left(\lambda_{l,4} - \lambda_{l,3}^2\right)} \tag{5.4}$$

Once F is evaluated at each concentration, the raw moments of the output variables are updated according to equations (5.5) and (5.6).

$$X(l,k) = F\left(\mu_{r_1}, \mu_{r_2}, \dots\dots, \mu_{r_{l,k}}, \dots\dots \mu_{r_{m-1}}, \mu_{r_m}\right) \tag{5.5}$$

$$E\left[X^j\right] \cong E\left[X^j\right] + \omega_{l,k}\left(X(l,k)\right)^j \tag{5.6}$$

Where $X(l,k)$ is the evaluation of F for a particular concentration, $E\left[X^j\right]$ is the expectation or the j-th raw moment of the output variable.

The first 2 central moments (mean and variance) of the output variable can then be computed using (5.7) and (5.8) respectively.

$$E[X^1] = \mu_x = \mu_1 \tag{5.7}$$

$$E[X^2] = \sigma_x^2 = \mu_2 - \mu_1^2 \tag{5.8}$$

μ_x and σ_x^2 are the mean and variance of the output random variable of interest respectively, μ_1 and μ_2 are the first and second raw moments of the output random variable.

Assuming the output variables are normally distributed, the probability density function (PDF) of the output variables can then be re-constructed by using equation (5.9).

$$f(x|\mu_x, \sigma_x) = \frac{1}{\sqrt{2\pi\sigma_x{}^2}} exp\left\{-\frac{(x-\mu_x)^2}{2\sigma_x{}^2}\right\} \quad (5.9)$$

Figure 5.1 shows the process flow chart for Hong's $2m + 1$ PEM scheme.

It begins by initializing the input random variable count to 1 and the raw moments of the output random variables to 0. Input random variables are then selected for which central

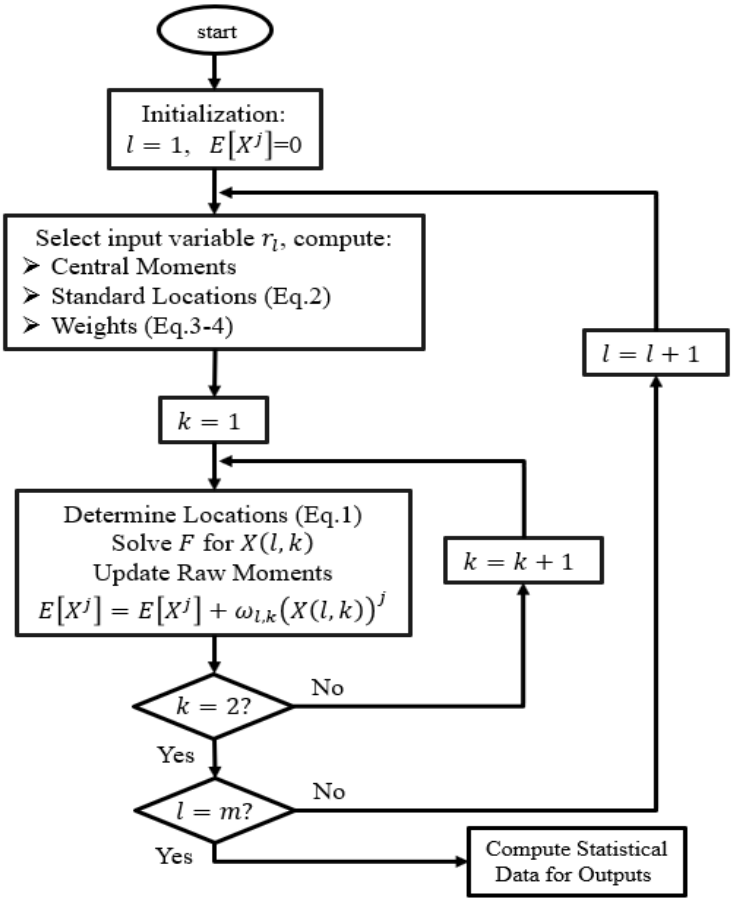

Figure 5.1: Flow chart for Hong's 2m+1 PEM scheme

moments, standard locations, and weights (their relative importance) are calculated.

Next, the input random variable locations are determined and then the function linking inputs to outputs is evaluated at these locations. Subsequently, the raw moments are updated at these evaluations. This process is repeated until all input random variables are exhausted.

After all evaluations are finalized and the raw moments are updated completely, the central statistical information is extracted from the generated raw moments. This information is

then used for generating the probability density functions (PDF) and the cumulative density functions (CDF) of the output variables of interest.

5.2.2 Implementation of Stochastic PSO-GD for PVHC estimation

The PVHC estimation process using the probabilistic approach begins with the uncertainty characterization of the input variables. In this case, the input variables are identified as the PV output and the load demand. The randomized input variables are then used to obtain random output variables through the PEM-based probabilistic load flow analysis.

The flow chart for the implementation of the PVHC estimation process is shown in figure 5.2. The process begins with determination of optimal PV sites and sizes using PSO-GD method proposed earlier. The sizes obtained in this phase are based on one scenario of PV outputs and load demand. Next, random PV output and load demand scenarios are generated based on their uncertainty characteristics. Thereafter, a PEM-based PLF analysis is used to obtain the output random variables including node voltages. The PDF of the node voltages are then plotted. If the voltage limit is not violated, the PV sizes on each node are proportionally incremented in preset step values. This process is repeated until an over-voltage is observed. The occurrence of an overvoltage at any node during the estimation process signals the end of the process. The final sum of the PV sizes in each location at the end of this process gives the PVHC of the DN in consideration.

5.2.3 Probabilistic Modelling of PV Output

The PV output variable is modeled as a random uncertain variable using random generated PV output scenarios considering the probabilistic representation of solar irradiation [48] and [20]. The driving formulation for the random generation of PV output scenarios is a beta distribution as given in (5.10).

$$f_i\left(P_{pv,i}\right) = \frac{\Gamma(\alpha_{pv}+\beta_{pv})}{\Gamma(\alpha_{pv})\Gamma(\beta_{pv})}\left\{\left(P_{pv,i}\right)^{(\alpha_{pv}-1)}\left(1-P_{pv,i}\right)^{(\beta_{pv}-1)}\right\} \tag{5.10}$$

Where $P_{pv,i}$ is the PV output of PV in i −th location; $\Gamma(\cdot)$ is a gamma scaling parameter; α_{pv} and β_{pv} are respective curve shaping parameters with $\alpha_{pv}, \beta_{pv} \geq 1$

The crude values of α_{pv} and β_{pv} are evaluated using the mean and standard deviation of the historical data on the PV outputs using equations (5.11) and (5.12).

$$\alpha_{pv} = {\mu_{pv}}^2\left(1-\mu_{pv}\right)/\left({\sigma_{pv}}^2-\mu_{pv}\right) \tag{5.11}$$

$$\beta_{pv} = \alpha_{pv}\left(1-\mu_{pv}\right)/\mu_{pv} \tag{5.12}$$

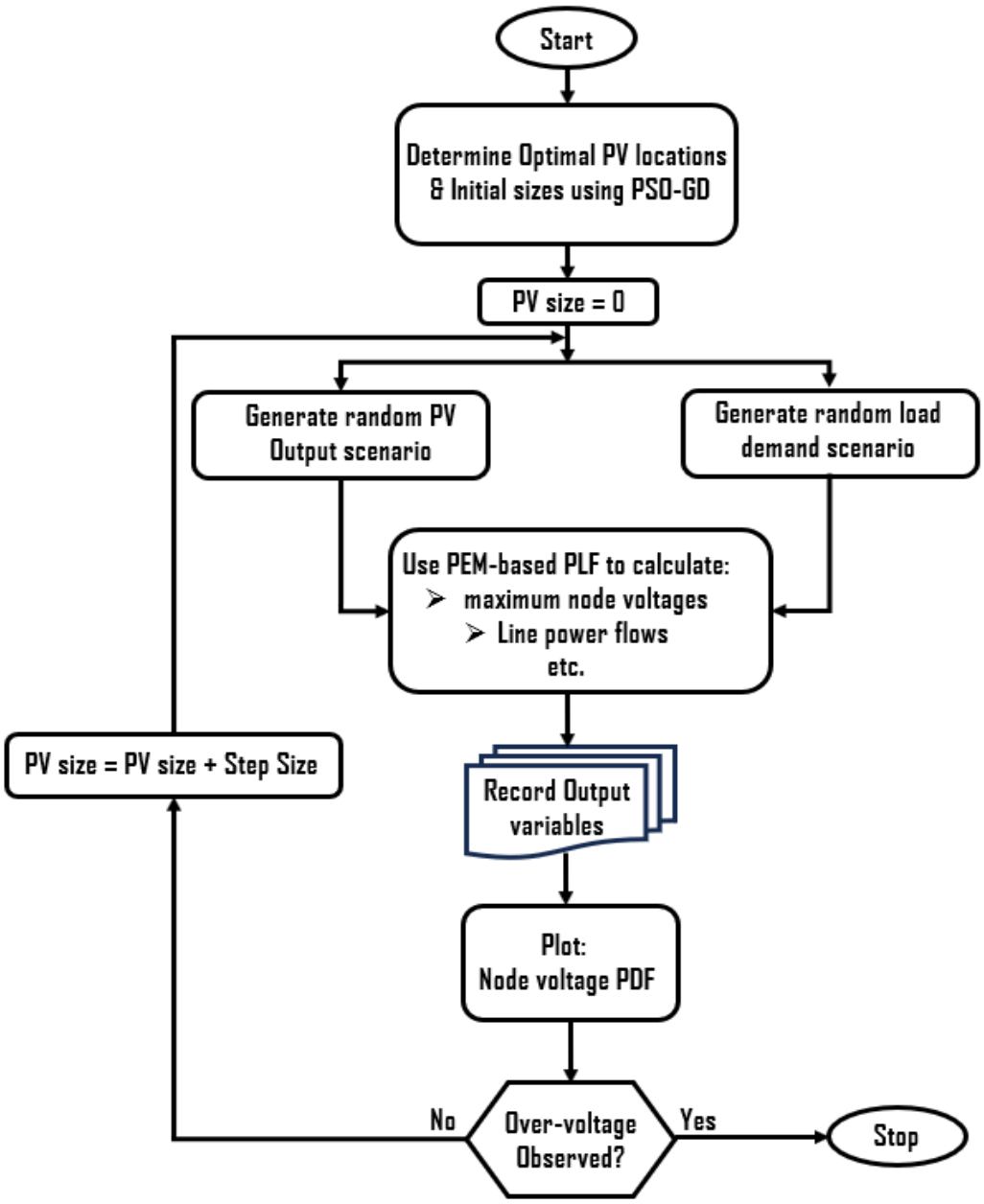

Figure 5.2: Flowchart for the PVHC estimation process in DN using stochastic PSO-GD

5.2.4 Probabilistic Modelling of Load Demand

The uncertainty characterization of load demand is modeled as a random variable with truncated Gaussian (normal) distribution [115]. The use of the truncated PDF is necessary to prevent generation of infinite number of loading scenarios which could result in difficulties in solving the problem. The random load demand scenarios are created using (5.13).

$$f_k(P_{L,k}) = \begin{cases} 0, & P_{L,k} < P_L^{min} \\ \frac{1}{\sqrt{2\pi{\sigma_L}^2}} exp\left\{-\frac{(P_{L,k}-\mu_L)^2}{2{\sigma_L}^2}\right\}, & P_L^{min} < P_{L,k} < P_L^{max} \\ 0, & P_{L,k} > P_L^{max} \end{cases} \quad (5.13)$$

Where $P_{L,k}$ is the load demand at the k −th node; μ_L is the mean of the load demand; ${\sigma_L}^2$ is the variance of the load demand; P_L^{min} and P_L^{max} are the minimum and maximum values of the load demand at the truncation points.

5.3 Case Studies

5.3.1 Case IA: Conservative Stochastic PVHC

This case explores the estimation of the PVHC under uncertainty with the network voltage set as a hard constraint. This gives a conservative estimate of the PVHC while considering the stochasticity of the network variables.

The procedure outlined in section 5.2.2 was applied to the problem discussed in chapter 2. The objective function given in equation (3.1) is modified to include the probabilistic formulation on which this chapter is hinged. Equation (5.14) indicates the modification to (3.1). The constraints given in equations (3.2) to (3.10) are maintained.

$$PVHC = max\{\textstyle\sum_i P_{pv,i} | (Pr[V_j^{max} \geq V_{lim}])\} \quad (5.14)$$

Where $Pr[V_j^{max} \geq V_{lim}]$ is the probability that the observed maximum node voltage does not exceed a preset maximum node voltage limit.

With this adjustment, the stochastic PVHC of the IEEE 33-bus test distribution network whose technical parameters are given in [116] was estimated.

Figure 4.3 shows the probability density functions of the maximum node voltages as a function of installed PV size in increments of 0.1 MW. The maximum voltage for the IEEE 33-bus test network is set at 1.05pu. This constraint must be strictly met.

As per algorithm set out in Fig. 5.2, the process of estimating the PVHC terminates when the termination criterion is met at the end of the last iteration in which the maximum voltage observed reaches 1.05 pu.

It can be appreciated that the variance of the probability distributions (PDF) is quite small at low values of installed PV sizes compared to the spread observed for high values of installed PV sizes. This is because at low values of installed PV sizes, the differences between the maximum values and minimum values due to uncertainty is quite small. Subsequently, the load flow analysis done within these realizations of input PV generation results in voltages which are in a very close range. Consequently, the resulting PDFs have a low variance.

On the contrary, because the difference between the maximum values and minimum values tenable are within the uncertainty framework at high installed PV sizes, the impact of the system voltage is quiet substantial at high values (at and near the maximum values), while being moderate at low values (at and near the minimum values). The situation is exacerbated because the network load remains substantially within the same range regardless of whether the installed PV size is the low end or on the high end. Figure 5.3 shows the PDFs of the maximum node voltages observed when the PVHC was estimated as outline in figure 5.2.

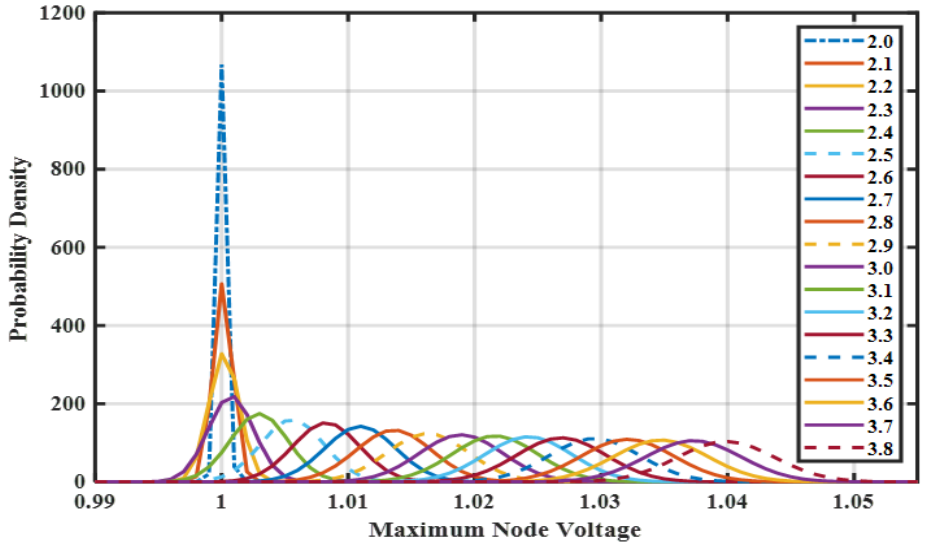

Figure 5.3: PDFs of maximum node voltages at each installed PV size.

Moreover, it has been observed that the stochastic PVHC value estimated in this case is 3700 kW. This is slightly higher than the value obtained in the previous chapter of 3461.9 kW. This is alluded to the fact that there was no consideration of uncertainty in the loading vis a vie, the load was kept at the average values. This results in a pessimistic result. With the stochastic load considered, it is possible for some loading levels and PV generation levels to have relatively low effects on the resulting maximum voltages. This then offers an optimistic result.

5.3.2 Case IB: Flexible Stochastic PVHC

The approach suggested in section 5.3.1 considers the voltage to be a hard constraint and all scenarios of input random variables which result in voltages outside this boundary are considered to violate the system performance. This approach, however, does not address the fact that some feeders may be more tolerant to slight over-voltages than others. Thus, we introduce case IB which seeks to apply a softened voltage constraint.

Figure 5.4 shows the principal differences between these two PVHC estimation cases. In (a), the voltage is set as a hard constraint such that when the installed PV vs node voltage curve crosses voltage limit line, the intercept defines the PVHC estimate. The region below

the voltage limit line defines the acceptable operating region in which there are no voltage violations while the region above the voltage limit line is the unacceptable region. In (b), however, the voltage limit boundary is relaxed to accommodate a small voltage violation, as may be acceptable to the network operators, to extend the PVHC. In this case, 3 operating regions are defined. As in (a), the region below the voltage limit line defines the acceptable operating region, the additional region where a small voltage violation is tolerable being the critical region and, the unacceptable region comes above the critical region. Operation in the critical region is very risky but may be permitted.

In case IB we consider estimating the PVHC under uncertainty while relaxing the network voltage constraint. We explore the idea that a very small over-voltage could not have a very severe impact on the network operation or its devices [82]. Instead, a slight over-voltage tolerance could find solutions with a high payout but less severe effects. This calls for a modification to the objective function to include this new reality. Equation 4.13 introduces the new objective function [20].

$$PVHC = max\{\sum_i P_{pv,i} | (Pr[V_j^{max} \geq (V_{lim} + \delta V)])\} \tag{5.13}$$

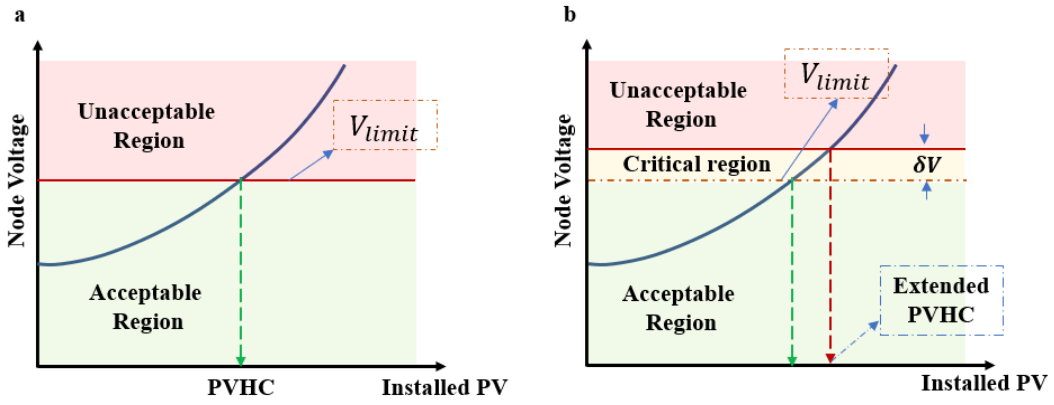

Figure 5.4: PVHC (a) with hard voltage constraint (b) with flexible voltage constraint

Where δV is the allowable tolerance in above the predefined voltage limit. Operation in this incrementally small voltage deviation from the preset value must generally be considered harmless to the network devices and equipment operation. Thus, care must be taken in setting the value of δV to ensure the payout for allowing such a slight abnormality in the network voltages is greater than the risk it poses. The typical value proposed for this variable is in the order of 0.5% of the nominal system voltage.

The flexibility offered by the relaxation on the voltage constraint enables heightened amounts of PV to be installed without requiring network reinforcement which might otherwise be a much more expensive proposition.

The formulation of Eq. 5.13 offers flexibility in the consideration of PVHC of the network. As with case IA, all the constraints defined by equation (3.2) to (3.10) are retained.

Figure 5.5 shows the probability density functions obtained by considering random PV output scenarios and load demand uncertainty on account of voltage limit constraint relaxation.

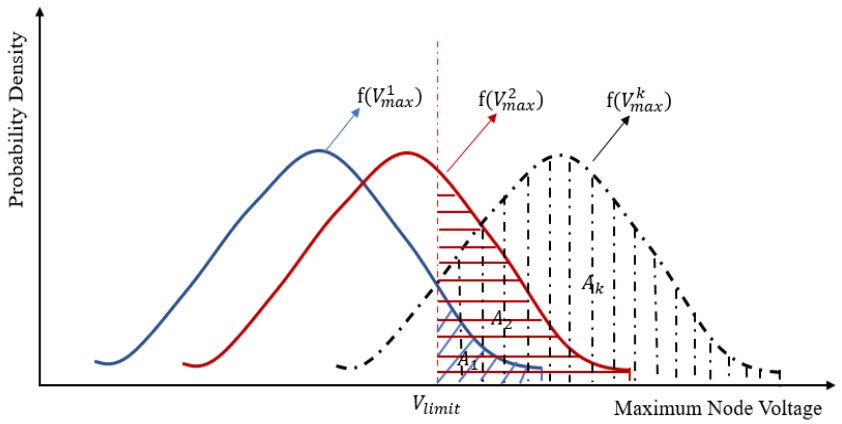

Figure 5.5: Probability density functions of maximum node voltages for different PV sizes.

In this instance, the extent of the maximum voltage magnitude and the number of scenarios out of the total number of runs which result in voltage violations occur is very important as it gives an idea of the level of voltages expected and, most crucially, the likelihood the extended voltage limit will be violated.

The probability of voltage violation is calculated by taking the area occupied by the curve to the right of the desired voltage limit using equation 5.14.

$$Pr[V.V^k] = Pr[V_{max}^k \geq V_{limit}] = \int_{V_{limit}}^{max\ (V_{max}^k)} f(V_{max}^k) dV_{max}^k \tag{5.14}$$

Where $Pr[\cdot]$ is the probability of the voltage violation for each installed PV size.

Fig 5.6 shows the probability density function (PDF) of the highest node voltages obtained when this argument is applied to IEEE 33 bus test DN.

It is obvious from figure 5.6 that, as the installed PV size is increased, the extent of the maximum node voltage that can be observed also increases. As alluded to earlier, no voltages are observed to be above the set threshold of 1.05 [pu] for PV installation sizes less than 3.7 [MW]. This situation changes as installed PV sizes increase above 3.7 [MW]. This increase in level of voltage seems to be in proportion to increases in installed PV sizes.

When a flexibility or relaxation on the allowable voltage limit is applied, the point at which the limit line is crossed increases thereby allowing higher PV sizes to be installed without abrogating the set voltage limit. Figure 5.7 shows the levels of voltage violations and points of PV installation sizes at which they occur for different over-voltage allowances.

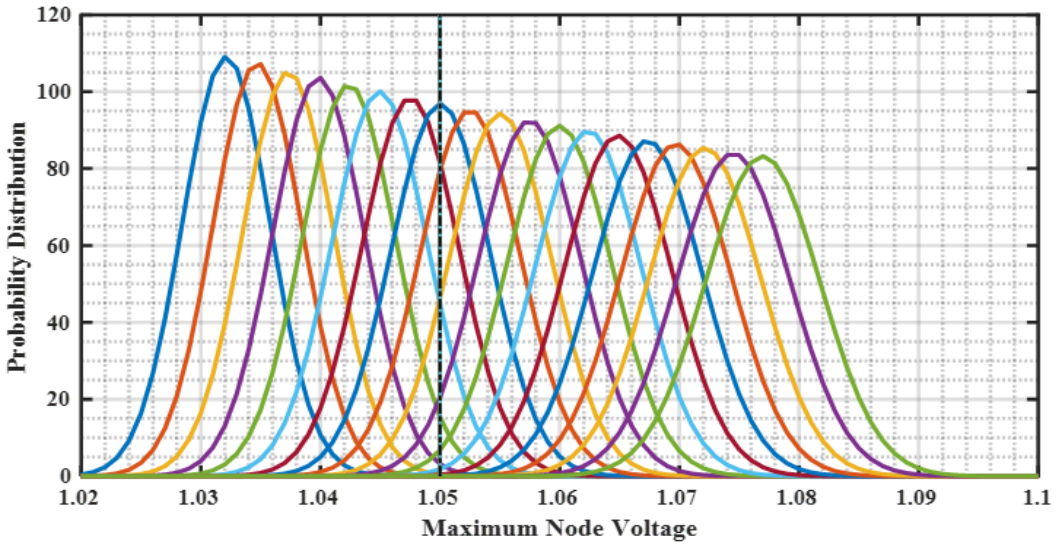

Figure 5.6: PDF of maximum node voltages for Installed PV capacities 3.2 - 5 MW

It has been seen that by increasing the voltage limit from 1.05 pu to 1.059 pu through various step sizes, the installed PV size was increased from 3.7 [MW] to about 4.0 MW. This intimates that increasing voltage limit flexibility by only 0.856% can potentially increase the PV hosting capacity of the DN by a substantial 8.108%. This is highly significant for DNs with less voltage sensitivity as it could enable the network operators to increase their PV installation sizes, reduce the carbon footprint, and subsequently contribute to reduce carbon emissions without many investments in system upgrades on equipment.

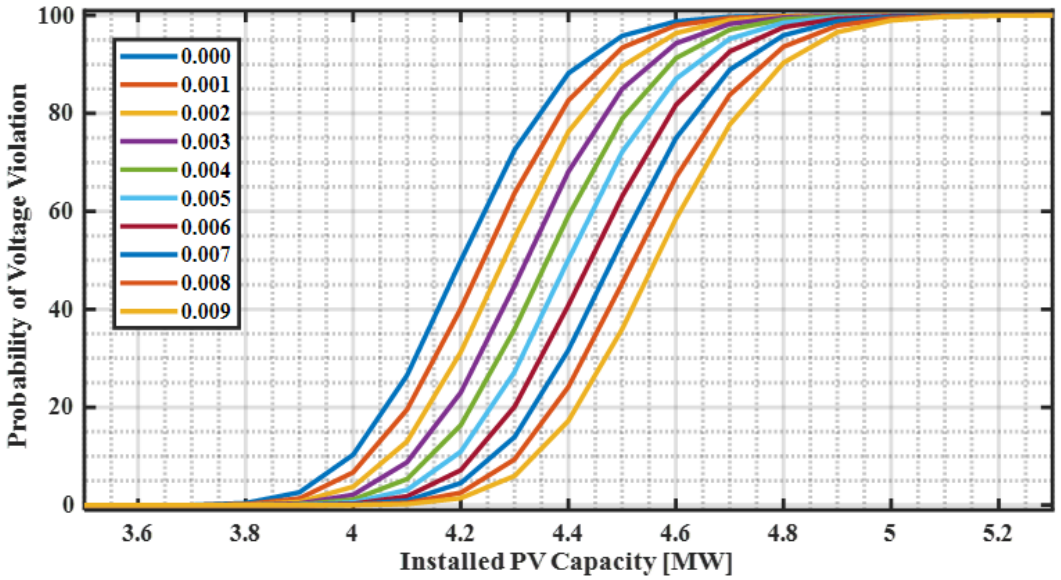

Figure 5.7: Probability of voltage violations as a function of Installed PV capacity

For a range of uncertainties on the load demand of from 3%, 5%, 7% to 10%, the variations of the PVHC estimates are shown in fig. 5.8.

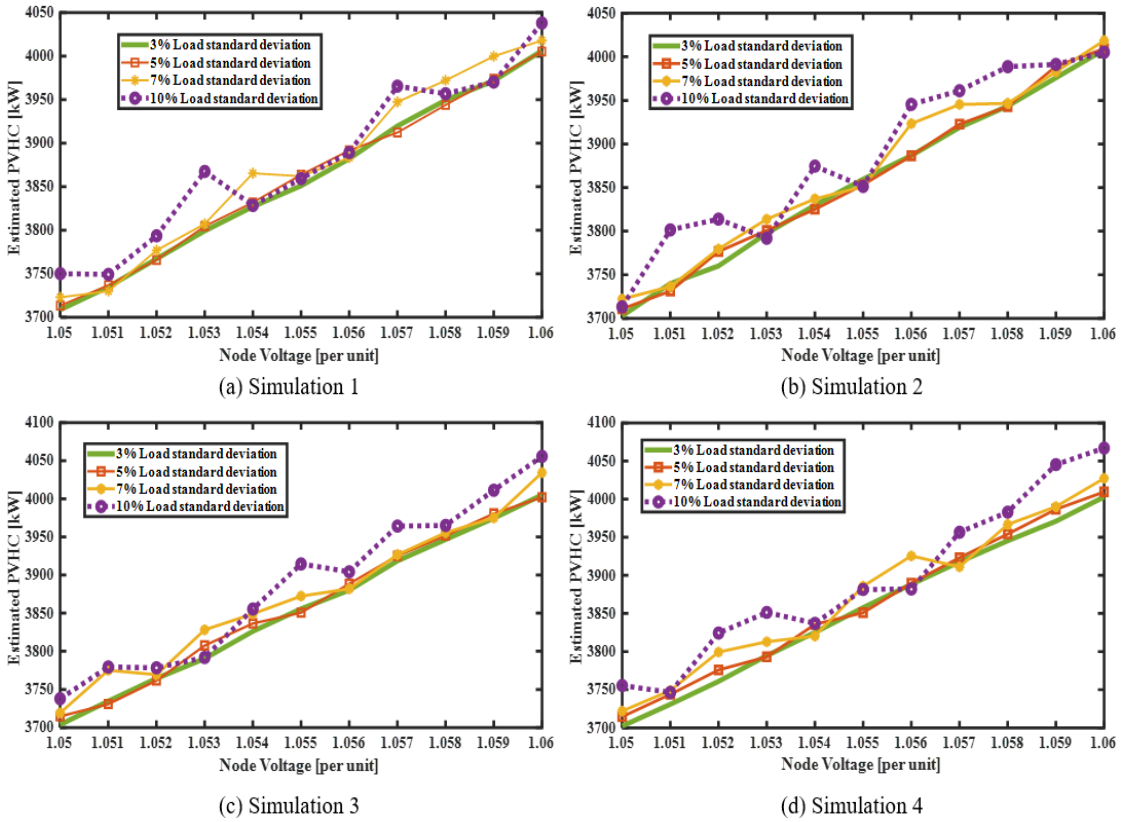

Figure 5.8: PVHC as a function of flexible voltage limit constraints.

The results of figure 5.8 show a near linear increase in estimated PVHC when the voltage tolerance is increased gradually between 1.05 per unit and 1.06 per unit for a load demand standard deviation of 3%. This is attributed to the very small uncertainty in the load demand variations having minimal impacts on the overall PVHC estimation process.

When the standard deviation in load demand increases to 5%, the results in all simulations are not nearly as linear as at 3% because the increased uncertainty in load demand results in higher variability between minimum and maximum values of load. The results become even more haphazard when the uncertainty is raised to 7% and 10 % standard deviations.

In all simulation cases, however, the trend is for the estimated PVHC to increase from a certain level at the lowest voltage limit to a higher value in subsequent voltage limit constraint relaxations. Thus, overall, for the voltage limit shift of about 0.962% (from 1.05 pu to 1.06 pu), the PVHC rises 8.108% for the 3% uncertainty, 8.11% for the 5% uncertainty, 8.054% for the 7% uncertainty and 7.733% for the 10% uncertainty in the load demand respectively.

There, it can be inferred that relaxations on the voltage limit constraints in certain areas of the DN have a potential to increase the PVHC of the DN by an appreciable amount.

5.4 Efficacy and Speed of Proposed Method

The calculation prowess and speed of the proposed method was benchmarked against the Monte-Carlo Simulation (MCS) based PVHC estimation on the IEEE 33 bus test DN and the existing 136 bus DN in Sao Paulo.

A 100000 MCS run was conducted per PV size. This included generation of 100000 scenarios of input variables of installed PV and load demand using their uncertainty characteristics. As in the previous case study, the installed PV sizes were increased from a certain low value (3.5 MW) to certain high value (5.2 MW) in preset steps (0.1 MW). The PV scenarios were generated at each PV size and a MCS was conducted at this PV size.

5.4.1 Computation Accuracy

The accuracy of the proposed method is tested by computing the errors in estimating the PVHC at different voltage violation levels relative to the results obtained at the same points using MCS. The errors of interest which were considered are the relative error (RE) and the room mean square error (RMSE).

Relative error is an important measure as it provides a valuation of the accuracy of the calculated values when benchmarked against standard values. In this case, the standard values are provided by the MCS calculations.

The relative error in calculating the PV hosting capacity for various values of probability of voltage violations are obtained using equation 5.15 [48].

$$\varepsilon_r = \frac{X_{MCS}^i - X_{PEM}^i}{X_{MCS}^i} \times 100\% \tag{5.15}$$

Where ε_r is the relative error, X_{MCS}^i is the i −th data point on the MCS result, X_{PEM}^i is the $i-th$ data point on the proposed method result.

A more significant error quantity is the RMSE. It measures the difference between values calculated by a model compared with the standard accurate values from the benchmark model. It measures how well the proposed model is able to predict the target value. It is evaluated using equation (5.16).

$$\varepsilon_{rmse} = \sqrt{\left\{\frac{1}{N}\sum_{i=1}^{N}\left(X_{MCS}^i - X_{PEM}^i\right)\right\}} \tag{5.16}$$

Where ε_{rmse} is the RMSE and N is the total number of data points on the graph under consideration.

The lower the values of both the RE and RMSE, the more accurate the proposed method is in calculating the PVHC of the DN.

Figure 5.8 shows estimated probability of voltage violations as a function of installed PV capacity for the IEEE 33 bus test DN and the existing136-bus DN. The dotted red lines are values obtained using the benchmark MCS method while the solid blue lines are values obtained using the proposed method.

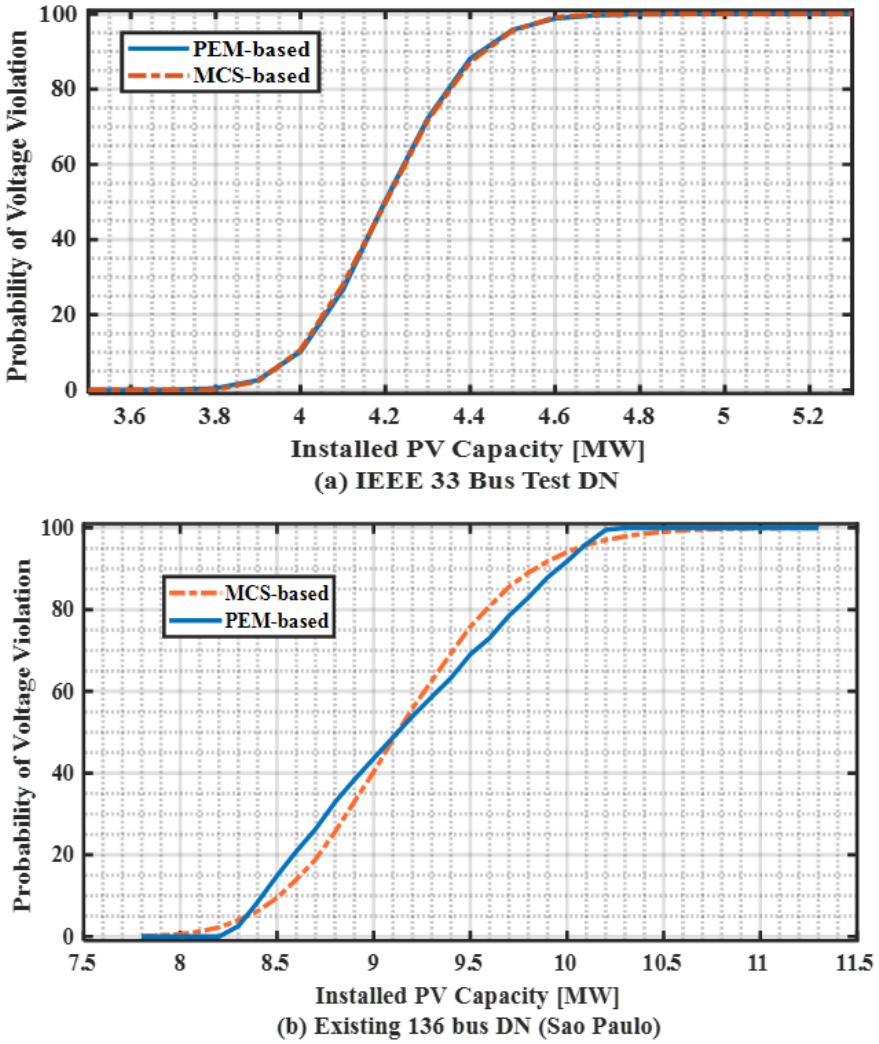

Figure 5.9: Probability of over-voltages as a function of installed PV size

The values obtained using the benchmark MCS method and the proposed method seem to be highly close when applied to the IEEE 33 bus DN estimations. However, the graphs in figure 5.8 (b) show slight differences between the MCS-evaluated results and those of the proposed method when applied to the existing 136-bus DN. This can be attributed to the differences between the IEEE bus DN and the existing 136-bus DN in terms of sheer physical size and load demand. The IEEE 33 bus network is 4 times smaller than the 136-bus DN and has a net active power demand of around 3.715 MW compared with 18.333 MW for 136-bus DN. These differences in physical size and demand render the 136-bus DN more susceptible to erroneous calculations.

Figure 5.9 shows the variations of estimated PVHC against probability of violations for the two systems being compared, with the accompanying errors in the estimations.

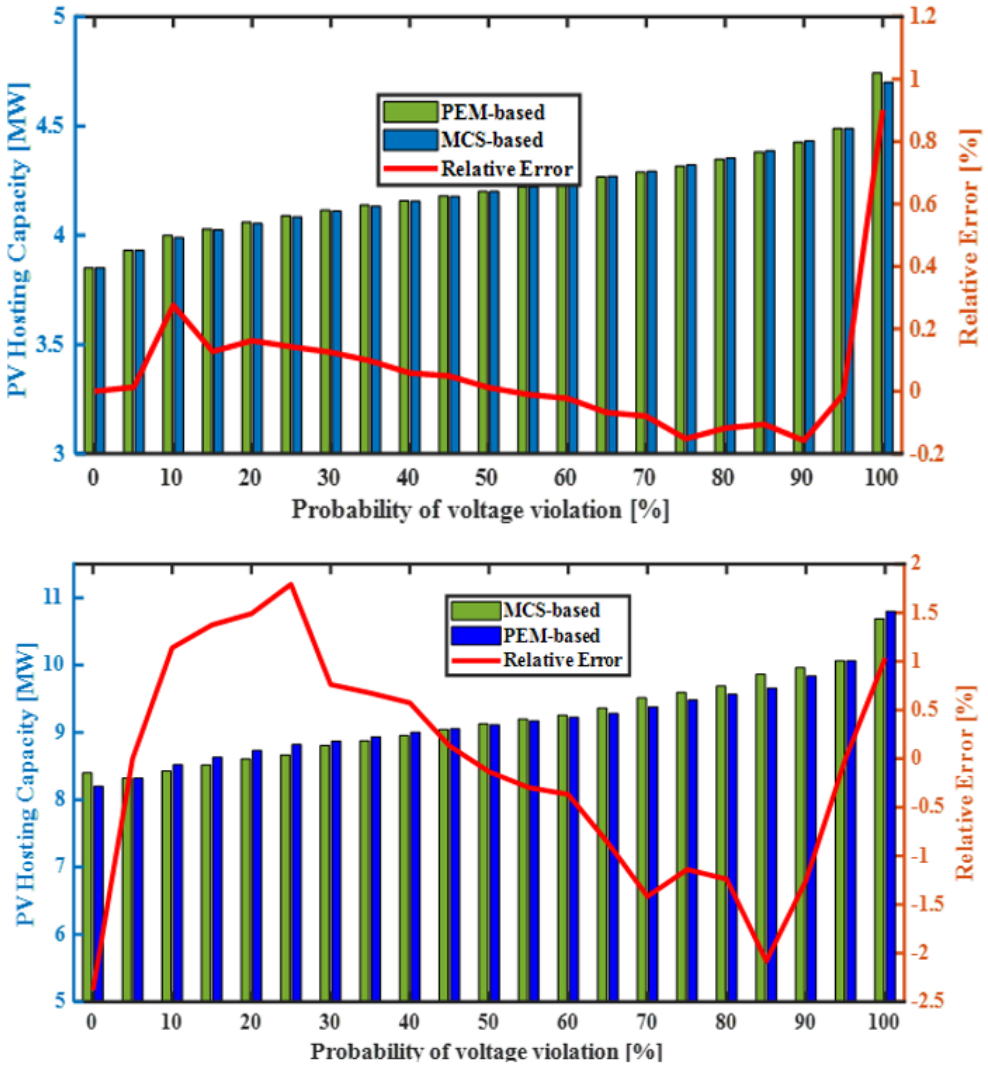

Figure 5.10: PVHC and error as a function of voltage violation probability

In both cases, the relative error starts from the positive values up to the mid-point of PV sizes and then goes to the negative side. This could be because, with the increase in PV sizes at the installation points, the variance of the PV outputs also increases. This acts to increase the spread of data for the PV output in the analysis. This essentially means, while the average values of PV output and, consequently, the calculated concentrations for the PEM estimation increase linearly, the MCS estimation is not affected by this spread thus generating a much different result.

The relative error for the IEEE 33 bus DN is in the range -0.20 % to 0.9 % for all probable values of voltage violation. For the 136-bus DN, it lies between -2.5% and +2%. The errors observed in the much larger 136-bus DN are nearly 3 times as high as those obtained for the IEEE 33 bus network, which is 4 times smaller. Clearly the error in calculation becomes bigger as the network becomes larger in size (number of buses). This is owed to the fact that the

number of variables increases as the network increases which in turn increases the possibility of inaccuracies when approximate methods such as the proposed method are applied.

However, the size of relative error obtained in both cases is quite low (2.5% maximum) and similar trends in relative error are observed for both the IEEE 33-bus DN and the 136-bus DN.

Furthermore, the RMSE calculated using equation 5.16 shows that the proposed method is relatively accurate and within plausible limits.

The RMSEs are 0.01031 MW and 0.10633 MW for the IEEE 33 bus and the 136 bus networks respectively. This, respectively, represents 2.413% and 1.33% when the individual PVHC estimates are used as base values for each network. Again, this means that the proposed method is of acceptable accuracy as the errors are substantially low.

5.4.2 Computation Speed

In as much as the accuracy of computing takes center-stage in the calculation of stochastic PVHC as it is used as a long-term planning metric, the speed of calculation is also important [30]. This is because existing distribution networks may have several hundreds to thousands of buses (nodes) and several distributed generators within the network. This means the number of input random variables may be too many and thus a slower method of calculation (like the MCS) may not give a result in a reasonable timeframe. A quicker method, however, might offer a solution in an acceptable timeframe.

Table 5.2 shows the computation speed for PEM-based and MCS-based stochastic PVHC estimation. The MCS is run with 100000 simulations per PV size consideration.

Table 5. 2: Calculation time (seconds) for PEM and MCS based PVHC estimation.

Method/Network	IEEE 33-bus	136-bus
MCS-based	103.839	4477.842
Proposed	2.712	254.642

From table V, the proposed method is about 40 times faster when estimating the stochastic PVHC for the IEEE 33-bus distribution network and about 18 times faster when calculating for the 136-bus distribution network. As can be observed in both methods, as the number of buses (nodes) for the network increases, the calculation time also increases. In this case, the number of buses has increased from 33 to 136, indicating an increase in nodes of about 4 times, while the calculation times for the proposed method and the MCS increase 94 times and 43 times respectively.

The higher calculation speed (lower computation time) is therefore preferrable for large networks with a lot of nodes to obtain a solution in an acceptable timeframe.

5.5 Chapter Summary

This chapter introduced a method for estimating the PVHC of a DN taking into consideration the uncertainties in PV output power and load demand. The method involves two stages. The first stage employs the deterministic PSO-GD approach proposed in chapter 2 while the second

stage uses the PEM-based probabilistic approach to incorporate the various uncertainties in the network variables.

The proposed approach was applied to the IEEE 33 bus test network and the existing 136 bus network in Sao Paulo. The results obtained were benchmarked against the MCS-based probabilistic approach to ascertain the proposed method's efficacy and speed of calculation.

It was established that the proposed method is relatively accurate with a 2.5% error margin and is extremely quick (up to 93 times quicker than the MCS-based calculation). Thus, in practical networks having a few hundred to thousands of nodes, the proposed method is to be preferred to the MCS method for its high speed in calculation for relatively small price in accuracy.

CHAPTER SIX IMPACTS OF EV AND BESS ON PVHC IN DISTRIBUTION NETWORKS

6. Impacts of BESS and EV on PVHC in DN

The transport sector is another sector which heavily depends on fossil fuels for its day-to-day operations. This results in enormous amounts of carbon being emitted into the atmosphere. To reduce these carbon emissions, the recent trend has seen a huge shift in the mobility sector towards the use of Electric Vehicles (EVs) [117] and hybrid Internal Combustion Engine Vehicles (ICEV) with Plug-in EV (PEV) capabilities. With this rise in EVs and hybrid ICEV/PEVs, the electrical power demand has also gone up due to charging demands imposed by these EVs and PEVs.

Additionally, the increased penetration of renewable energy sources has prompted the integration of battery energy storage systems (BESS) in active distribution networks to improve the system resilience. The energy storage systems not only participate in the backup power supply but also have the potential to provide various distributed ancillary services [118]. The deployment of BESS also increases the distribution network potential for self-consumption PV by their charging requirements [119].

As a balancing act, EVs and ICEV/PEVs could be charged from excess PV produced by private owners. Because EVs may not necessarily park during times of excess PV production, battery energy storage systems (BESS) may be used to store the energy from PV to enable EV charging at desired times. With a higher proliferation of EV/BESS in the DN, the self-consumption of PV is increased and thus could potentially improve the PVHC of the DN [120].

As a result of increasing EV penetrations in the transport sector, the electrical power distribution system must accommodate an increased load demand for charging EVs. In this vein, the importance of robust planning in DNs cannot be overemphasized. During the planning or network reinforcement stage of the DN, it's important to have some estimations and analyses done on a wide range of EV and BESS charging loads that will be placed in the network [121]. This would ensure that during operation, the DN equipment is not overloaded or overstressed by high power flows (thermal overloads) or high operating voltages respectively.

This chapter investigates the impact of BESS and EV on the PVHC of the distribution network. It endeavors to develop models for EV and BESS charging which could be used to quantify the impact of EVs and BESSs on the PVHC of a DN. A stochastic charging schedule based on the 'Need-and-Availability' approach, is used to derive the random charging demand of the EV. A similar model is used for BESS charging demand execution. These charging demand models are then augmented to the normal demand and, ultimately, used in PVHC estimation with uncertainty consideration.

6.1 BESS Charging load demand Model

The reduced Feed-in-Tariffs (FiT) in the electricity market have made essential to increase the self-consumption of PV generated power at domestic level in the distribution network [122]. It is therefore necessary to develop a model for BESS charging load that could be useful in scheduling and/or sizing the PV system.

The BESS charging load demand is determined by the SoC of the BESS as well as the time of charge allocated to the BESS.

The state of charge of the h-th BESS at time, t depends on the previous state of charge at a time $t-1$ and the allocated time of charge, t_{ch}^{BESS}.Thus,

$$SOC_t^{BESS,h} = SOC_{t-1}^{BESS,h} + \frac{\zeta_h^{BESS}\left(\eta_{ch}^{BESS,h} P_{ch,t}^{BESS,h} t_{ch}^{BESS}\right)}{E_{max}^{BESS,h}} - (1-\zeta_h^{BESS})\left(\frac{P_{dis,t}^{BESS,h} t_{dis}^{BESS}}{E_{max}^{BESS,h}\eta_{dis}^{BESS,h}}\right) \tag{6.1}$$

Where $SOC_t^{BESS,h}$ is the state-of-charge of the BESS of h-th type (defined by capacity and/or make); $SOC_{t-1}^{BESS,h}$ is previous state charge before BESS charging begins; ζ_h^{BESS} is a binary variable ($\zeta_h^{BESS} \in \{0,1\}$) which represents the status of the BESS operating mode (charging/discharging); $\eta_{ch}^{BESS,h}$ BESS charging efficiency; $\eta_{dis}^{BESS,h}$ discharge efficiency of the h-th BESS $E_{max}^{BESS,h}$ maximum capacity of h-th BESS; $P_{ch,t}^{BESS,h}$ charging power of the h-th BESS at time t; $P_{dis,t}^{BESS,h}$ discharging rate of the h-th BESS at time t; t_{ch}^{BESS} charging time of BESS, t_{dis}^{BESS} discharge time of the BESS.

From equation (6.1), the charging demand of the h-th BESS is given by equation (6.2).

$$P_{ch,t}^{BESS,h} = \begin{cases} \frac{E_{max}^{BESS,h}\left(SOC_{t+1}^{BESS,h} - SOC_t^{BESS,h}\right)}{\eta_{ch}^{BESS,h} t_{ch}^{BESS}}, \zeta_j^{BESS,h} = 1 \\ -\left(\frac{P_{dis,t}^{BESS,h} t_{dis}^{BESS}}{\eta_{dis}^{BESS,h}}\right) \quad , \zeta_j^{BESS,h} = 0 \end{cases}, SOC_{min}^{BS,h} \le SOC_t^{,h} \le SOC_{max}^{BS,h} \tag{6.2}$$

Where $SOC_{min}^{BS,h}$ and $SOC_{max}^{BS,h}$ are the minimum and maximum values of the SoC of the h-th BESS.

It should be noted that when the power flows from the grid into the BESS, charging occurs while discharging happens when the power flows in the opposite direction vis-a-vie, from the BESS to the grid.

The aggregate load imposed by a total of N_B BESS is given by equation (6.3).

$$P_{ch,t}^{BESS} = \sum_{h=1}^{N_B} P_{ch,t}^{BESS,h} \tag{6.3}$$

6.2 EV charging load demand model

The EV charging is characterized by its arrival time (plug-in time), mounted-battery capacity, plug-in period, and EV departure time (plug-out time). The aggregate charging load presented by the EV also depends on the type of EV. According to, there are five distinct EV types as shown in Table 6.1 [121].

Table 6. 1:Charging, storage, and endurance characteristics of different EV types

EV type	Battery Capacity (kWh)	Charging Power (kW)		Endurance mileage (km)
		Slow	Fast	
Private	24/40	6.6	11	150/250
Utility	40	6.6	11	250
Public	40	-	11	250
Bus	202	-	50	200
Truck	240	-	80	250

The amount of energy stored on the EV at time of departure depends on the amount of energy it had at the time of it being plugged in vis-a-vie state-of-charge (SoC). Thus, the state of charge of the EV at the departure is given as:

$$SOC_{t+1,j}^{EV,k} = SOC_{t,j}^{EV,k} + \frac{\zeta_j^{EV,k}\left(\eta_{ch}^{k} P_{ch,t,j}^{EV,k} t_{ch}^{EV,k}\right)}{E_{j,max}^{EV,k}} - \left(1 - \zeta_j^{EV,k}\right)\left(\frac{P_{dis,t,j}^{EV,k} t_{dis}^{EV,k}}{\eta_{dis}^{k} E_{j,max}^{EV,k}}\right) \quad (6.4)$$

Where $SOC_{t,j}^{EV,k}$ is the SoC of k-th EV type in the j-th fleet at time t, η_{ch}^{k} and η_{dis}^{k} are the EV charging and discharging efficiencies respectively for the k-th fleet, $t_{ch}^{EV,k}$ and $t_{dis}^{EV,k}$ are the charging and discharging time periods of k-th EV type in the j-th fleet respectively, k represents the EV type, j is the EV assigned number in the fleet, $\zeta_j^{EV,k}$ is a binary variable indicative of whether the EV is charging or discharging (moving) i.e. $\zeta_j^{EV,k} \in \{0,1\}$, $E_{j,max}^{EV,k}$ is the maximum energy storage capacity of k-th EV type in the j-th fleet.

The SoC of the EV is predefined within a prescribed finite range. The mounted battery cannot charge above a certain maximum level. It should also not be allowed to discharge below a certain minimum level. Therefore,

$$SOC_{j,min}^{EV,k} \leq SOC_{t,j}^{EV,k} \leq SOC_{j,max}^{EV,k} \quad (6.5)$$

Where, $SOC_{j,min}^{EV,k}$, $SOC_{j,max}^{EV,k}$ are the minimum and maximum allowable values of state-of-charge of EV energy storage.

Given that the vehicle is either plugged-in (arrival) for charging or plugged out (departure), the charging power depends on the initial SoC at the plug-in time and the desired SoC at the plug-out time and the available charging time. Therefore, the charging power as derived from equation 6.5 is obtained as:

$$P_{ch,t,j}^{EV,k} = \frac{\zeta_j^{EV,k} E_{j,max}^{EV,k}\left(SOC_{t+1,j}^{EV,k} - SOC_{t,j}^{EV,k}\right)}{\eta_{ch}^{k} t_{ch}^{EV,k}} \quad (6.6)$$

The EV's charging demand is thus estimated for the time between the plug-in and plug-out. This is approximated to the available charging option of either slow or fast charging. Thus,

$$P_{ch,t,j}^{EV,k} = \begin{cases} P^{ch,k}, & t_{pi} \leq t \leq t_{po} \\ 0, & otherwise \end{cases} \quad (6.7)$$

Where, $P^{ch,k}$ is the variable charging power demand by an EV of type k, t_{pi} and t_{po} are the plug-in and plug-out times of the EV respectively.

From the foregoing therefore, the aggregate charging demand imposed by the EVs on the network at any time t is estimated using equation (6.8).

$$P_{ch,t}^{EV} = \sum_{k=1}^{N_p} \sum_{j=1}^{N_j} P_{ch,j,t}^{EV,k} \tag{6.8}$$

6.3 Quantification of the Effects of BESS and EV deployment in DNs on PVHC

In this section, a case study on the impact of the EV and BESS on the PVHC is presented. Figure 6.1 shows the flow chart of the PVHC estimation process in the wake of EV and BESS deployment with their uncertainty characterizations. The solution proceeds as explained in [20]. First the optimal locations for PV installation are determined using Particle Swarm Optimization and Gradient Descent (PSO-GD) algorithm [123]. For the obtained locations, several PV output scenarios are generated using the uncertainty characteristics in equation (5.12). The loads at all nodes also generate stochastic scenarios based on the characteristics in equation (5.13).

Once the PV output and load demand stochastic scenarios are generated, they are analyzed to determine the node voltages, line power flows and other network variables using probabilistic load flow (PLF) analysis based on the point estimate method (PEM).

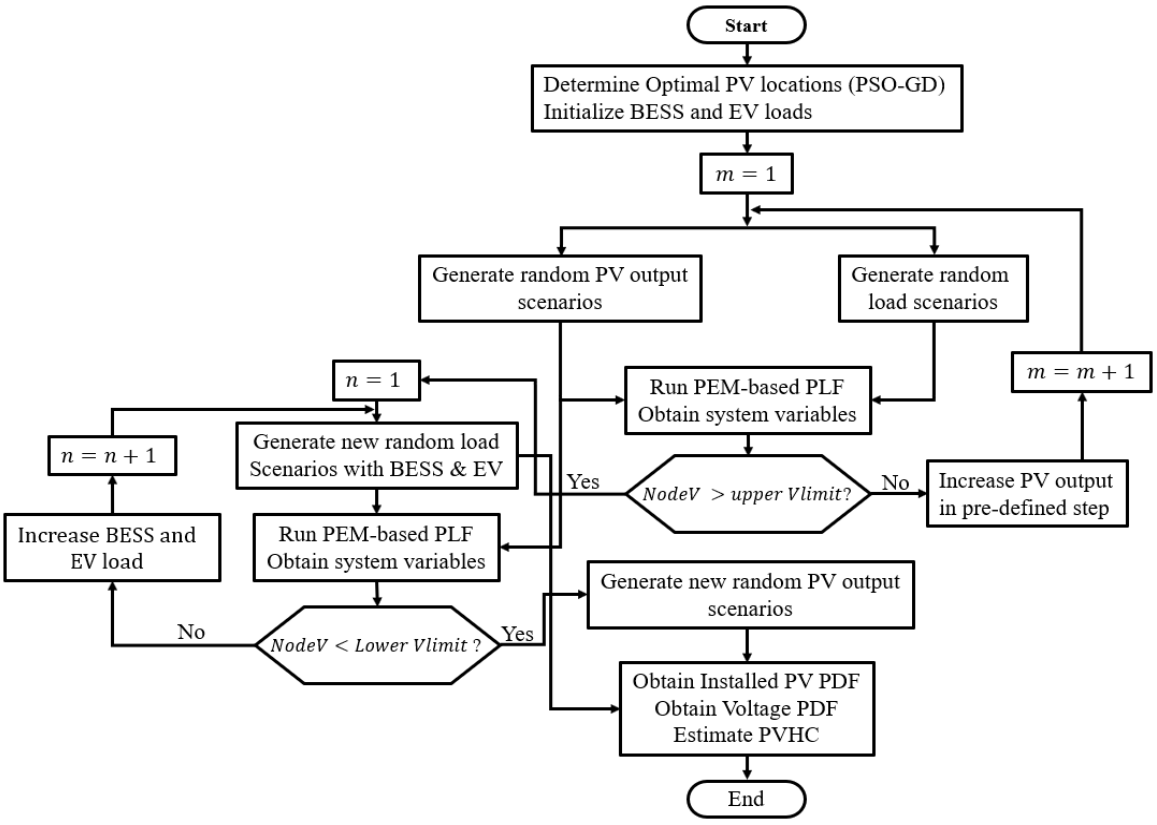

Figure 6.1: Flow chart of multi-stage estimation of PVHC of DNs with EV and BESS.

The next phase involves adding BESS and EV deployment in the network as charging loads given by equations (6.3) and (6.8). At the locations with PV installation, the BESS and EV sizes are increased by adding several EVs and BESSs in predetermined sizes until the network voltage falls just below the lower voltage bound.

Afterwards, the BESS and EV charging load (with their stochastic characteristics) at the final iteration are augmented with the normal load at the locations with PV installation. New load stochastic behavior is modeled, and new PV output scenarios are generated. With the new stochastic PV output and load demand scenarios, the procedure for estimating the PVHC, described earlier, is undertaken. The resulting PVHC is the hosting capacity of the network in the wake of BESS and EV deployment in the system.

6.4 Case Studies

6.4.1 Case A: EV Charging Station and BESS Located at PV Installation Sites

In case A, an investigation was carried out to establish the impact of deploying BESS and EV charging stations at the same nodes where there is installed PV. The procedure outlined in section 6.3 was used to generate the results.

The PSO-GD/PEM-based Stochastic tool developed in chapters 2 and 5 respectively, was employed in estimating the PVHC of the network with the increases in BESS and EV charging load demand. In this case, the PV sizes were increased in steps of 10 kW at each of the participating nodes until an over-voltage was observed.

The simulations were conducted on the IEEE 33 Test DN. Figure 6.2 shows the PDFs of the highest node voltages obtained by increasing the number of EVs and BESSs at the PV

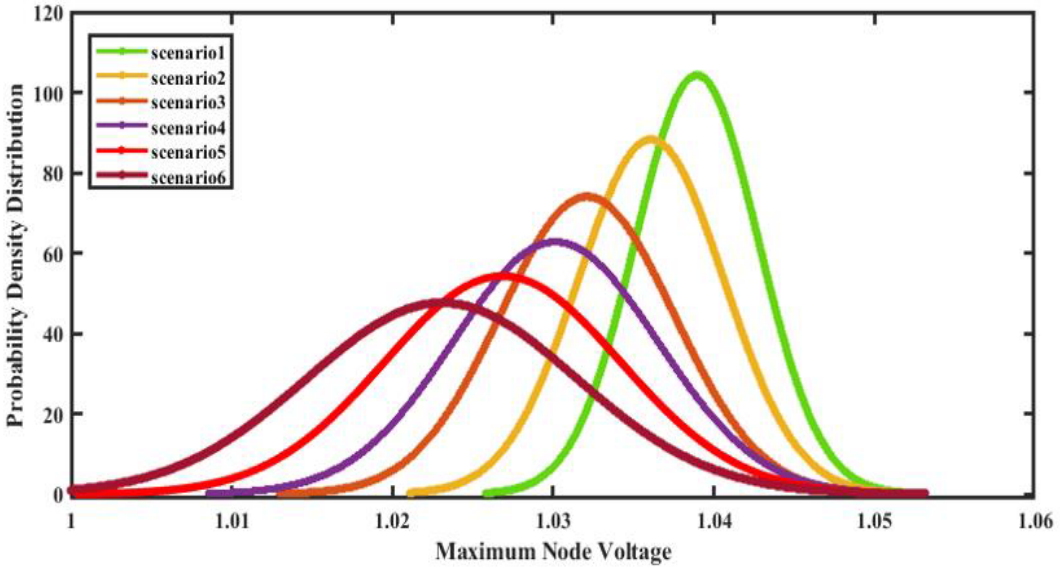

Figure 6.2: PDFs of the maximum node voltages in each EV and BESS penetration scenarios.

installation sites from 0 to 50 in steps of 10. It is observed that, as the EVs and BESSs increase, the PVHC also increases until the stopping criteria is met.

In figure 6.2, scenario 1 represents the lowest number of BESS and EVs. At this point, it is 0, in scenario 2, the number of BESS and EV is increased by 10 at each of the participating nodes (nodes with PV installation). We observe that the highest node voltage PDF of scenario 2 has a bigger spread compared to the one in scenario 1. This is because of the relative increase in load owing to the BESS and EV charging demand. This increases the PV self-consumption resulting in reduced rises in voltages due to increases in PV size increases. Figure 6.3 shows the changes in standard deviation of the highest node voltages against the mean values of the node voltages for each scenario.

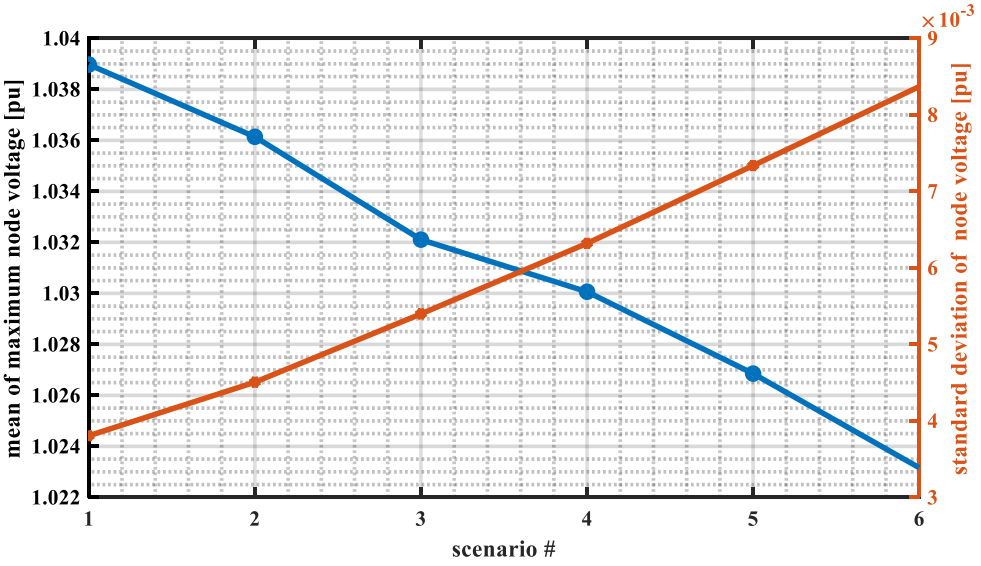

Figure 6.3: Variations of mean and standard deviation of maximum node voltages

Table 6.2 gives the estimated changes in mean voltages observed, the standard deviation of the voltages and the PVHC as the BESS and EV charging load is increased through the scenarios.

Table 6. 2: Variations of PVHC and observed node voltages against BESS and EV load changes.

Scenario	EV load [kW]	BESS load [kW]	Min node Vmax [pu]	Max node Vmax [pu]	Mean Vmax [pu]	Std Vmax [pu]	PVHC [kW]
1	0	0	1.026	1.050	1.0390	0.0038	3764
2	70	40	1.022	1.050	1.0361	0.0045	4200
3	140	80	1.013	1.050	1.0321	0.0054	4594
4	210	120	1.009	1.050	1.0301	0.0063	5063
5	280	160	1.001	1.050	1.0264	0.0073	5485
6	350	200	1.000	1.050	1.0230	0.0084	5890

For the subsequent scenarios, the trend continues until scenario 6 when all PV installed nodes have 50 BESS and EV. At this penetration level, the highest node voltage observed falls below

the threshold set by the stopping criteria of 1 pu. The PVHC for this final scenario is calculated at 5890 kW. Figure 6.4 shows the variations of PVHC and BESS/EV load demand changes.

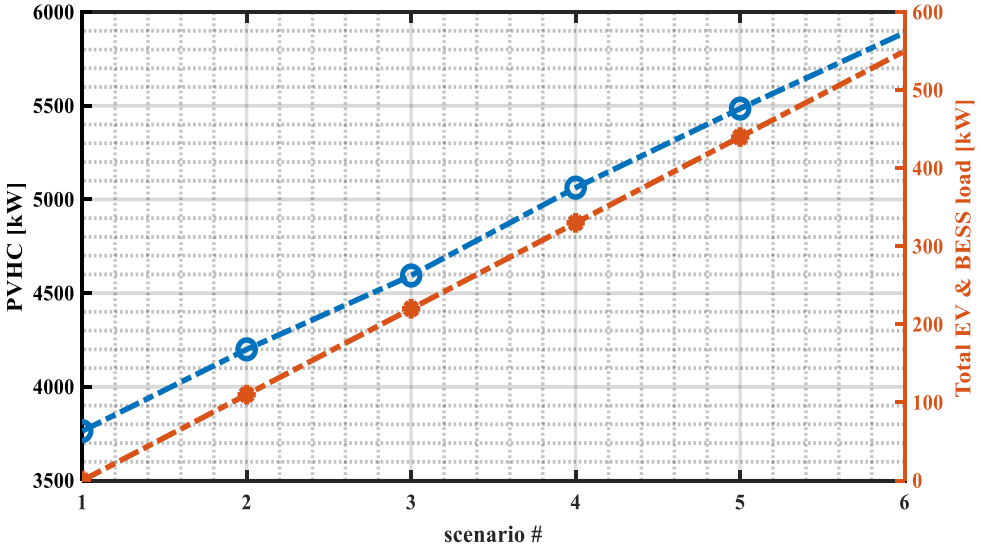

Figure 6.4: Variations of PVHC estimates with BESS/EV load for each scenario.

It is observed that there is a strong correlation between the BESS and EV load demand and the estimated PVHC as increases in BESS and EV load demand result in subsequent increases in estimated PVHC values.

For the scenarios under discussion, the net demands are shown in figure 6.5. The net demand at 0 EV results in excess PV generation compared to the network demand. This results in a net export of power to the grid. This export progressively reduces as the number of BESS and EV increases until there is a net import of power for the final scenario.

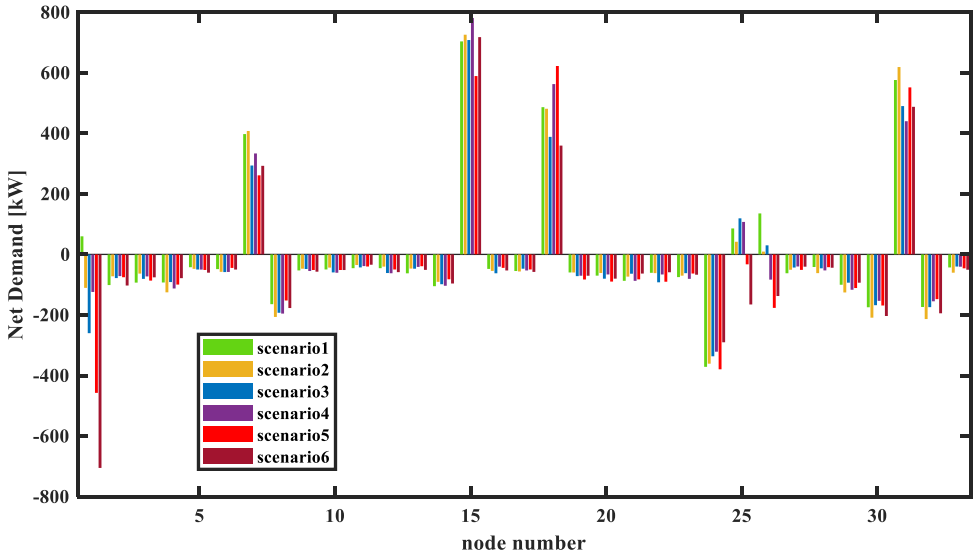

Figure 6.5: Net demand on the DN nodes for each scenario

6.4.2 Case B: EV Charging Station Randomly Located within DN

In this case, the location of BESS is fixed at the PV installation sites while the locations of EV charging stations are randomly selected from the available network nodes. The approach described in the earlier section was also applied to this case. Table 6.3 gives the simulation results for 10 different runs of the algorithm. For each run, the EV charging sites are randomly generated, the PVHC for each EV size is estimated and its correlation coefficient is obtained.

Table 6. 3: PVHC, correlation coefficients for randomly generated PV sites

Simulation	EV Charging Sites	PVHC [kW]						Correlation
		0EV	10EV	20EV	30EV	40EV	50EV	
1	6,7,23,24,27,29	3830	3990	4370	4940	5690	6000	0.98314641
2	9,15,17,19,28	3850	4340	5270	6000	6000	6000	0.929926683
3	3,10,14,23,25,27	3800	4100	4650	5500	6000	6000	0.975684072
4	3,5,13,15,20,33	3800	4150	4800	5700	6000	6000	0.966299397
5	7,9,11,13,19,27	3800	4150	4900	5900	6000	6000	0.948700624
6	3,15,22,24,27,31	3800	4000	4500	5200	6000	6000	0.939141881
7	12,13,20,27,29	3800	4200	4950	6000	6000	6000	0.977045987
8	10,18,21,29,30,32	3840	4220	4980	6000	6000	6000	0.938687407
9	11,12,18,19,19,32	3840	4270	5100	6000	6000	5930	0.928136107
10	4,6,21,22,26,31	3820	3960	4270	4680	5210	5910	0.974052764

It has been established that in these cases, the highest amount of PVHC attained is limited to 6000 kW. This is slightly higher than that obtained in case 1 were the locations of BESS and EV charging sites where the same as the locations for PV installation nodes.

In the same vein, the correlation coefficient between estimated PVHC and the number of EVs is found to lie between 0.928 and 0.983. This indicates that there is a significantly strong

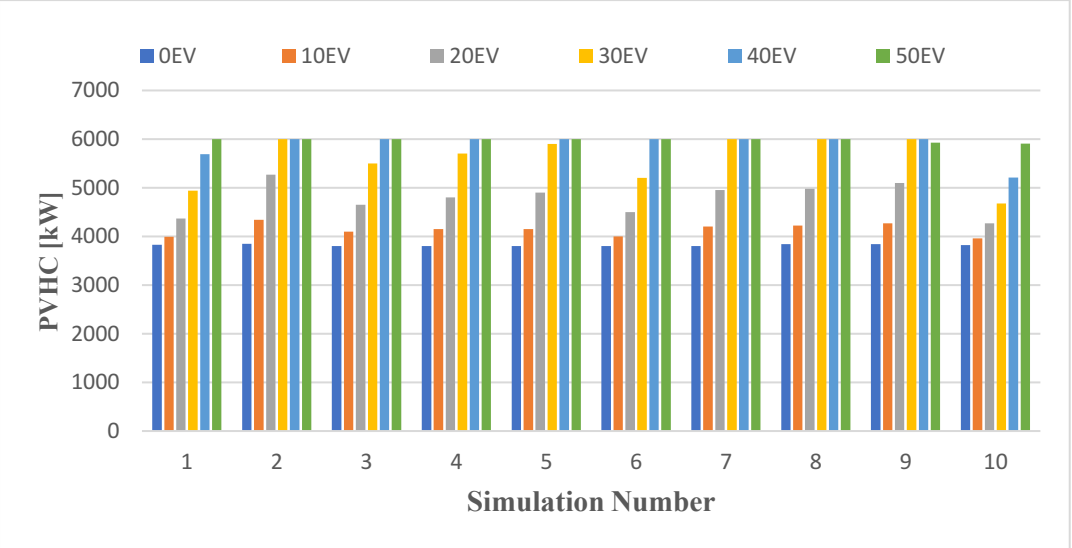

Figure 6.6: Variations of PVHC estimates in simulation runs against number of EVs.

relationship between changes in EV sizes and estimated PVHC. Figure 6.6 shows the variations of PVHC estimates in each simulation run.

In all simulation runs, the PVHC increases when the number of EV increases. However, when the EVs reach a total of between 40 and 50 per node (representing a total prospective EV charging load of 1680-2100 kW), the PVHC seems to reach its peak value of 6000 kW. Figure 6.7 shows these simulation results.

It has been seen that the EV charging load increases result in increases in the estimated PVHC of the DN up to a certain level. Above this level, the increased line power flows from the PV generators result in violations and thus the power from PVs is restricted.

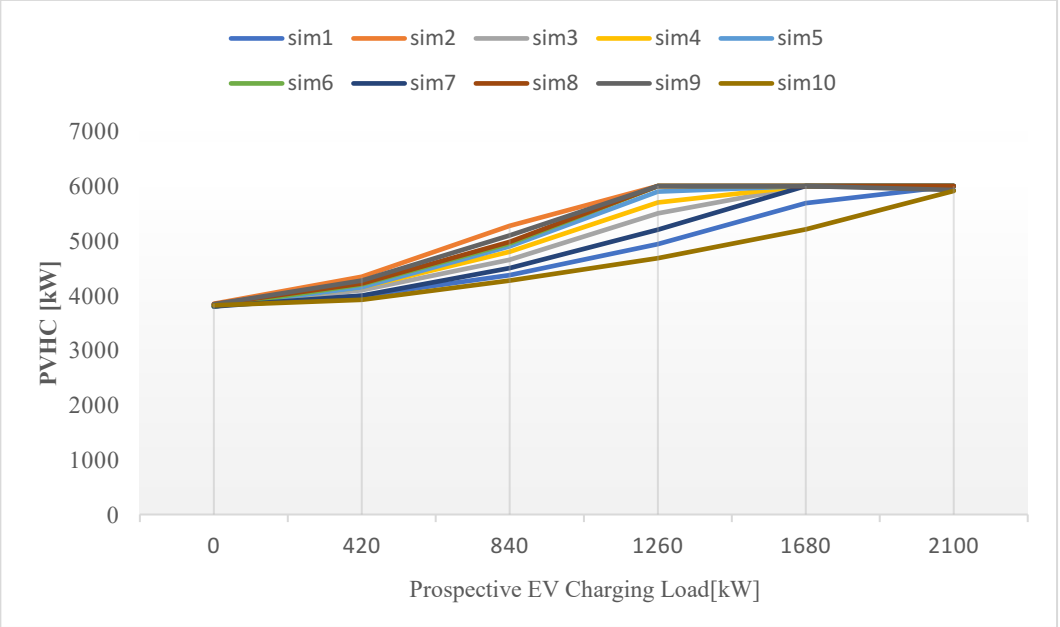

Figure 6.7: PVHC estimate as a function of EV charging load.

6.5 Chapter Summary

In this chapter, an investigation into the potential effects of EV and BESS charging was carried out. The chapter has presented a load demand model for BESS and EV charging load to use in quantifying the impacts of BESS and EV charging on the PVHC of the DN. For both the EV load model and the BESS charging load model, the state of charge of the storage system as well the available period of charging is pivotal to the estimation of the demand imposed by these loads.

Even though there are several kinds of EVs available, this study was restricted to privately owned vehicles with storage capacities ranging from 24 to 40 kWh and charging requirements of 6.6 kW, for slow chargers, and 11 kW for fast chargers. The BESS was also restricted to home-owned BESS with capacities of 20-30 kWh and charging demands between 4 and 5kW.

A multi-stage PVHC estimation algorithm encompassing the normal load as well as BESS and EV charging load has also been developed and described in detail. It uses a forward-backward method. First it estimates the PVHC of the DN without having the EV and BESS deployed in the network. Then it deploys EV and BESS in predetermined step sizes to estimate how much EV and BESS load would reduce the observed node voltages just below a certain minimum

threshold. Finally, PV sizes in exact ratios of the values estimated for a case without EV and BESS are incremented until the upper node voltage limit is observed. The amount which leads to this conclusion stands as the PVHC at a particular penetration of EV and BESS. This algorithm has been applied to 2 distinct cases.

In the first case, the locations of BESS and EV charging stations were the sites (nodes) with PV installed. In the second case, the EV charging sites were randomly selected. When applied to the IEEE 33 bus network, the first case had a lower value of PVHC of about 5850 kW compared with simulation results of the second case which yielded 6000 kW in most simulation scenarios.

Moreover, it was observed that there was a limit to the amount of PVHC which could be obtained at the higher values of EV numbers because of the line flow limitations.

CHAPTER SEVEN
CONCLUSIONS

7. Conclusions

This thesis proposes an optimization method based on hybrid particle swarm intelligence and the steepest gradient descent philosophy. In its execution, the method is aimed at addressing the challenges and limitations of both the particle swarm optimization and the gradient descent algorithm while harnessing the optimization power which lies in each of the methods.

The first chapter introduces the background to the research, gives the current state of the research in the estimation of PV hosting capacity and highlights the need for further research. It also highlights the mainstream approaches to estimating the hosting capacity of photovoltaics in the distribution networks available at the present.

The second chapter focuses on describing the proposed optimization method using hybrid particle swarm and gradient descent algorithms (PSO-GD). It highlights the way the method is made amiable to the PVHC problem by modifying the velocity component of the standard PSO using the first derivative of the objective function provided by the problem structure and its gradient component.

In the third chapter, the problem of PVHC is defined. A formulation of the problem is provided, and a model algorithm for solving the problem using PSO-GD is given. This model algorithm is applied to three distinct cases. These cases are the 2 IEEE test cases vis-a-vie IEEE 33 test bus network and the IEEE 69 bus test network and the existing 136 bus network of Brazil's Sao Paulo. The generated results showed that the proposed algorithm is superior to many other methods also presented in the chapter. The results also show that the proposed method is highly robust through its show of order-1 and order-2 stability.

Chapter 4 introduces the concept of PVHC enhancement using the PV inverters with volt-var function. The proposed method developed in chapters 2 and 3 is extended to this chapter to validate the efficacy of the proposal. It is shown that the use of PV inverters with the volt-var control capability can massively increase the PVHC of the distribution network.

In chapter 5, the proposed algorithm is applied in estimating the PVHC of the network with uncertain random variables. The proposed method is combined with PEM-based probabilistic power flow analysis to estimate the hosting capacity of IEEE 33 bus test system and the existing 136 bus network. The results obtained indicate that the proposed method is much faster compared to mainstream probabilistic methods such as the Monte Carlo Simulations.

In the final chapter, an investigation into the impacts BESS and EV have on the PVHC of the distribution networks is launched. The chapter begins by presenting a load demand model for BESS and EV charging load to use for quantifying the impacts of BESS and EV charging on the PVHC of the DN. The chapter proceeds to propose a method of incorporating the charging load demand into the system normal loading structure and an algorithm to solve this issue is also presented. Two case studies are analyzed in this chapter. One case study considered the BESS and EV to be located at the PV sites. The other case study considered random EV sites. The results of the studies show a certain limit of PVHC for a given number of EV due to operating limitations of the DNs.

Overall, a new method of estimating the distribution network's maximum potential to host photovoltaic generated power using PSO-GD presented in this study is superior to other

methods and is validated to be faster and order-1 and order-2 stable. The study has shown that the proposed method yields remarkable results when combined with stochastic analysis to incorporate uncertainties in network variables.

REFERENCES

References

[1] M. Schmela, A. Beauvais, N. Chevillard, M. Paredes, M. Heisz and R. Rossi, “Global market outlook for solar power 2018-2022,” Africa-EU renewable energy cooperation programme (RECP), solar power europerue, Brussels, 2022.

[2] P. K. C. a. M. O. Denholm, “On the Path to SunShot: Emerging Issues and Challenges in Integrating High Levels of Solar into Electrical Generation and Transmission,” Golden, CO: National Renewable Energy Laboratory. NREL/TP-6A20-65800, California, 2016.

[3] A. O. H. M. H. S. M. M. Busra Uzum, “Rooftop SolaPenetration Impacts on Distribution Network and Further Growth Factors-A Comprehensive Review,” *Electronics 2021, Vol 10, No. 55,* vol. 10, no. 55, pp. 1-31, 2021.

[4] J. D. Zulu Esau, “Reliability assessment in active distribution networks with detailed effecte of PV systems,” *Modern Power Systems and Clean Energy,* vol. 2, no. 1, pp. 59-68, 2014.

[5] R. R. Pathomthat Chiradeja, “An Approach to Quantify the Technical Benefits of Distributed Generation,” *IEEE TRANSACTIONS ON ENERGY CONVERSION,* vol. 19, no. 4, pp. 764-773, December 2004.

[6] P. Bryan, R. Broderick, B. Mather, M. Coddington, K. Baker, F. Ding, M. Reno, M. Lave and A. Bharatkumar, “On the Path to SunShot: Emerging Issues and Challenges in Integrating Solar with the Distribution System,” Golden, CO: National Renewable Energy Laboratory, Denver, 2016.

[7] B. P. I. K. D. K. Himanshu Jain, “Studying the Impact of Distributed Solar PV on Power Systems using Integrated Transmission and Distribution Models,” in *2018 IEEE PES T&D Conference and Exposition*, Denver, Colorado, 2018.

[8] M. Karimi, H. Mokhlis, K. Naidu, S. Uddin and A. Bakar, “Photovoltaic penetration issues and impacts in distribution network- A review,” *Renewable and Sustainable Energy Reviews,* pp. 594-605, 2016.

[9] L. A. C. L. T. H. M. E.-F. Reinado Tonkoski, “Coordinated Active Power Curtailment of Grid Connected PV Inverters of Overvoltage Prevention,” *IEEE Transactions on Sustainable Energy,* vol. 2, no. 2, pp. 139-147, April 2011.

[10] H. K. Jacobsen and S. T. Schroder, “Curtailment of renewable generation: Economic optimality and incetives,” *Energy Polic,* vol. 49, pp. 663-675, 2012.

[11] O. Eric, J. Cruce and K. Xu, “Solar PV curtailment in changing grid and Technological contexts,” Golden, CO: National Renewable Energy Laboratory, Denver.

[12] L.M.Cipcigan and P. Taylor, “Investigation of the reverse power flow requirements of high penetrations of small-scale embedded generation,” *IET Renewable Power Generation,* vol. 1, no. 3, pp. 160-166, 2007.

[13] R. Singh, P. Tripathi and K. Yatendra, “Impact of Solar Photovoltaic Penetration in Distribution Network,” in *2019 3rd International Conference on Recent Developments in Control, Automation and Power Engineering (RDCAPE)*, 2019.

[14] S. Lewis, “Analysis and management of the impacts of a high penetration of photovoltaic systems in an electricity distribution network,” in *Innovative Smart Grid Technologies Asia (ISGT), 2011 IEEE PES* , 2011.

[15] I. T. Papaioannou, A. S. Bouhouras, A. G. Marinopulos, M. C. Alexiadis, C. S. Demoulias and D. P. Labridis, “Harminc Impact of Small Photovoltaic Systems Connected to the LV Distribution Network,” in *5th International Conference on European Electricity Market*, 2008.

[16] S. S. Alanzi and R. M. Kamel, “Photovoltaic maximum penetration limits on medium voltage overhead and underground cable distribution feeders: A comparative study,” *Energies,* vol. 14, 2021.

[17] S. S. Anamika Dubey, “On estimation and sensitivty Analysis of distribution circuits photovoltaic hosting capacity,” *IEEE Transactions on Power Systems,* vol. 32, no. 4, pp. 2779-2789, 2017.

[18] J. M. D. Z. A. S. A. H. M. Mohammad Seydali Seyf Abad, “Probabilistic Assessment of Hosting Capacity in Radial Distribution Systems,” *IEEE TRANSACTIONS ON SUSTAINABLE ENERGY,* vol. 9, no. 4, pp. 1935-1947, 2018.

[19] M. B. N. E. Enock Mulenga, “Solar PV stochastic Hosting Capacity in Distribution Networks considering Aleatory and Epistemic uncertainties,” *Electrical Power and Energy Systems,* vol. 130, 2021.

[20] E. Zulu, R. Hara and H. Kita, “A flexible stochastic PV hosting capacity framework considering network over-voltage tolerance,” *Energy Reports,* vol. 9, no. supplement 1, pp. 529-538, 2023.

[21] A. Koirala, T. V. Acker, R. D'hulst and D. V. Hertem, “Hosting Capacity of photovoltaic Systemsin low-voltage distribution systems: A benchmark of deterministic and stochastic approches,” *Renewable and Sustainable Energy Reviews,* vol. 155, 2022.

[22] M. H. B. Sarah K. Ronnberg, “Hosting Capacity of the Power Grid for Renewable Electricity Production and New Large Consumption Equipment,” *Energies,* vol. 10, pp. 1-28, 2017.

[23] M. B. H. E. N. Mulenga Enock, “A review of hosting capacity quantification methods for photovoltaics inlow-voltage distribution grids,” *Electrical Power and Energy Systems,* vol. 115, pp. 1-13, 2020.

[24] I. M. J. F. Simon Heslop, “Maximum PV generation estimation method for residential low voltage feeders,” *Sustainable Energy, Grids and Networks,* vol. 7, pp. 58-69, 2016.

[25] M. B. K. K. A. Y. C. Schwaegerl, “Voltage Control in Distribution Systems as a Limitation of the Hosting Capacity for Distributed Energy Resources,” in *18th International Conference on Electricity Distribution (CIRED)*, Turin, 2005.

[26] D. L. J. W. Rasmus Luthander, “Large-scale integration of photovoltaic power in a distribution grid using power curtailment and energy storage,” *Solar Energy,* vol. 155, pp. 1319-1325, 2017.

[27] J. U. P. S. A. A. Chathurangi D., “A generalized Deterministic Approach to Evaluate PV Hosting Capacity of LV Distribution Networks Under Different Operating Conditions,” in *Hosting Capacity for Smart Grids*, Zurich, Springer, 2020, pp. 141-177.

[28] S. P. A. S. N. G. K. R. N. Nand Kishor Meena, “Improved Elephant Herding Optimization for Multi-objective DER Accomodation in Distribution Systems,” *IEEE Transactions on Industrial Informatics,* pp. 1029-1039, 2018.

[29] B. S. J. D. Imran Ahmad Quadri, “A comprehensive technique for optimal allocation of distributed energy resources in radial distribution systems,” *Applied Energy,* pp. 1245-1260, 2017.

[30] K. M. U. L. J. A. Aamir Ali, “Optimal Site and Size of Distributed Generation Allocation in Radial Distribution Network Using Multi-Objective Optimization,” *Modern Power Systems and Clean Energy,* vol. 9, no. 2, pp. 404-415, 2021.

[31] A. M. Moradi M. H., “A combination of genetic algorithm and particle swarm optimization for optimal DG location and sizing in distribution systems,” *Electrical Power and Energy Systems,* pp. 66-74, 2012.

[32] S. Kikuchi, M. Machida, J. Tamura, M. Imanaka, J. Baba, D. Iioka, K. Miura, M. Takagi and H. Asano, “Hosting Capacity Analysis of Many Distributed Photovoltaic Systems in Future Distribution Networks,” in *IEEE Innovative smart grid technologies - Asia 2017*, 2017.

[33] P. McNutt and J. Hambrick, “Impact of SolarSmart subdivisions on SMUD's distribution system,” National Renewable Energy Laboratory, Sacramento, California, 2009.

[34] R. Pandi, Z. H. and W. Xiao, “Determining Optimal Locations and Size of Distributed Generation Resources Considering Harmonic and Protection Coordination Limits,” *IEEE Transactions on Power Systems,* vol. 28, no. 2, pp. 1245-1254, 2013.

[35] M. Ebad and W. M. Grady, “An approach for assessing high-penetration PV impact on distribution feeders,” *Electric Power Systems Research,* vol. 133, pp. 347-354, 2016.

[36] K. Coogan, M. Reno, S. Grijalva and R. J. Broderick, “Locational Dependence of PV Hosting Capacity Correlated with Feeder Load,” in *2014 IEEE PES TD conference and exposition*, 2014.

[37] K. P. B., A. D. T. and C. A. J, “An Investigation into the technical impacts of microgeneration UK-type LV distribution networks,” in *Australasian Universities Power Engineering Conference (AUPEC2016)*, 2016.

[38] T. Gush, C.-H. Kim, S. Admasie, J.-S. Kim and J.-S. Song, “Optimal Smart Inverter Control for PV and BESS to Improve PV Hosting Capacity of Distribution Networks using Slime Mould Algorithm,” *IEEE Access,* vol. 9, pp. 52164-52176, 2021.

[39] O. P. V. Tejna Khosla, “An Adaptive Hybrid Particle Swarm Optimizer for Constrained Optimization Problem,” in *2021 International Conference in Advances in Power, Signal, and Information Technology (APSIT)*, New Delhi, 2021.

[40] R. K. A. A. F. Vahid Behravesh, “Stochastic analysis of solar and wind hybrid rooftop generation systems and their impact on voltage behavior in low voltage distribution systems,” *Solar Energy,* vol. 166, pp. 317-333, 2018.

[41] I. S. T. K. J. N. J. D. M. O. D. F. Yaosuo Xue, “Voltage Impact Analyses of Solar Photovoltaics on Distribution Load Tap Changer Operations,” in *North American Power Symposium (NAPS)*, 2017.

[42] M. S. Misurovic Filip, “Numerical Probabilistic Load Flow Analysis in Modern Power Systems with Intermittent Energy Sources,” *Energies 2022,* vol. 15, pp. 1-20, 2022.

[43] I. M. S. Constante-Flores G. E., “Data Driven Probabilistic Power Flow Analysis for Distribution Systems with Renewable Energy Sources using Monte-Carlo Simulations,” *IEEE Transactions on Industry Applications,* vol. 55, no. 1, pp. 174-181, 2019.

[44] R. K. A. A. F. Vahid Behravesh, “Stochastic analysis of solar and wind hybrid rooftop generation systems and their impact on voltage behavior in low voltage distribution systems,” *Solar Energy,* pp. 317-333, 2018.

[45] T. M. D. J. Vikas Singh, “Probabilistic Load Flow Considering Load and Wind Power Uncertainties using Modified Point Estimation Method,” in *2022 3rd Internationational Conference on Smart Grid and Renewable Energy (SGRE)*, Doha, 2022.

[46] M. T. J. D. Singh V., “Uncertainty handling techniques in power systems: A critical review,” *Electri Power Systems Research,* 2022.

[47] F. W. Y. L. F. X. Chenxi Wu, “Probabilistic load flow analysis of photovoltaic generation with plug-in electric vehicles,” *Electrical Power and Energy Systems,* vol. 64, pp. 1221-1228, 2015.

[48] F. B. J. Cordero B. Luis, “Probabilistic Power Flow Analysis Based on Point Estimate Method for High Penetration of Photovoltaic Generation in Electrical Distribution Systems,” *Sociedade Brasileira de Automatica,* vol. 2, no. 1, 2020.

[49] Y. M. R. B. M. N. Kabir, “Probabilistic load flow for distribution systems with uncertain PV generation,” *Applied Energy,* vol. 163, pp. 343-351, 2016.

[50] N. Nima and N. R. Sajad, “Solving probabilistic load flow in smart distribution grids using heuristic methods,” *Journal of Renewable and Sustainable Energy,* vol. 7, p. 043138, 2015.

[51] S. D., M. F., Ronnberg S.K, M. J. and B. M.H.J, “Stochastic assessment of voltage unbalance due to single phase-connected solar power,” *IEEE Transactions on Power Delivery,* vol. 32, no. 2, pp. 852-861, 2017.

[52] W. C., D. Z.Y. and W. K.P., “Probabilistic load flow computation using first-order second-momeent method,” in *IEEE Power and Energy Society Meeting*, 2012.

[53] L. D.D., P. K.V., N. D. V., N. N.T.A. and B. A., “An enhancement to cumulant-based probabilistic power flow methodologies,” in *IEEE Innovative Smart Grid Technologies - Asia (ISGT)*, 2015.

[54] M. Aien, M. Fotuhi-Firuzabad and F. Aminifar, “Probabilistic Load Flow in Correlated Uncertain Environment using Uncented Transformation,” *IEEE Transactions on Power Systems,* vol. 27, no. 4, pp. 2233-2241, 2012.

[55] R. Torquato, D. Salles, C. O. Pereira, P. C. M. Meira and W. Freitas, “A comprehensive Assement of PV hosting capacity on Low-voltage distribution systems,” *IEEE Transactions on Power Delivery,* vol. 33, no. 2, pp. 1002-1012, 2018.

[56] F. Ding and B. Mather, “On distributed PV hosting capacity estimation sensitivity study, and improvement,” *IEEE Transactions on sustainable energy,* vol. 8, no. 3, pp. 1010-1020, 2017.

[57] D. J. M. B. Reno M.J., “Motivation and requirements for quasi-static time series (QSTS) for distribution system analysis,” *IEEE Power and Energy Society,* pp. 1-5, 2017.

[58] S. G. M. J. R. R. J. B. Jeremiah Deboever, “Fast Quasi-Static Time-Series (QSTS) for yearlong PV impact studies using vector quantization,” *Solar Energy,* vol. 159, pp. 538-547, 2018.

[59] M. A. D. M. A. C. I. P. M. Y. S. A.-K. v. K. Mark Z. Jacobson, “Impacts of the greeg new deal energy plans on grid stability, costs, jobs, health, and climate in 143 Countries,” *One Earth,* vol. 1, pp. 449-463, 2019.

[60] S. K. R. Math H. J. Bollen, “Hosting Capacity of the Power Grid for Renewable Electricity Production and New Large Consumption Equipment,” *Energies,* vol. 10, pp. 1-28, 2017.

[61] S. H. A. A. A. Y. A. A. F. Z. Sherif M. Ismael, “State-of-the-art of Hosting capacity in modern power systems with distributed generation,” *Renewable Energy,* vol. 130, pp. 1002-1020, 2019.

[62] T. F. Moro Vinicius, “A Review on Techniques to Increase Hosting Capacity of Distribution Systems to DERs,” in *2021 Workshop on Communication Networks and Power Systems (WCNPS)*, 2021.

[63] S. V. D. G. B. G. Emiliano Dall'Anese, “Optimal Dispatch of Photovoltaic Inverters in Residential Distribution Systems,” *IEEE Transactions on Sustainable Energy,* vol. 5, no. 2, pp. 487-498, 2014.

[64] R. H. H. K. Esau Zulu, “Distribution Network PV Hosting Capacity Improvement by Volt-Var Optimization using Hybrid PSO-GD Algorithm,” in *2022 National Conference of the Institute of Electrical Engineers of Japan*, 2022.

[65] M. L. Ammar Ashard, “A stochastic Assessment of PV Hosting Capacity Enhancement in Distribution Network Utilizing Voltage Support Techniques,” *IEEE Access,* vol. 7, pp. 46461-46471, 2019.

[66] L. F. O. Andreas T. Procopiou, “Voltage Control in PV-Rich LV Networks Without Remote Monitoring,” *IEEE Transactions on Power Systems,* vol. 32, no. 2, pp. 1224-1236, 2017.

[67] R. K. Varma, “PV STATCOM,” in *Smart Solar PV inverters with Advanced Grid Support Functionalities*, IEEE Press, 2022, pp. 107-144.

[68] K. D. M. K. D. G. S. S. M. B. T. Stetz, “Techno-Economic Assessment of Voltage Control Strategies in Low Voltage Grids,” *IEEE Transactions on Smart Grids,* vol. 5, no. 4, pp. 2125-2132, 2014.

[69] C. L. T. B. J. M. Jader F. B. Sousa, “PV hosting capacity of LV distribution networks uisng smart inverters and storage systems: a practical margin,” *IET Renewable Power Generation,* vol. 14, no. 8, pp. 1332-1339, 2020.

[70] A. V.-J. S. D. S.-Z. Carlos D. Zuluaga-Rios, “Evaluation of Distributed Generation and Electric Vehicles in Islanded DC Grids Considering EV Uncertainty,” *Energies 2022,* vol. 15, pp. 1-17, 2022.

[71] O. D. M.-D. C. S. B. V. A. P.-F. Darwin A. Quijano, “Increasing distributed generation hosting capacity in distribution systems via optimal coordination of electric vehicle aggregators,” *IET Generation Transmission and Distribution,* pp. 1-12, 2020.

[72] T. T. L. R. Z. Jun Su, “Modelling of Large-scale electric vehicles charging demand: A New Zealand case study,” *Electric Power Systems Research,* vol. 167, pp. 171-182, 2019.

[73] T. F. Hideharu Sugihara, “Increasing Electric Vehicle Capacity and Equality for Fast Charging Stations Using Residential Photovoltaics in Medium- and Low-voltage Distribution Networks,” *IEEJ Transactions on Electrical and Electronic Engineering,* vol. 15, pp. 364-371, 2020.

[74] H. S. E. O. G. O. G. A. Can Duman, “Optimal sizing of PV-BESS units for home energy management system-equipped households considering day ahead load scheduling for demand response response,” *Energy and Buildings,* vol. 267, 2022.

[75] L. F. O. H. M. N. D. H. Florin Capitanescu, “Assessing the Potential of Network Reconfiguration to improve distributed generation hosting capacity in active distrubtion systems,” *IEEE Transactions on Power Systems,* pp. 346-356, 2015.

[76] S. K. Y. H. N. Y. S.-i. M. Yuji Takenobu, “Maximizing Hosting Capacity of Distributed Generation by Network Reconfiguration in Distribution System,” in *19th Power System and Computing Conference (PSCC2016)*, 2016.

[77] I. M. J. F. S. L. Simon Heslop, “Method for determining a PV generation limit on low voltage feeders for evenly distributed PV and load,” *Energy Procedia,* pp. 207-216, 2014.

[78] T.Stetz, “High Penetration PV in Local Distribution Grids Outcomes of the IEA PVPS Task 14 Subtask 2,” in *29th European Photovoltaic Solar Energy Conference and Exhibition (EU PVSEC 2014)*, Kassel, 2014.

[79] J. M. D. Z. A. S. A. H. M. Mohammad Seydali Seyf Abad, “Probabilistic Assessment of Hosting Capacity in Radial Distribution Systems,” *IEEE Transactions on Sustainable Energy,* vol. 9, no. 4, pp. 1935-1947, 2018.

[80] S. S. Anamika Dubey, “On Estimation and Sensitivity Analysis of Distribution Circuit's Photovoltaic Hosting Capacity,” *IEEE Transactions on Power Systems,* vol. 32, no. 4, pp. 2779-2789, 2017.

[81] M. A. K. J. B. N. Sai Munikoti, “A novel framework for hosting capacity analysis with spatio-temporal probabilistic voltage sensitivity analysis,” *Electrical Power and Energy Systems,* vol. 134, 2022.

[82] W. F. T. Hermann W. Dommel, “Optimal Power Flow Solutions,” *IEEE Transactions on Power Systems,* pp. 1866-1876, 1969.

[83] K. B. C. Tabak Daniel, Optimal Control by Mathematical Programming, E. Cliffs, Ed., New Jersey: Prentice Hall, 1971, pp. 19-20.

[84] S. D. S. S. A. Santos Jr., “A Dual Augmented Approach for Optimal Power Flow,” *IEEE Transactions on Power Systems,* vol. 3, no. 3, pp. 1020-1025, 1988.

[85] S. G. E. A. A. A. V. Mojtaba Ghasemi, “Solving non-linear, non-smooth and non-convex optimal power flow problems using chaotic invasive weed optimization algorithms based on chaos,” *Energy,* vol. 73, pp. 340-353, 2014.

[86] E. R. Kennedy J., “Particle Swarm Optimization,” in *IEEE International Conference on Neural Networks (ICNN'95)*, Perth, 1995.

[87] A. G. Gad, “Particle Swarm Optimization Algorithm and its Applications: A Systematic Review,” *Archives of Computational Methods in Engineering,* pp. 2531-25-61, 2022.

[88] S. M., C. K. and W. J, “Three-dimensional wind turbine positioning using gaussian particle swarm optimization with different evolution,” *Journal of Wind Engineering and Industrial Aerodynamics,* vol. 172, pp. 317-324, 2018.

[89] S. F. and N. N.J, “Service allocation in the cloud environment using multi-objective particle swarm optimization algorithm based on crowding distance,” *Swarm Evolution Computing,* vol. 35, pp. 53-64, 2017.

[90] N. B. Y. D. A. S. R. Priem, “Upper trust bound criterion for mixed constrained Bayesian optimization with application to aircrft design,” *Aerospace Science and Technology,* vol. 105, 2020.

[91] W. M. F. R. A. Noureen, “Constrained optimization based on hybrid version of superiority of feasibility solution strategy,” *Soft Computing,* vol. 26, pp. 8117-8132, 2022.

[92] S. Fatima, V. Puvi and M. Lehtonen, “Review on the PV Hosting Capacity in Distribution Networks,” *Energies,* vol. 13, 2020.

[93] R. Torquato, D. Salles, C. O. Pereira, P. C. M. Meira and W. Freitas, “A comprehensive Assessment of PV hosting capacity on low-voltage distribution systems,” *IEEE Transactions on Power Delivery,* vol. 33, no. 2, pp. 1002-1012, 2018.

[94] A. Hoke, R. Butler, J. Hambrick and B. Kroposki, “Steady-state analysis of maximum photovoltaic penetration levels on typical distribution feeders,” *IEEE Transactions on sustainable energy,* vol. 4, no. 2, pp. 350-357, 2013.

[95] G. Radman and J. Shultz, “A New Derivation for Newton-Based Optimal Power Flow Solution,” *Electric Power Components and Systems,* vol. 33, no. 6, pp. 673-684, 2006.

[96] F. F. W. Mesut E. Baran, “Network Reconfiguration in Distribution Systems for Loss Reduction and Load Balancing,” *IEEE Transactions on Power Delivery,* vol. 4, no. 2, pp. 1401-1407, 1989.

[97] S. Nawaz and A. Tandon, “Power loss minimization of rural feeder in Jaipur city by renewable-based DG technologies,” *Australian Journal of Electrical and Electronics Engineering,* pp. 1-10, 2018.

[98] J. Mantovani, F. Casari and R. Romero, “Reconfiguracao de sistemasde distrbuicaoradiais utilizando o criterio de queda de tensa,” *Bras Controle Automacao-SBA,* vol. 11, no. 2, pp. 150-159, 2000.

[99] R. Zimmerman, C. Murillo-S'anchez and R. Thomas, “MATPOWER: Steady-State Operations, Planning and Analysis Tools for Power Systems Research Education,” *IEEE Transactions on Power Systems,* vol. 26, no. 1, pp. 12-19, 2011.

[100] R. D. Utkarsh Mahadeo Khaire, “Stability Investigation of Improved Whale Optimization Algorithm in Feature Selection,” *IETE,* vol. 39, no. 2, pp. 286-300, 2020.

[101] Q. Liu, “Order-2 Stability Analysis of Particle Swarm Optimization,” *Evolutionary Computation,* vol. 23, no. 2, pp. 187-216, 2014.

[102] E. Dall'Anese, S. V. Dhople and G. B. Giannakis, “Optimal Dispatch of Photovoltaic Inverters in Residential Distribution Networks,” *IEEE Transactions on Sustainable Energy,* vol. 5, no. 2, pp. 487-498, 2014.

[103] Z. Esau and H. Hara Ryoichi Kita, “Distribution Network PV Hosting Capacity Improvement by Inverter Volt/Var Optimization using hybrid PSO/GD Algorithm,” in *2020 National Conference of the Institute of Electrical Engineers of Japan*, Sapporo, 2022.

[104] David Narang etal., “IEEE Standard for Interconnection and Interoperability of Distributed Resources with Associated Electric Power Interfaces,” IEEE Press, New York, 2018.

[105] S. R. S. Conti, “Probabilistic load flow using Monte Carlo techniques for distribution networks with photovoltaic generators,” *Solar Energy,* pp. 1473-1481, 2007.

[106] M. H. J. B. N. E. Enock Mulenga, “A review of hosting capacity quantification methods for photovoltaics in low-voltage distribution grids,” *Electrical Power and Energy Systems,* vol. 115, 2020.

[107] A. T. S. V. T. G. Valverde, “Probabilistic load flow with non-Gaussian correlated random variables using Gaussian mixture models,” *IET Generation, Transmission & Distribution,* vol. 6, no. 7, pp. 701-709, 2012.

[108] P. C. P. V. Guido Carpinelli, “Multi-linear Monte Carlo simulation method for probabilistic load flow of distribution systems with wind and photovoltaic generation systems,” *Renewable Energy,* vol. 76, pp. 283-295, 2015.

[109] J. P.-R. Juan M. Morales, “Point Estimate Schemes to Solve the Probabilistic Power Flow,” *IEEE Transactions on Power Systems,* vol. 22, no. 4, pp. 1594-1601, 2007.

[110] M. E. Harr, “Probabilistic estimates for multivariate analyses,” *Applied Mathethatical Modelling,* vol. 13, pp. 313-318, 1989.

[111] L. K. S., “Point-estimate method for calculating statistical moments,” *Journal of Engineering Mechanics, ASCE,* vol. 188, no. 7, pp. 1506-1511, 1992.

[112] E. Rosenblueth, “Point estimates for probability moments,” in *National Academic of Science - Mathematics* , USA, 1975.

[113] R. L. A. H.-S. A. Z. L. Wenliang Fan, “A new point estimation method for statistical moments based on dimension-reduction method and direct numerical integration,” *Applied Mathematical Modelling,* vol. 62, pp. 664-679, 2018.

[114] H. Hong, “An efficient point estimate method for probabilistic analysis,” *Reliability and Systems Safety,* vol. 59, pp. 261-267, 1998.

[115] M. I. Constante-Flores E. Gonzalo, “Data-driven Probabilistic Power Flow Analysis for a Distribution System with Renewable Energy Sources using Monte Carlo Simulation,” *IEEE Transactions on Industry Applications,* vol. 55, no. 1, pp. 174-181, 2019.

[116] C. F. R. R. A. Mantovani J.R.S, “Reconfiguracao de sistemas de distribuicao radiais utilizando o criterio de queda de tensa,” *Bras Controle Automacao-SBA,* vol. 11, no. 2, pp. 150-159, 2000.

[117] M. Tran, D. Banister, j. D. Bishop and M. D. McCulloch, “Realizing the Electric-vehicle revolution,” *Nature Climate Change,* vol. 2, pp. 328-333, 2012.

[118] A. Kumar, N. K. Meena, A. R. Singh, Y. Deng, X. He, R. Bansal and P. Kumar, “Strategic integration of battery energy storage systems with provision of distributed ancillary services in active distribution systems,” *Applied Energy,* vol. 253, 2019.

[119] A. Ahmadian, M. Segghi and M. Aliakbar-Golkar, “Stochastic Modeling of plug-in Electric vehicles load demand in residential grids considering non-linear battery charge characteristic,” in *20th Iranian Electrical Power Distribution Conference (EPDC2015)*, Zahedan, 2015.

[120] R. Fachrizal, U. H. Ramadhani and J. W. Joakim Munkhammar, “Combined PV-EV hosting capacity assessment for residential LV distribution grid with smart EV charging and PV curtailment,” *Sustainable Energy, Grids and Networks,* vol. 6, 2021.

[121] J. Su, T. Lie and R. Zamora, “Modeling of Large-scale electric vehicles charging demand: A New Zealand case study,” *Electric Power Systems Research,* vol. 167, pp. 171-182, 2019.

[122] C. A. Duman, O. G. Hamza Salih Erden and O. Guler, “Optimal sizing of PV-BESS units for home energy management system-euipped households considering day-ahead load scheduling for demand response and self-consumption,” *Energy & Buildings,* vol. 267, 2022.

[123] Z. Esau, H. Ryoichi and K. Hiroyuki, “An Efficient Hybrid Particle Swarm and Gradient Descent Method for the Estimation of the Hosting Capacity of Photovoltaics in Distribution Networks,” *Energies,* vol. 16, no. 13, p. 5207, 2023.

[124] S. S. Anamika Dubey, “On Estimation and Sensitivity Analysis of Distribution Circuit's Photovoltaic Hosting Capacity,” *IEEE Transactions on Power Systems,* vol. 32, no. 4, pp. 2779-2789, 2017.

[125] A. Kumar, N. K. Meena, A. R. Singh, Y. Deng, X. He, R. Bansal and P. Kumar, “Strategic integration of battery energy storage systems with provision of distributed ancillary services in active distribution systems,” *Applied Energy,* vol. 253, 2019.

[126] E. Zulu, R. Hara and H. Kita, “A flexible stochastic PV hosting capacity framework considering network over-voltage tolerance,” *Energy Reports,* vol. 9, pp. 529-538, 2023.

Acknowledgements

My sincere gratitude goes to all those who helped and supported me in my quest to achieve success in my doctoral research.

I would like to thank my supervisors Associate Professor Hara Ryoichi and Professor Kita Hiroyuki for their unwavering guidance, engagement, and encouragement during my studies and research. Their constant and considerable efforts in weekly meetings provided a source of direction, inspiration, and hope without which this research wouldn't have been completed.

Associate Professor Hara provided invariable advice on the direction of the research. He provided ideas to solve many challenges faced during the research process and relentlessly corrected my errors which occurred during the research tenure. His help in my transition to Japanese lifestyle cannot be overemphasized. It was really a pleasure working under his supervision.

Profound gratitude to Professor Kita for his valuable advice on the research direction of this study, and his exemplary patience on the guidance in shaping the presentation results of the research. Professor Kita gave advice on the presentation of style and content of engineering research presentations. With his help my ability to present at scientific and/or engineering conferences has improved tremendously. I cannot overemphasize his contribution to my life during my time in Japan.

Many thanks to many Professors who taught me in various coursework. Professor Yuh Yamashita, Professor Hagime Igarashi and Professor Atsushi Konno offered insights in various fields related to information science and technology.

To the laboratory members of staff Mr. Ko Rinoie, and Mrs. Ozaki Chiemi, Thank you for your kindness, patience, and unmatched help during my time in the power and energy laboratory. My sincere gratitude to all the students in the PES laboratory. Special thanks to Ohsawa Takuto, who was my tutor since the time I came to Sapporo. Special thanks to Kida-san, Kawashima-san, Yida-san, Takada-san and Akasaka-san, Nakamura-san, to mention but a few, for making my life easy with constant help throughout my stay in Japan.

Gratitude also goes to the Ministry of Education, Culture, Sports, Science and Technology (MEXT), and the President of Hokkaido University for the financial support for tuition fees and living expenses since October 2019. The support allowed me to devote myself to my research work without having to worry about finances too much.

More importantly, I would like to extend my heartfelt gratitude to my wife Violet Mwandu Banda Zulu for all the support and sacrifices made during the long period I was away to pursue the studies. I understand how difficult this was for her. I also tender my apologies to my two daughters Tikambenji Mary Zulu and Temwani Catherine Zulu for being away from them when they were so young.

To God the Almighty, I give all the glory!

Esau Zulu

November 2023

Appendix I-A: Line power flows of IEEE 33 without PV

Load Flow Results After PV Installation – IEEE 33 Bus Test DN				
From Bus	*To Bus*	*Current [pu]*	*Power [MW]*	*Reactive Power [MVAr]*
1	2	0.864755661	3.879361274	1.909349345
2	3	0.762196836	3.407469652	1.682788648
3	4	0.529830261	2.333205336	1.162808649
4	5	0.50056145	2.19717926	1.074646735
5	6	0.486739038	2.122284746	1.037060733
6	7	0.254643098	1.095039958	0.527687699
7	8	0.207639501	0.893146558	0.421428962
8	9	0.160401678	0.68836239	0.319847913
9	10	0.147039858	0.624228798	0.296878148
10	11	0.133612025	0.560707983	0.274382551
11	12	0.12213715	0.515160529	0.244201552
12	13	0.107293725	0.454289357	0.208913488
13	14	0.092375583	0.391653346	0.171839514
14	15	0.061873244	0.270932461	0.090890625
15	16	0.048891273	0.21057955	0.080576527
16	17	0.035174599	0.150301291	0.060373324
17	18	0.021449043	0.090052529	0.040041191
2	19	0.079307747	0.361137118	0.161078468
19	20	0.059544437	0.270976221	0.120924929
20	21	0.039709929	0.180144341	0.080175341
21	22	0.019861342	0.090043619	0.040057672
3	23	0.212373166	0.939590424	0.457226217
23	24	0.191406721	0.846416175	0.405057287
24	25	0.095866841	0.421284451	0.201005054
6	26	0.218964888	0.936979217	0.463246345
26	27	0.205356066	0.875461057	0.437473056
27	28	0.191722287	0.813591616	0.411521233
28	29	0.178457561	0.747519868	0.386167889
29	30	0.148859475	0.623524962	0.312687621
30	31	0.101005107	0.421770833	0.211794139
31	32	0.06544411	0.270220244	0.140261691
32	33	0.015520395	0.060012812	0.040019921

Appendix I-B: Line Flows for IEEE 33 with PV

Load Flow Results after PV Installation - IEEE 33 Bus Test DN				
From Bus	*To Bus*	*Current [pu]*	*Power [MW]*	*Reactive Power [MVAr]*
1	2	0.37855415	0.335053272	1.862879621
2	3	0.32939351	-0.12814005	1.640755049
3	4	0.27832358	-0.78582511	1.143613907
4	5	0.28032679	-0.91024747	1.061361647
5	6	0.28393562	-0.9749188	1.028982467
6	7	0.22728384	-0.99487328	0.546768789
7	8	0.14767981	-0.58982167	0.4417827
8	9	0.17250385	-0.79224175	0.340982926
9	10	0.18215128	-0.85702262	0.317548122
10	11	0.19214428	-0.92242565	0.293718387
11	12	0.19902384	-0.96855782	0.263344069
12	13	0.20890627	-1.03087105	0.227579171
13	14	0.21920667	-1.10086418	0.184716727
14	15	0.24066134	-1.22492355	0.099373437
15	16	0.09077257	-0.45764271	0.084621497
16	17	0.10173598	-0.51860188	0.063921045
17	18	0.11296758	-0.58068289	0.041142595
2	19	0.07914358	0.361132406	0.161073999
19	20	0.05942092	0.270972174	0.120921095
20	21	0.0396275	0.180143742	0.080174614
21	22	0.01982009	0.090043438	0.040057433
3	23	0.14435981	0.559341538	0.452891529
23	24	0.12402092	0.467874862	0.401889365
24	25	0.04147411	0.0457204	0.200188108
6	26	0.09131821	-0.05034455	0.453323063
26	27	0.08801474	0.0991114	0.428188568
27	28	0.0811245	0.038767995	0.403013723
28	29	0.07688352	-0.02231911	0.382055241
29	30	0.06895432	-0.1430606	0.311409276
30	31	0.08112977	-0.34343698	0.211217561
31	32	0.06120318	0.270192624	0.140228873
32	33	0.01451421	0.060011205	0.040017422

Appendix II: PSO-GD Program Code

Appendix II-A Main Program Code

```
clc;
clear;
close all;
tic;
%% Problem Definition
problem.CostFunction = @(x) Hosting_Capacity(x);    % Objective Function of problem
nbus = 33;                                    % Number of buses in the IEEE 33-bus DN
PV_max = params.PV_max;                          % Declare maximum size of PV plants
problem.nVar = (nbus-1);          % Search space of solution, all buses in network
problem.VarMin = zeros(1, problem.nVar);                 % Lower bound of solution
problem.VarMax = PV_max*ones(1, problem.nVar);           % Upper bound of solution

%% Common Parameters of Meta-Heuristics
params.MaxIt = params.MaxIt;                           % maximum number of iterations
params.nPop = params.nPop;                                        % population size

%% Parameters of PSO
params.c1 = 2;                % coefficient of acceleration of individual particle
params.c2 = 2;                   % coefficient of acceleration of social behavior
params.w = 1;                                     % Inertia weight of acceleration
params.d = 0.99;                                             % Damping coefficient

%% Run PSO-GD algorithm to Generate Results

out1a = RunPSO_GD(problem, params);     % Generates solution for PVHC using PSO-GD

%% Results

PVHC = out1a.BestValues(end);                 % Calculation for PV Hosting Capacity
plot(out1a.voltage);grid on; xlabel('node number'); ylabel('voltage [pu]');

toc;
```

Appendix II-B: PSO-GD Sub-routine

```
%%Particle_Swam_Optimization with Gradient Descent for PV siting and sizing
function out1a = RunPSO_GD(problem, params)
%% Problem Definition
ObjFunction = problem.CostFunction;                          % Objective function
nVar = problem.nVar;                                         % number of variables
VarSize = [1, nVar];                                         % size of the control
variable
VarMin = problem.VarMin;                                     % Minimum values of
variables
VarMax = problem.VarMax;                                     % Maximum values of
variables
% MaxVelocity =0.35*(VarMax-VarMin);                           % Maximum velocity of
particles
```

```
MaxVelocity =1.00*(VarMax-VarMin);                          % Maximum velocity of
particles
MinVelocity = -MaxVelocity;                                 % Minimum velocity of
particles
%% Parameters of PSO
MaxIt = params.MaxIt;                                       % Maximum number of
Iterations
nPop = params.nPop;                                         % Initial swam
population
c1 = params.c1;                                             % Personal acceleration
coefficient
c2 = params.c2;                                             % Global acceleration
coefficient
w = params.w;                                               % Inertia coefficient
d = params.d;                                               % Damping ratio of
inertia (weight) coefficient
z = 10^(-5);                                                % Damping coefficient
of gradient
%% Initialization
empty_particle.PVsizes = [];                                % Initialize particles
sizes
empty_particle.Velocity = [];                               % Initialize particle
velocity
empty_particle.value = [];                                  % Initialize particle
value
empty_particle.feasibility = [];                            % Initialize particle
feasilbility
empty_particle.violation = [];                              % Initialize particle
constraint violation
empty_particle.gradient = [];                               % Initialize particle
gradient
empty_particle.V = [];                                      % Initialize particle
node voltages
empty_particle.Pg = [];                                     % Initialize particle
PV generations
empty_particle.Qg = [];                                     % Initialize particle
PV inverter Q output
empty_particle.PowerLoss = [];                              % Initialize particle
power loss
empty_particle.alpha = [];                                  % Initialize particle
VVC droop characteristic
empty_particle.Best.PVsizes = [];                           % Initialize particle
node PV sizes
empty_particle.Best.value = [];                             %  Initialize particle
PVHC value
empty_particle.Best.feasibility = [];                       % Initialize particle
feasilbility flag
empty_particle.Best.violation = [];                         % Initialize particle
constraint violation flag
empty_particle.Best.gradient = [];                          % Initialize particle
gradient
particle = repmat(empty_particle, nPop,1);                  % Initialize particle
population
GlobalBest.PVsizes = VarMin;
[GlobalBest.value, GlobalBest.feasibility, GlobalBest.violation,
GlobalBest.gradient,~,~,~,~,~] = ObjFunction(GlobalBest.PVsizes);
for i = 1:nPop
    %Generate a random position for each particle
```

```
    particle(i).PVsizes = unifrnd(VarMin, VarMax, VarSize);
%     input.PV_injection = particle(i).location;
    %Initialize velocity
    particle(i).Velocity = zeros(VarSize);
    %Evaluate the particle
    [particle(i).value, particle(i).feasibility, particle(i).violation,
particle(i).gradient,~,~,~,~,~] = ObjFunction(particle(i).PVsizes);
%     particle(i).location = input.PV_injection ;
    %Update personal best of particle
    particle(i).Best.PVsizes = particle(i).PVsizes;
    particle(i).Best.value = particle(i).value;
    particle(i).Best.feasibility = particle(i).feasibility;
    particle(i).Best.violation = particle(i).violation;
    particle(i).Best.gradient = particle(i).gradient;
    % Update Global Best
    if (particle(i).Best.feasibility == 1 && GlobalBest.feasibility ==0)
        GlobalBest = particle(i).Best;
    elseif (particle(i).Best.feasibility == 1 && GlobalBest.feasibility == 1)
        if particle(i).Best.value > GlobalBest.value
             GlobalBest = particle(i).Best;
        elseif particle(i).Best.value == GlobalBest.value
            if particle(i).Best.violation < GlobalBest.violation
                GlobalBest = particle(i).Best;
            end
        end
    elseif (particle(i).Best.feasibility == 0 && GlobalBest.feasibility == 0)
        if (particle(i).Best.violation < GlobalBest.violation)
           if particle(i).Best.gradient < GlobalBest.gradient
             GlobalBest = particle(i).Best;
           elseif particle(i).Best.gradient == GlobalBest.gradient
               if particle(i).Best.value > GlobalBest.value
                 GlobalBest = particle(i).Best;
               end
           end
        end
    end
end
% alpha = NaN(MaxIt,33);
Vmax = zeros (MaxIt, 1);
Gradient = NaN(MaxIt, 1);
BestValues = NaN(MaxIt, 1);
Solution_feasibility = NaN(MaxIt, 1);
Constraint_violation = NaN(MaxIt, 1);
%% Main Loop of PSO
for it = 1:MaxIt
   % Calculating the particle velocity and particle position
 for i = 1:nPop

        particle(i).Velocity = (particle(i).gradient).*particle(i).Velocity...
            +c1.*rand(VarSize).*( particle(i).Best.PVsizes -
particle(i).PVsizes)...
            +c2.*rand(VarSize).*( GlobalBest.PVsizes - particle(i).PVsizes);
        particle(i).Velocity = max(particle(i).Velocity, MinVelocity);
        particle(i).Velocity = min(particle(i).Velocity, MaxVelocity);
        particle(i).PVsizes =(particle(i).PVsizes + particle(i).Velocity);
        particle(i).PVsizes = max(particle(i).PVsizes, VarMin);
        particle(i).PVsizes = min(particle(i).PVsizes, VarMax);
```

```
        [particle(i).value, particle(i).feasibility, particle(i).violation,
particle(i).gradient,particle(i).V, particle(i).Pg, particle(i).Qg,
particle(i).PowerLoss,particle(i).alpha] = ObjFunction(particle(i).PVsizes);
        % Update the particle best
      if (particle(i).Best.feasibility == 0 && particle(i).feasibility ==1)
             particle(i).Best = particle(i);
      elseif(particle(i).Best.feasibility == 1 && particle(i).feasibility == 1)
          if (particle(i).Best.value < particle(i).value)
              particle(i).Best = particle(i);
          elseif (particle(i).Best.value == particle(i).value)
              if particle(i).Best.violation > particle(i).violation
                   particle(i).Best = particle(i);
              end
          end
      elseif particle(i).Best.feasibility == 0 && particle(i).feasibility == 0
           if (particle(i).Best.gradient > particle(i).gradient)
              particle(i).Best = particle(i);
          elseif particle(i).Best.gradient == particle(i).gradient
              if particle(i).Best.value < particle(i).value
                   particle(i).Best = particle(i);
              end
           end
      end
      % Update the global best solution
  if (particle(i).Best.feasibility == 1 && GlobalBest.feasibility ==0)
        GlobalBest = particle(i).Best;
    elseif (particle(i).Best.feasibility == 1 && GlobalBest.feasibility == 1)
        if particle(i).Best.value > GlobalBest.value
             GlobalBest = particle(i).Best;
        elseif particle(i).Best.value == GlobalBest.value
            if particle(i).Best.violation < GlobalBest.violation
                GlobalBest = particle(i).Best;
            end
        end
    elseif (particle(i).Best.feasibility == 0 && GlobalBest.feasibility == 0)
        if particle(i).Best.violation < GlobalBest.violation
           if particle(i).Best.gradient < GlobalBest.gradient
             GlobalBest = particle(i).Best;
           elseif particle(i).Best.gradient == GlobalBest.gradient
               if particle(i).Best.value > GlobalBest.value
                 GlobalBest = particle(i).Best;
               end
           end
        end
  end
 end
   Solution_feasibility(it) = GlobalBest.feasibility;
%    Vmax(it) = max(GlobalBest.V);
   BestValues(it) =  GlobalBest.value;
   Constraint_violation(it) = GlobalBest.violation;
   Gradient(it) = GlobalBest.gradient;
%    alpha(i)= particle(i).alpha;
   w = w*d;
   disp(['Iteration#:' num2str(it) ' Best PSO_Value: ' num2str(BestValues(it)) '
Feasibility: ' num2str(Solution_feasibility(it)) ' ' 'Gradient:'
num2str(Gradient(it))])
%    input.penaltyfactor = input.penaltyfactor*penaltycorrection;
end
```

```
%% Results
out1a.particle = particle;
out1a.BestValues = BestValues;
out1a.BestSol = GlobalBest.PVsizes;
out1a.Feasibility = GlobalBest.feasibility;
out1a.Constraint_Violation = Constraint_violation;
out1a.Gradient = Gradient;
out1a.voltage = particle.V;
out1a.realPV = particle.Pg;
out1a.reactivePV = particle.Qg;
out1a.PowerLoss = particle.PowerLoss;
out1a.alpha = particle.alpha;
out1a.Vmax = Vmax;
end
```

Appendix II-C: PVHC Cost-function Sub-routine

```
function [FitnessValue, Feasibility, constraint_violation,
Gradient,V,Pg,Qg,PowerLoss,alpha] = Hosting_Capacity(x)
penaltyfactor = 10;
[V, Pg, Qg, J, ~, busd, del, npv, npq, G, B, ~, pq, ~, nbus,alpha] =
LoadFlow(x); % Calling the load flow progam
[~, ~, ~, ~, ~, PowerLoss] = linepowerflows(V, G, B, nbus, del);
Vlb = 0.95;                                % Lower bound of the voltage
Vub = 1.05;                                % Upper bound of the voltage
Qlb = -1;                                  % Lower bound of the reactive power
(IEEE 33-1.0 , IEEE-69-1.50, IEEE 119-1.50)
Qub = 1;                                   % Upper bound of the reactive power
(IEEE 33+1.0 , IEEE-69+1.50, IEEE 119+1.50)
Pub = 1;                                   % Lower bound of the reactive power
(IEEE 33-1.0 , IEEE-69-1.50, IEEE 119-1.50)
Plb = -1;                                  % Upper bound of the reactive power
(IEEE 33+1.0 , IEEE-69+1.50, IEEE 119+1.50)
wp = 0;                                    % Initializing the real power violation
wq = zeros(nbus,1);                        % Initializing the reactive power
violation
wv = zeros(nbus,1);                        % Initializing the bus voltage violation
Gradient = min(abs(LagrangeGrad(V, del, J, G, B, npv, npq, busd, pq, nbus, Pg)));

%% Penalties for violation of constraints
for i = 1:nbus
    % voltage constraints
    if V(i) > Vub
        wv(i) = (V(i)-Vub)^2;
    else
        if V(i) < Vlb
            wv(i) = (V(i)-Vlb)^2;
        end
    end
    % reactive power constraints
    if Qg(i) > Qub
        wq(i) = (Qg(i)-Qub)^2;
    else
        if Qg(i) < Qlb
            wq (i)= (Qg(i)-Qlb)^2;
        end
    end
```

```
end
% real power constraints at the slack bus
    if Pg(1) < Plb
        wp =(Pg(1)-Plb)^2;
    else
        if Pg(1) > Pub
             wp =(Pg(1)-Pub)^2;
        end
    end
%% Feasibilty check
constraint_violation = sum(wp)+sum(wq)+sum(wv);
if constraint_violation == 0
    Feasibility = 1;
else
    Feasibility = 0;
end
%% Fitness value calculation
FitnessValue = 1.0*sum(x) - 1.0*penaltyfactor*sum(wv)-0.5*penaltyfactor*sum(wq)-
1*penaltyfactor*wp-0.2*PowerLoss;
end
```

Appendix II-D: Lagrange Gradient Sub-routine

```
function Gradient = LagrangeGrad(V, del, J, G, B, npv, npq, busd, pq, nbus,
PV_Sizes)
%% Initilization of elements
dFdDelta = zeros([nbus, 1]);              % derivatives of Lagrange wrt voltage
angles
dFdVolt = zeros([npq, 1]);                % derivatives of Lagrange wrt voltage
magnitudes
dFdPpv = zeros([2*npq + npv - 1, 1]);     % derivatives of Lagrange wrt PV power
dGdPpv = zeros([2*npq + npv - 1, 1]);     % derivatives of Lagrange wrt PV power
nbus = length(busd(:,1));                 % total number of buses
for i = 1 : nbus
     if (busd(i,2) == 1 || busd(i,2) == 2)
        for j = 1:nbus
           dFdDelta(i) = dFdDelta(i) + PV_Sizes(i)*(V(i)*V(j)*(-G(i,j)*sin(del(i)-
del(j))+B(i,j)*cos(del(i)-del(j))));
%            dFdDelta(i) = dFdDelta(i) + (V(i)*V(j)*(-G(i,j)*sin(del(i)-
del(j))+B(i,j)*cos(del(i)-del(j))));
        end
          dFdPpv(i) = dFdPpv(i) + PV_Sizes(i);
          dGdPpv(i) = dGdPpv(i) - PV_Sizes(i);
     end

end
dFdDelta = dFdDelta(2:nbus);
for i = 1: npq
      m = pq(i);
      for j = 1:nbus
          dFdVolt(i) = dFdVolt(i) + (V(j)*(G(m,j)*cos(del(m)-
del(j))+B(m,j)*sin(del(m)-del(j))));
      end

end
dFdx = [dFdDelta;dFdVolt];
```

```
Lambda = J^(-1)*(dFdx);
Gradient = dFdPpv - dGdPpv'*Lambda;

end
```

Appendix II-E: LoadFlowAnalysis Sub-routine

```
function [V, Pg, Qg, J, Y, busd, del, npv, npq, G, B, pv, pq, Pl, nbus, alpha1] =
LoadFlow(x)
num = 33;                           % IEEE-33 Bus RDN
%num = 69;                          % IEEE 69-bus RDN
%num = 136;                         % Sao Paulo 136 Bus DN
Y = ybusppg(num);                   % Calling ybusppg.m to get Bus Admittance
Matrix..
busd = busdatas(num);
% busd = busdatas;                  % Calling busdata33.m to get busdatas..
BMva = 5;                           % Base MVA ....for IEEE 33, 69
bus = busd(:,1);                    % Bus Number.
type = busd(:,2);                   % Type of Bus 1-Slack, 2-PV, 3-PQ..
V = busd(:,3);                      % Specified Voltage..
del = zeros(length(V),1);           % Voltage Angle..
t = 2:num;                          %IEEE 33 Bus PV locations
% t = [7 10 12 20 23 26 35 43 56 62 64 73 76 77 83 86 90 98 100 105 112 118 122
129 136];
% x = input;
for j = 1:length(t)
    busd(t(j),5) = x(j);
end
Pg = busd(:,5)/BMva;                % PGi
Qg = busd(:,6)/BMva;                % QGi..
Pl = 1.00*busd(:,7)/BMva;           % PLi..
Ql = 1.00*busd(:,8)/BMva;           % QLi..
Qmin = busd(:,9)/BMva;              % Minimum Reactive Power Limit..
Qmax = busd(:,10)/BMva;             % Maximum Reactive Power Limit..
nbus = max(bus);                    % To get no. of buses..
Psp = Pg - Pl;                      % Pi = PGi - PLi..Net bus real power
Qsp = Qg - Ql;                      % Qi = QGi - QLi..Net bus reactive power
%Psp = P;                           % P Specified
%Qsp = Q;                           % Q Specified
G = real(Y);                        % Conductance..of bus matrix elements
B = imag(Y);                        % Susceptance..of bus matrix elements
pv = find(type == 2 | type == 1);       % Index of PV Buses..
pq = find(type == 3);                   % Index of PQ Buses..
npv = length(pv);                       % Number of PV buses..
npq = length(pq);                       % Number of PQ buses..
alpha1=zeros(nbus,1);
Tol = 1;              % Tolerance (for error) setting
Iter = 1;             % iteration starting
while (Tol > 1e-5 )
    %(Tol > 1e-5 && Iter <= 50)     % Iteration starting..
    P = zeros(nbus,1);
    Q = zeros(nbus,1);
    % Calculate P and Q
    for i = 1:nbus
        for k = 1:nbus
            P(i) = P(i) + V(i)* V(k)*(G(i,k)*cos(del(i)-del(k)) +
B(i,k)*sin(del(i)-del(k)));
```

```
            Q(i) = Q(i) + V(i)* V(k)*(G(i,k)*sin(del(i)-del(k)) -
B(i,k)*cos(del(i)-del(k)));
        end
    end

    % Checking Q-limit violations..
    if Iter <= 7 && Iter > 2    % Only checked up to 7th iterations..
        for n = 2:nbus
            if type(n) == 2
                QG = Q(n)+Ql(n);
                if QG < Qmin(n)
                    V(n) = V(n) + 0.01;
                elseif QG > Qmax(n)
                    V(n) = V(n) - 0.01;
                end
            end
         end
    end
% %     [alpha, Qg] = VVC(V, Pg, nbus);
% %     Qsp = Qg - Ql;

    % Calculate change from specified value
    dPa = Psp-P;          % Real Power mismatch between specified and calculated
values
    dQa = Qsp-Q;          % Reactive Power mismatch between specified and
calculated values
    k = 1;
    dQ = zeros(npq,1);    % Initializing the power mistmatch matrix
    for i = 1:nbus
        if (type(i) == 3)||(type(i) == 4)
%             type(i) == 3 (alterations(1))
            dQ(k,1) = dQa(i);
            k = k+1;
        end
    end
    dP = dPa(2:nbus);
    M = [dP; dQ];       % Mismatch Vector

    % Jacobian
    % J1 - Derivative of Real Power Injections with Angles..
    J1 = zeros(nbus-1,nbus-1);             %Initializing dP/dDel elements
    for i = 1:(nbus-1)
        m = i+1;
        for k = 1:(nbus-1)
            n = k+1;
            if n == m
                for n = 1:nbus
                    J1(i,k) = J1(i,k) + V(m)* V(n)*(-G(m,n)*sin(del(m)-del(n)) +
B(m,n)*cos(del(m)-del(n)));
                end
                J1(i,k) = J1(i,k) - V(m)^2*B(m,m);
            else
                J1(i,k) = V(m)* V(n)*(G(m,n)*sin(del(m)-del(n)) -
B(m,n)*cos(del(m)-del(n)));
            end
        end
    end
```

```
    % J2 - Derivative of Real Power Injections with V..
    J2 = zeros(nbus-1,npq);             %Initializing dP/dV elements
    for i = 1:(nbus-1)
        m = i+1;
        for k = 1:npq
            n = pq(k);
            if n == m
                for n = 1:nbus
                    J2(i,k) = J2(i,k) + V(n)*(G(m,n)*cos(del(m)-del(n)) +
B(m,n)*sin(del(m)-del(n)));
                end
                J2(i,k) = J2(i,k) + V(m)*G(m,m);
            else
                J2(i,k) = V(m)*(G(m,n)*cos(del(m)-del(n)) + B(m,n)*sin(del(m)-
del(n)));
            end
        end
    end

    % J3 - Derivative of Reactive Power Injections with Angles..
    J3 = zeros(npq,nbus-1);               %Initializing dQ/dDel elements
    for i = 1:npq
        m = pq(i);
        for k = 1:(nbus-1)
            n = k+1;
            if n == m
                for n = 1:nbus
                    J3(i,k) = J3(i,k) + V(m)* V(n)*(G(m,n)*cos(del(m)-del(n)) +
B(m,n)*sin(del(m)-del(n)));
                end
                J3(i,k) = J3(i,k) - V(m)^2*G(m,m);
            else
                J3(i,k) = V(m)* V(n)*(-G(m,n)*cos(del(m)-del(n)) -
B(m,n)*sin(del(m)-del(n)));
            end
        end
    end

    % J4 - Derivative of Reactive Power Injections with V..
    J4 = zeros(npq,npq);                        %Initializing dQ/dV elements
    for i = 1:npq
        m = pq(i);
        for k = 1:npq
            n = pq(k);
            if n == m
                for n = 1:nbus
                    J4(i,k) = J4(i,k) + V(n)*(G(m,n)*sin(del(m)-del(n)) -
B(m,n)*cos(del(m)-del(n)));
                end
                J4(i,k) = J4(i,k) - V(m)*B(m,m);
            else
                J4(i,k) = V(m)*(G(m,n)*sin(del(m)-del(n)) - B(m,n)*cos(del(m)-
del(n)));
            end
        end
    end

    J = [J1 J2; J3 J4];         % Jacobian Matrix
```

```
    X = J\M;                    % INV(J) x M, Correction Vector..
    dTh = X(1:nbus-1);          % Change in Voltage Angle..
    dV = X(nbus:end);           % Change in Voltage Magnitude..

    % Update State Vectors (Voltage Angle & Magnitude)
    del(2:nbus) = dTh + del(2:nbus);
    k = 1;
    for i = 2:nbus
        if type(i) == 3
            V(i) = dV(k) + V(i);
            k = k+1;
        end
    end
    Iter = Iter + 1;
    Tol = max(abs(M));


end

       for k = 1:nbus
           if (type(k)== 1 || type(k)==2)
             Pg(k)= P(k)+Pl(k);
             Qg(k)= Q(k)+Ql(k);
           end
       end
end
```

Appendix II-F: Volt-Var Control Sub-routine

```
function [alpha, Qg] = VVC(V, Pg, nbus)
% function for calculating the inverter volt/var set points%%
%% Parameter declaration
Vmax = 1.050;                       % maximum allowable node voltage
Vmin = 0.950;                       % minimum allowable node voltage
Vdmin = 0.98;                      % minimum dead-band voltage
Vdmax = 1.02;                      % maximum dead-band voltage
Vref = 1.00;
%% Calculation of Decision Variables
Qgmax = sqrt((Pg/0.9).^2-Pg.^2);   % maximum reactive power output (injection)
Qgmin = -Qgmax;                     % minimum reactive power output (absorption)
alpha = Qgmax/(Vref-Vmin);         % inverter reactive power operating
characteristic
Qg = zeros(nbus,1);
%% volt-var control loop
for i = 1:nbus
    if Pg(i) > 1e-3                                % To avoid conflicting with Power
mismatch tolerance
        if V(i) < Vmin
           Qg(i) = Qgmax(i);
        elseif ((V(i) > Vmin) && (V(i) < Vref))
             Qg(i) = -alpha(i)*(V(i)-Vref);
        elseif ((V(i) > Vref) && (V(i) < Vmax))
               Qg(i) = -alpha(i)*(V(i)-Vref);
        else
            Qg(i) = Qgmin(i);
```

```
        end

    end
end
end
```

Appendix II-G: PEM Moments Generator

```
% Input data capture
clear;
close all;
clc;
tic;
% Declaration of Parameters of Distribution Network
nbus = 136;
params.nbus = 136;                                          % Number of bus in
the network
params.Y = ybusppg(nbus);                                  %PLF generation
params.BMVA = 5;                                           % MVA base for the
nework
params.busd = busdatas(nbus);                              % Network bus
information
params.Pg = params.busd(:,5)/params.BMVA;                  % PGi..active power
generated
params.Qg = params.busd(:,6)/params.BMVA;                  % QGi..reactive
power generated
params.Pl = params.busd(:,7)/params.BMVA;                  % Active power
demand
params.Ql = params.busd(:,8)/params.BMVA;                  % Reactive power
demand
params.type = params.busd(:,2);                            % Type of node
(slack=1, P-V=2, P-Q=3)
params.PV_sizes = [0.7 0.9 0.7 0.5 0.2 0.8];               % PV plant sizes at
different nodes
params.t = [7 15 18 25 26 31];                             % PV plant locations
params.Number_of_Runs = 100000;                            % Number of points
on the random variable distribution
% n = 3.6:0.1:5.2
% for b = 1:length(n)
%   params.PV_sizes  = n(b)*params.PV_sizes1/length(params.PV_sizes1);
% call the random variable generator
Random_Var = Stochastic_Random_Variables(params);          % Random generation
of input variables
PVgen = Random_Var.PVgen';                                 % PV output
distribution
Plgen = Random_Var.Plgen';                                 % Load demand active
power demand
Qlgen = Random_Var.Qlgen';                                 % Load demand
reactive power demand
% calculate mean of the random input variables
mu_LoadP = mean(Plgen);                                  % Mean of the node
active power demands
```

```
mu_LoadQ = mean(Qlgen);                                    % Mean of the node
reactive power demands
mu_PV = mean(PVgen);                                       % Mean of the node PV
injections
% standard deviation of random input variables
sigma_LoadP = std(Plgen);                                  % Standard deviation
of the node active power demands
sigma_LoadQ = std(Qlgen);                                  % Standard deviation
of the node reactive power demands
sigma_PV = std(PVgen);                                     % Standard deviation
of the node PV injections
% calculate skewness of random input variables
Skew_LoadP = skewness(Plgen,1);                              % Skewness of the
node active power demands
Skew_LoadQ = skewness(Qlgen,1);                              % Skewness of the
node reactive power demands
Skew_PV = skewness(PVgen,1);                                 % Skewness of the
node PV injections
% calculate kurtosis of random input variables
Kurtos_LoadP = kurtosis(Plgen,1);                            % Kurtosis of the
node active power demands
Kurtos_LoadQ = kurtosis(Qlgen,1);                            % Kurtosis of the
node reactive power demands
Kurtos_PV = kurtosis(PVgen,1);                               % Kurtosis of the
node PV injections
% Extracting the mean values of the random variables
Mean_Pl = mu_LoadP(2:params.nbus);
Mean_Ql = mu_LoadQ(2:params.nbus);
Mean_PV = mu_PV(params.t);
% Extracting the standard deviation values of the random variables
std_Pl = sigma_LoadP(2:params.nbus);
std_Ql = sigma_LoadQ(2:params.nbus);
std_PV = sigma_PV(params.t);
% Extracting the skewness values of the random variables
skew_Pl = Skew_LoadP(2:params.nbus);
skew_Ql = Skew_LoadQ(2:params.nbus);
skew_PV = Skew_PV(params.t);
% Extracting the kurtosis values of the random variables
kurtos_Pl = Kurtos_LoadP(2:params.nbus);
kurtos_Ql = Kurtos_LoadQ(2:params.nbus);
kurtos_PV = Kurtos_PV(params.t);
% Mean, stndard deviation, skewness and kurtosis of all input random variab
mean_Var = [Mean_PV,Mean_Pl,Mean_Ql];                        % Mean values of
all random input variables
sigma_Var = [std_PV,std_Pl,std_Ql];                          % Standard
deviation of all random input variables
skew_Var = [skew_PV,skew_Pl,skew_Ql];                        % Skewness of all
random input variables
kurtos_Var = [kurtos_PV,kurtos_Pl,kurtos_Ql];                % Kurtosis of all
random input variables
% Computing the PEM concentrations (locations and weights)
K = 2;                                                        % For 2m+1 Point
Estimate Method (PEM) scheme
```

```
Std_locations = zeros(K,length(mean_Var));                  % Standard
locations of the variables
rnd_Var_weight = zeros(K,length(mean_Var));                 % Weights of the
random variables in each standard location
rnd_Var_locations = zeros(K,length(mean_Var));              % locations of
random variables
for k = 1:K
    Std_locations(k,:) = (skew_Var./2) +((-1)^(3-k))*sqrt(kurtos_Var-
0.75.*skew_Var.^2);
end
for k = 1:K
    % Computing actual weights
    rnd_Var_weight(k,:) = ((-1)^(3-
k))./(Std_locations(k,:).*(Std_locations(1,:)-Std_locations(2,:)));
    % Computing actual locations
    rnd_Var_locations(k,:) = mean_Var + sigma_Var.*Std_locations(k,:);
end
% Random Variable input data
 %=============================================================================
======================%
 % Mean(column 1)   locations(columns 2,3)     weights(columns 4,5)
%  Rnd_Var_Dat = [mean_Var', rnd_Var_locations', rnd_Var_weight']
Var_input = mean_Var';
Var_Locations = rnd_Var_locations';
Var_Weights = rnd_Var_weight';
a = length(params.t); b = a+1; c = b+params.nbus-2;
Max_NodeVoltage = zeros(length(Var_input),K);
meanNODE_Vmax = 0;
stdNODE_Vmax = 0;
 % Initial weight for 2m+1 PEM
 w0 = 1-sum(1./(kurtos_Var-(skew_Var).^2));
 for l = 1:length(Var_input)
     for k = 1:K
         Pg = zeros(params.nbus,1);
         Pl = zeros(params.nbus,1);
         Ql = zeros(params.nbus,1);
         x = Var_Locations(l,k);
         y = Var_input;
         y(l)=(x);
         PV1 = y(1:a);
         Pl1 = y(b:c);
         Ql1 = y((c+1):end);
         Pl(2:params.nbus)=Pl1;Ql(2:params.nbus)=Ql1;Pg(params.t)=PV1;
         [Vmax, PV_inj, Pg1] = PLFTest2(Pl, Ql, Pg,params);
         Max_NodeVoltage(l,k)=Vmax;
         meanNODE_Vmax = meanNODE_Vmax +
         Max_NodeVoltage(l,k)*Var_Weights(l,k);
     end
 end
```

Appendix II-H: Main program for comparison of PSO-GD/PEM and MCS

```
tic;
clear;
close all;
clc;
tic;
% Declaration of Parameters of Distribution Network
nbus = 33;
% nbus = 136;
params.Steps = 0.05;                                    % Increment steps
for PVHC [100kW]
params.PVHC_min = sum(out1a.PV_sizes);                                  %
Starting value of PVHC [MW] IEEE 33 bus
params.nbus = 33;                                      % Number of bus in
the network(IEEE33)
params.Y = ybusppg(params.nbus);                              %PLF
generation
params.BMVA = 5;                                       % MVA base for the
nework
params.busd = busdatas(params.nbus);                          % Network bus
information
params.Pg = params.busd(:,5)/params.BMVA;                % PGi..active power
generated
params.Qg = params.busd(:,6)/params.BMVA;                % QGi..reactive
power generated
params.Pl = params.busd(:,7)/params.BMVA;                % Active power
demand
params.Ql = params.busd(:,8)/params.BMVA;                % Reactive power
demand
params.type = params.busd(:,2);                          % Type of node
(slack=1, P-V=2, P-Q=3)
params.PV_sizes1 = out1a.PV_sizes;             % PV plant sizes at different
nodes(IEEE33)
params.t = out1a.PV_locations;                           % PV plant
locations(IEEE33)
params.Vlim = 1.05;
params.Number_of_Runs = 20000;
PV_sizes2 = params.PVHC_min :params.Steps:params.PVHC_max;
runs = length(PV_sizes2);
ProbVVMCS = 0;
Node_VmaxMCS = zeros(params.Number_of_Runs,runs);
PVRandGen = zeros(params.Number_of_Runs,runs);
RandLoad = zeros(params.Number_of_Runs,runs);
Installed_PV = zeros(runs,1);
Observed_Vmax=zeros(runs,1);
ProbVVPEM = zeros(runs,1);
ProbVVMCS = zeros(runs,1);
meanVmaxNodePEM = zeros(runs,1);
stdVmaxNodePEM = zeros(runs,1);
Node_V = zeros(params.nbus,runs);
```

```
for z = 1:runs
       params.PV_sizes =
      PV_sizes2(z)/(sum(params.PV_sizes1))*params.PV_sizes1;
       params.Random_Var = Stochastic_Random_Variables(params);
       %%     MCS-based results
       figure(1)
       [ProbVVMCS(z,1),Node_VmaxMCS(:,z), Node_V(:,z), PVRandGen(:,z),
       RandLoad(:,z)]=MCS_MaxNodeVoltage_Curves(params);
       Installed_PV(z,1) = sum(params.PV_sizes);
       pd = fitdist(Node_VmaxMCS(:,z), 'Normal');
       x =
       linspace(min(Node_VmaxMCS(:,z)),max(Node_VmaxMCS(:,z)),params.Number_o
       f_Runs);
       y1 = pdf(pd,x);
       y = y1/params.Number_of_Runs;
       hold on;
       plot(x,y1,'LineWidth',5);
       xlabel('Maximum Node Voltage');
       ylabel('Probability Density Distribution');
        % %    PEM based results
       [ProbVVPEM(z,1),meanVmaxNodePEM(z,1),stdVmaxNodePEM(z,1)] =
       PEM_MaxNodeVoltage_Curves(params);
       NodeVmax = 1.02:0.001:1.1;
       pdfNodeVmax = (1/(sqrt(2*pi*stdVmaxNodePEM(z,1)^2)))*(exp(-((NodeVmax-
       meanVmaxNodePEM(z,1)).^2)/(2*stdVmaxNodePEM(z,1)^2)));
       hold on;
       plot(NodeVmax,pdfNodeVmax,'LineWidth',2.5); grid on;
       hold on;
    end                                          % end the ProbVV simulation
end
toc;
```

Appendix II-I: PEM-based PVHC Estimation sub-routine

```
function [ProbVVPEM,meanVmaxNode,stdVmaxNode] =
PEM_MaxNodeVoltage_Curves(params)
ProbVV = 0;
meanVmaxNode = 0;
stdVmaxNode = 0;
params.PV_sizes  = params.PV_sizes;


% call the random variable generator
% Random_Var = Stochastic_Random_Variables(params);       % Random generation
of input variables
Vlim = params.Vlim;                                       % The maximum
allowed voltage
PVgen = params.Random_Var.PVgen';                         % PV output
distribution
Plgen = params.Random_Var.Plgen';                         % Load demand active
power demand
Qlgen = params.Random_Var.Qlgen';                         % Load demand
reactive power demand
```

```
PV1 = PVgen(:,params.t);                                % PV injections at
PV nodes t
Pl1 = Plgen(:,2:params.nbus);                           % Active power load
demand at P-Q nodes
Ql1 = Qlgen(:,2:params.nbus);                           % ReActive power
load demand at P-Q nodes
mu_PV = (mean(PV1))';                                   % Mean values of
random PV injections
mu_Pl = (mean(Pl1))';                                   % Mean values of
random load demands
mu_Ql = (mean(Ql1))';                                   % Mean values of
random load demands
sigma_PV = (std(PV1))';                                 % standard deviation
values of random PV injections
sigma_Pl = (std(Pl1))';                                 % standard deviation
values of random load demands
sigma_Ql = (std(Ql1))';                                 % standard deviation
values of random load demands
skew_PV = (skewness(PV1,0))';                           % skewness values of
random PV injections
skew_Pl = (skewness(Pl1,0))';                           % skewness values of
random load demands
skew_Ql = (skewness(Ql1,0))';                           % skewness values of
random load demands
kurtos_PV = (kurtosis(PV1,0))';                         % kurtosis values of
random PV injections
kurtos_Pl = (kurtosis(Pl1,0))';                         % kurtosis values of
random load demands
kurtos_Ql = (kurtosis(Ql1,0))';                         % kurtosis values of
random load demands
meanVar = [mu_PV;mu_Pl;mu_Ql];                          % Mean values of
random variables
sigmaVar = [sigma_PV;sigma_Pl;sigma_Ql];                % standard
deviations of random variables
skewVar = [skew_PV;skew_Pl;skew_Ql];                    % skewness of random
variables
kurtosVar = [kurtos_PV; kurtos_Pl; kurtos_Ql];          % kurtosis of random
variables
% 2m scheme of Point Estimate Method (PEM)
K = 2;                                                  % PEM scheme related
value
m = length(meanVar);                                    % Total number of
variables
Var_weight = zeros(m,K);
std_location = zeros(m,K);
Var_locations = zeros(m,K);
NVmax = zeros(m,K);
mu_NodeVmax = 0;
moment2 = 0;
a = length(params.t); b = a+1; c = a+params.nbus-1; d = c+1; e =
length(meanVar);
% generating standard locations
for k = 1:K
```

```
    std_location(:,k) = (skewVar/2)+((-1)^(3-k))*sqrt(m+(skewVar/2).^2);
end
for k = 1:K
    Var_weight(:,k) = (((-1)^k)/m)*(std_location(:,(3-k))./(std_location(:,1)-
std_location(:,2)));
    % calculating concetrations
    Var_locations(:,k) = meanVar + std_location(:,k).*sigmaVar;
end
for l = 1:m
    for k = 1:K
        y = meanVar;
        Pg = zeros(params.nbus,1);
        Pl = zeros(params.nbus,1);
        Ql = zeros(params.nbus,1);
        x = Var_locations(l,k);
        y(l) = x;
        PV2 = y(1:a); Pl2 = y(b:c); Ql2 = y(d:e);
        Pg(params.t) = PV2; Pl(2:params.nbus) = Pl2; Ql(2:params.nbus) = Ql2;
        [Vmax, ~, ~] = PLFTest2(Pl, Ql, Pg,params);
        NVmax(l,k) = Vmax;
        mu_NodeVmax = mu_NodeVmax + Vmax*Var_weight(l,k);
        moment2 = moment2 + ((Vmax)^2)*Var_weight(l,k);
    end
end
meanVmax = mu_NodeVmax;
sigmaVmax = sqrt(moment2-meanVmax.^2);
% NodeVmax = 1.02:0.001:1.095; r = min(NodeVmax); s = max(NodeVmax);
% pdfNodeVmax = (1/(sqrt(2*pi*sigmaVmax^2)))*(exp(-((NodeVmax-
meanVmax).^2)/(2*sigmaVmax^2)));
% plot(NodeVmax,pdfNodeVmax,'LineWidth',2); grid on; xlabel('Maximum Node
Voltage'); ylabel('Probability Density');
% hold on;
syms x;
f = (1/(sqrt(2*pi*sigmaVmax^2)))*(exp(-((x-meanVmax).^2)/(2*sigmaVmax^2)));
F = vpaintegral(f,x,[Vlim,1.1]);
ProbVV = double(F);
meanVmaxNode = meanVmax;
stdVmaxNode = sigmaVmax;
ProbVVPEM = 100*ProbVV;
end
```

Appendix II-J: MCS-based PVHC Estimation sub-routine

```
function [ProbVVMCS,Node_Vmax,V, PVRandGen, RandLoad] =
MCS_MaxNodeVoltage_Curves(params)
% Monte Carlo Parameter Declaration
Number_of_Runs = params.Number_of_Runs;
Vllimit = 1.05;
Node_Vmax = zeros(Number_of_Runs,1);
Volt_vio = 0;
params.PV_sizes = params.PV_sizes;
```

```
PVRandGen = zeros(Number_of_Runs,1);
RandLoad = zeros(Number_of_Runs,1);
% call the random variable generator
% Random_Var = Stochastic_Random_Variables(params);
PVgen = params.Random_Var.PVgen;
Plgen = params.Random_Var.Plgen;
Qlgen = params.Random_Var.Qlgen;
  for i = 1:Number_of_Runs
      Pg = PVgen(:,i);
      Pl = Plgen(:,i);
      Ql= Qlgen(:,i);
      [Vmax, ~, V] = PLFTest2(Pl, Ql, Pg,params);
      Node_Vmax(i,1) = Vmax;                      % Maximum node voltage in
iteration
      if Node_Vmax(i,1)>Vllimit
         Volt_vio = Volt_vio+1;
      end
      PVRandGen(i,1) = sum(Pg);                  % Aggregate Random PV
generation
      RandLoad (i,1) = sum(Pl);                  % Aggregate Load demand

   end
   volt_violation = Volt_vio/Number_of_Runs;
%    PVHC = sum(params.PV_sizes);
   ProbVVMCS = volt_violation*100;               % Percent probability of
overvoltage.
%    Installed_PV =  PVHC;
% Net_Load = PVRandGen - RandLoad;                % Net demand imposed on
the network.
end
```